



Ana Teresa Vilhena Pontes do Carmo Rodrigues

LONG-TERM EFFECTS ON STRUCTURAL GLASS

EFEITOS DIFERIDOS EM VIDRO ESTRUTURAL

Dissertação de Mestrado Integrado em Engenharia Civil, na área de Especialização em Mecânica Estrutural,
orientada pela Professora Doutora Sandra Filomena da Silva Jordão Alves e pela Professora Doutora Chiara Bedon.

Coimbra, 8 de Setembro de 2017



UNIVERSIDADE DE COIMBRA



FCTUC DEPARTAMENTO DE ENGENHARIA CIVIL
FACULDADE DE CIÊNCIAS E TECNOLOGIA
UNIVERSIDADE DE COIMBRA

Ana Teresa Vilhena Pontes do Carmo Rodrigues

Long-term Effects on Structural Glass

Efeitos Diferidos em Vidro Estrutural

Dissertação de Mestrado Integrado em Engenharia Civil, na área de Especialização em Mecânica Estrutural, orientada pela Professora Doutora Sandra Filomena da Silva Jordão Alves e pela Professora Doutora Chiara Bedon.

Esta Dissertação é da exclusiva responsabilidade do seu autor.
O Departamento de Engenharia Civil da FCTUC declina qualquer
responsabilidade, legal ou outra, em relação a erros ou omissões
que possa conter.

Coimbra, 8 de Setembro de 2017

AGRADECIMENTOS

A conclusão da presente dissertação assinala o final de uma marcante etapa da minha vida. Importa por isso agradecer não só a todos os que contribuíram para o desenvolvimento deste trabalho, mas também aos que permaneceram sempre ao meu lado ao longo destes anos.

Em primeiro lugar, queria exprimir os meus mais sinceros agradecimentos à Professora Doutora Sandra Jordão e à Professora Doutora Chiara Bedon, não só pelo apoio ao longo de todo o processo, mas também pelos conhecimentos transmitidos e pelos desafios propostos, que tanto contribuíram para a valorização desta dissertação.

A todos os funcionários do Laboratório de Construções, Estruturas e Mecânica Estrutural, gostaria também de deixar aqui uma palavra de agradecimento pelos seus contributos para o bom desenvolvimento dos ensaios experimentais realizados.

À Fundação da Ciência e Tecnologia, tenho a agradecer o apoio financeiro através do programa PTDC/ECM/116609/2010 relativo ao projeto S-GLASS, no qual se insere a presente dissertação; e à empresa Sosoares pelo fornecimento das vigas de vidro ensaiadas.

Os meus maiores agradecimentos vão para a minha mãe e para o meu pai, sem vocês nada disto teria sido possível. **MUITO OBRIGADA POR TUDO.** Pelo amor, pelo apoio incondicional, por todos os conselhos e pela paciência (sei que por vezes não foi fácil).

Ao meu irmão Afonso, pela cumplicidade que sempre partilhámos e por me entender melhor que ninguém.

Aos meus amigos de curso, porque sem vocês, sem a vossa companhia e ajuda, este percurso teria sido ainda mais difícil.

Aos meus amigos de Coimbra, por tudo. Particularmente ao Gonçalo Santos, ao Nuno Caixeiro e ao Diogo Lemos, por me terem acompanhado desde sempre. Obrigada por crescerem comigo.

Por ultimo, ao Ricardo. Não é fácil expressar o quanto influenciaste todo este percurso. Obrigada por estares presente em todos os momentos, nos bons e nos menos bons, e por me teres sempre encorajado a fazer melhor, a ser melhor. Sei que contigo vou mais longe.

Teresa Rodrigues

RESUMO

Ao longo das últimas décadas tem-se verificado uma expansão considerável na utilização do vidro em vários setores da indústria. As suas excelentes propriedades estéticas e o seu potencial para melhorar o comportamento energético dos edifícios, tornam este material extremamente apelativo para a arquitetura e para a engenharia modernas. O crescente interesse no vidro como material estrutural potenciou o desenvolvimento de numerosas aplicações, e permitiu o aparecimento de estruturas modernas com um nível de transparência cada vez maior.

No entanto, e apesar da considerável evolução que se tem verificado na indústria vidreira, o comportamento dos laminados de vidro como elementos estruturais está ainda pouco estudado e a atual regulamentação torna-se incompleta, conduzindo à obtenção de soluções pouco económicas e dificultando a expansão da sua utilização.

No âmbito da investigação das propriedades e da resposta mecânica dos elementos de vidro laminado, a influência das ações de longa duração torna-se de particular interesse, afetando significativamente o seu comportamento e tendo como principal consequência a redução da capacidade de carga e resistência destes elementos ao longo do tempo. Um dos principais responsáveis por esta deterioração das propriedades efetivas do vidro é um fenómeno ambiental designado como “*Stress Corrosion*”. Adicionalmente, os materiais utilizados como película de laminação caracterizam-se por possuir propriedades dependentes de fatores mecânicos e ambientais e por se deformarem ao longo do tempo devido a fenómenos de fluência e relaxação, contribuindo também para diminuição da resistência do vidro laminado.

A presente dissertação pretende aprofundar o estudo desta problemática, reduzindo o grau de incerteza relativamente ao comportamento expectável a longo prazo de vigas de vidro laminado, tanto intactas como fraturadas, através do desenvolvimento de ensaios de longa duração à escala real, tendo-se adotado um esquema estrutural e de carregamento semelhantes a uma situação frequente em estruturas reais.

O trabalho elaborado encontra-se no âmbito do projeto “S-GLASS: Desempenho Estrutural e Regras de Projeto de Vigas de Vidro Reforçadas Externamente”, desenvolvido na Universidade de Coimbra.

Palavras-chave: Vidro estrutural; Vigas de vidro laminado; SentryGlas®; Efeitos de longa duração; “*Stress Corrosion*”; Fluência; Temperatura; Ensaios de longa duração; Carregamentos de longa duração.

ABSTRACT

Over the last few decades, there has been a considerable expansion in the use of glass in several sectors of the industry. Its excellent aesthetic properties and potential to improve the energy performance of buildings make this material extremely appealing for both modern architecture and engineering structures. The growing interest in glass as a structural material potentiated the development of numerous applications and has allowed the emerging of modern structures with an increased level of transparency.

However, and in spite of the considerable evolution that has occurred in the glass industry, the behavior of glass laminates as structural elements is still insufficiently studied and the existing regulation is incomplete, leading to the development of uneconomical solutions and hampering the expansion of the utilization of this material.

In the investigation regarding the properties and the mechanical response of structural glass, the influence of long-term actions is of particular interest, affecting its behavior significantly and having as main consequence the reduction of the load bearing capacity and resistance of this element overtime. One of the main aspects responsible for the deterioration of the effective properties of glass is an environmental phenomenon designated as Stress Corrosion. In addition to that, the materials applied as lamination films are characterized by having properties that depend on mechanical and environmental factors and by deforming over time due to phenomena of creep and relaxation, which results in a contribution to the diminishment of the resistance of laminated glass and ultimately leads to the occurrence of delamination.

The present dissertation aims to deepen the study of this theme, reducing the level of uncertainty regarding the expectable long-term behavior of laminated glass beams, both in intact and fractured conditions, through the development of full-scale long-term experimental tests, in which the considered structural layout and loading strategy resemble a real structure situation.

The elaborated work lies within the framework of the “S-GLASS: Desempenho Estrutural e Regras de Projeto de Vigas de Vidro Reforçadas Externamente” is being developed at the University of Coimbra.

Keywords: Structural glass; Laminated glass beams; SentryGlas®; Long-term effects; Stress Corrosion; Creep; Temperature; Long-term tests; Long-term loadings.

INDEX

AGRADECIMENTOS	ii
RESUMO	iii
ABSTRACT	iv
INDEX	v
ABREVIATIONS	vii
SYMBOLOLOGY	vii
1. INTRODUCTION	1
1.1 Framework	1
1.2 Objectives	3
1.3 Structure and Contents of the Dissertation	4
2 STRUCTURAL GLASS	5
2.1 Introduction	5
2.2 Historical Review	6
2.3 The Industrial Production	8
2.4 Composition and Mechanical Properties	9
2.5 The Fracture	11
2.5.1 Introduction	11
2.5.2 Fracture Mechanics	11
2.5.3 Stress Corrosion	13
2.6 Reinforcing Techniques	14
2.6.1 Introduction	14
2.6.2 Lamination	15
2.6.3 Thermal Treatment	18
3 LONG-TERM EFFECTS ON STRUCTURAL GLASS	22
3.1 Introduction	22
3.2 Mechanisms Responsible for the Long-term Behavior of Laminated Glass	22
3.2.1 In the Glass	22
3.2.2 In the Adhesive	24
3.3 State of Knowledge	27
3.3.1 Introduction	27
3.3.2 Glass	27
3.3.3 Laminated Compounds	29
3.4 Design Code Framework	34

4	EXPERIMENTAL TESTS	39
4.1	Introduction.....	39
4.2	Geometry and Experimental Layout	40
4.3	Instrumentation	41
4.4	Test Protocol	43
4.5	Experimental Results	47
5	COMPARATIVE ANALYSIS	51
5.1	Introduction.....	51
5.2	Evaluation of the Recorded Deflections	52
5.3	Evaluation of the Recorded Strains	55
5.3.1	Model 1.....	56
5.3.2	Model 2.....	57
5.3.3	Model 3.....	57
5.3.4	Model 4.....	58
5.3.5	Model 5.....	58
5.3.6	Model 6.....	59
5.3.7	Final Notes.....	59
5.4	Data Treatment	60
5.5	Final Deflections.....	60
5.5.1	Analysis of the Final Deflections	62
5.6	Final Strains	63
5.6.1	Comparison of the Strains in 2A, 2C and 2A(B).....	65
5.6.2	Comparison of the Strains in 1A, 3A and 3C	67
5.6.3	Analysis of the Final Strains.....	70
5.6.4	Isolation of time-related strains	71
6	FINAL COMMENTS	74
6.1	Conclusions.....	74
6.2	Proposals for Future Developments.....	75
6.3	Publications.....	75
7	IMAGE CREDITS	76
8	BIBLIOGRAPHIC REFERENCES	77

ABREVIATIONS

BSG	Borosilicate Glass
CNR	Advisory Committee on Technical Recommendations for Construction
DIN	German Standards
EN	European Norm
EVA	Ethyl Vinyl Acetate
GFRP	Glass Fiber Reinforced Polymer
JRC	Joint Research Centre of the European Commission
LEFM	Linear Elastic Fracture Mechanics
NBN	Belgium Standards
NEN	Netherlands Standards
ÖNORM	Austrian Standards
prEN	pre-European Norm
PVB	Polyvinyl Butyral
SGP	SentryGlas® Plus
SG	SentryGlas®
SLS	Serviceability Limit State
SLSG	Silicate Glass
TPU	Thermoplastic Polyurethane
ULS	Ultimate Limit State
UV	Ultraviolet
4PB	Four-point Bending

SYMBOLOLOGY

a	Crack size
b	Width of the beam
c	constant of corrosion
c_p	Specific thermal capacity
d	Distance between the gravity centre of the glass ply and the gravity centre of the laminated element

$f_{y,k}$	Yield strength
$f_k; f_{g,k}$	Characteristic bending strength of annealed glass
f_t	Tensile bending strength
$h_{ef,w}$	Deflection-effective thickness
h_i	Thickness of the i^{th} glass ply
h_{int}	Thickness of the interlayer
$h_{i,ef,\sigma}$	Stress-effective thickness
k_a	Coefficient for the on-linearity of loads
k_b	Coefficient dependent on traction distribution
k_b	Coefficient depending on the type of loading
k_c	Coefficient respecting the type of construction
k_e	Coefficient depending on the type of loading
$k_{ed}; k'_{ed}$	Coefficients on the edge and/or holes finishing
k_{mod}	Factor of load duration
k_{sp}	Factor for the glass surface profile
k_{sf}	Coefficient dependent on the surface treatments
k_v	Coefficient dependent on the prestress or chemical treatment
l	Length of the beam
l_b	Length of the edge subjected to traction
r_0	Equilibrium spacing of the atoms
t	Load duration
v	Crack velocity
z	Distance between each section point and the sections neutral axis
A	Loaded Area
A^*	Generic area of the glass plies cross sections
E	Young's modulus
G_{int}	Shear modulus of the interlayer
$H_{K0,1/20}$	Knoop hardness
I_y	Moment of inertia around y axis
I_s	Moment of inertia per unit of length
K_I	Stress intensity factor
K_{IC}	Critical stress intensity factor
K_{th}	Stress intensity threshold
M_y	Bending moment around y axis
N	Average refractive index within the visible spectrum

R_d	Design resistant force
$R_M; R_{M,v}$	Multiplicative factors dependent on the class of consequence
T_G	Glass Transition Temperature
Y	Geometry factor
α	Coefficient of thermal expansion
γ	Fracture surface energy
$\gamma_M; \gamma_{M,A}; \gamma_{M,v}$	Material partial factor
ε	Extension
ε_T	Elongation at tear
λ_{gA}	Size effect coefficient
λ_{gl}	Edge quality coefficient
λ	Thermal conductivity
ρ	Density
σ	Stress
σ_m	Theoretical failure stress
σ_n	Nominal tensile stress normal to the crack's plane
ν	Poisson's ratio
Γ	Shear transfer coefficient
ΔL	Length variation
ΔT	Temperature Variation

1. INTRODUCTION

1.1 Framework

Glass is commonly known for being a fragile and transparent material. Its remarkable aesthetic properties and potential to improve the energetic efficiency of buildings made glass a highly-desired material in modern day structures. This architectural tendency powered a massive evolution in the glass industry, which led to the development of numerous applications in the various industry sectors and allowed the creation of some of the most impressive constructions ever built, in which glass is acknowledged as a noble material (Figure 1.1).



a) *The Glass Home - Milan, Italy* [Image 1]



b) *The Dome of the Reichstag Building - Berlin, Germany* [Image 2]



c) *The Louvre Pyramid - Paris, France*
[Image 3]



d) *The Sage Gateshead - Gateshead, United Kingdom* [Image 4]

Figure 1.1 - Photographs of examples of structural glass applied in buildings.

In spite of the considerable interest demonstrated by building industry in glass as a load-bearing component, it is important to take into consideration that the brittleness that characterizes this material makes it relatively unsafe for structural applications. In addition to this particularity of glass, the material is known to break without any kind of warning, not allowing the visualization of significant deformations before its complete failure. For that reason, and in order to overcome the fragility of the material, it is necessary to include reinforcement techniques when using glass elements for load-bearing applications. These measures should delay the fracture of the glass structure and minimize the consequences of an eventual collapse.

The technological breakthroughs that occurred over the past few decades had a considerable impact on the safety of structural glass applications. The development of safety techniques and enhancement procedures made it possible to obtain glass components with noticeably increased bearing capacity, residual post-breakage strength, and failure mechanisms that are not only safer but also easier to predict. The improvement of the properties of glass increased the confidence of architects and designers in the material, which translated in the diffusion of the utilization of the material.

Nevertheless, and despite all the technological progress in glass industry, many aspects of the behavior of glass are still unregulated, which prevents a larger expansion of the utilization of load-bearing glass elements. The generalization of structural glass applications will only be able to take place with the creation of extensive regulatory documents that include design formulations, as well as execution and project recommendations. The currently existing normative documents for glass are mainly focused in framed glass, lacking sufficiently detailed information regarding structural glass. Nowadays, the European Standard for structural glass (Eurocode 10) is being prepared. In order to do so, extensive investigation work must be executed so that the behavior of structural glass can be properly assessed.

Part of the referred research must address the effects of long-term actions in the mechanical response of laminated glass beams. These aspects are extremely important in what concerns the behavior of glass since they can significantly reduce its strength and resistance, even in situations of constant stress values. The main phenomenon that contributes to this diminishment of the practical strength of glass over time is “Stress Corrosion”, which is responsible for the deterioration of the glass in the presence of water or humidity. Besides that, the polymeric materials utilized to bond the glass layers are known to present deformations over time due to phenomena of creep and relaxation. This characteristic of the interlayer, allied to its considerable susceptibility to environmental factors like UV-radiation, temperature, and humidity, can also result in the reduction of the laminated glass resistance. Ultimately, long-

term mechanical and environmental actions can result in not only significant loss tensile strength but also in the collapse of glass elements.

The intents of the current investigation were to study and characterize the behavior of laminated glass beams under the influence of long-term actions. It was considered important that the obtained results corresponded to real parameters. For this purpose, several measures were taken regarding the structural layout, the experimented models, and the applied loads. Both the layout and the loading strategy were established in a way that they could simulate a real situation. In addition to that, the experimental tests were performed on full-scale laminated glass beams, composed by sheets of annealed float glass, and bonded by a SentryGlas interlayer, which are widely used materials in structural glass applications. To determine the influence of the lamination film in the long-term behavior of laminated glass beams, both intact and fractured models were included in the experimental tests, as it is the interlayer the main responsible for the load-bearing capacity that these composite structures can display after the breakage of all the glass plies.

It was expected that the options taken during this experimental campaign would originate results with great applicability and that the respective conclusions allowed a deepening of the knowledge regarding the security that these structural glass elements are able to provide when applied in the building industry.

1.2 Objectives

The main purpose of the present dissertation was to characterize the behavior of full-scale laminated glass beams under long-term loading by means of an experimental investigation, which was carried out in the context of the S-GLASS project.

The experimental investigation consisted on the development of 4-point bending tests (Figure 1.2), including both intact and cracked models. The applied load-term actions included the self-weight of the beams and environmental temperature. The impact of these actions in the strains and vertical displacements of the tested models were analyzed during approximately 13 months.



Figure 1.2 – Layout of the experimental tests.

It was expected that this experimental research would be able to provide accurate information regarding the long-term behavior of the laminated glass beams and to allow a better comprehension of the impact that the duration of the considered loads had on the global structural response of the analyzed models.

1.3 Structure and Contents of the Dissertation

The present dissertation is divided into 8 chapters which are organized in order to provide a better understanding of the addressed issues, of the performed experimental research and of the obtained results and conclusions.

In Chapter 1, a general introduction to the explored theme is presented. The structure of the document and the main objectives of developed investigation are also defined.

Chapter 2 is focused on providing the theoretical background of structural glass. Firstly, this chapter exhibits information about the history of glass and the evolution of its production techniques. The physical properties of glass and the mechanics of its fracture are also thoroughly explained in this chapter, as well as several commonly applied reinforcing techniques.

In Chapter 3, a thorough explanation of the numerous factors that affect the long-term behavior of glass, of the laminate film and of the laminated glass elements is presented. Additionally, it is expected that this chapter will enlighten the readers in relation to the significant contributions that have been made in this particular field by other authors.

Chapter 4 concerns the developed experimental research and the obtained results, which are the focus of this dissertation. Details about the geometry and components of the models, experimental layout, utilized instrumentation, results and initial conclusions are presented.

Chapter 5 contains the detailed analysis of the experimental results and consequent conclusions.

In Chapter 6, several comments are included regarding the performed investigation, as well as recommendations for future developments concerning the behavior of laminated glass beams and the influence of long-term effects.

Image credits and bibliographic references are registered in the final chapters.

2 STRUCTURAL GLASS

2.1 Introduction

Glass is a millennial material and its industry has significantly evolved since the first discovered technique. Over the past years, glass started to be used in load bearing components, in addition to its most common application in the building industry: as infill panels. Nowadays it is possible to use glass in main structural components such as floors, beams (Figure 2.1 a)), columns (Figure 2.1 b)), walls, stairs (Figure 2.1 c)) or even in pedestrian bridges (Figure 2.1 d)).



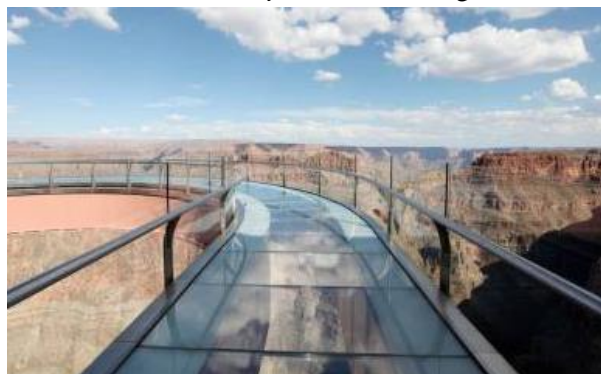
a) *Structural glass applied in beams – Industrie Handelskammer, Munich, Germany [Image 5]*



b) *Structural glass applied in columns – St. Germain-en-Laye, France [Image 6]*



c) *Structural glass applied in stairs – Apple store in 5th Avenue, New York, USA [Image 7]*



d) *Structural glass applied in a pedestrian bridge – Grand Canyon Skywalk, Arizona, USA [Image 8]*

Figure 2.1 - Photographs of examples of structural glass applications.

However, as previously mentioned, glass is a brittle material and its resistance is susceptible to several parameters such as load-duration, humidity, and temperature which are responsible for the degradation of the mechanical properties of glass. To overcome this fragility, several reinforcing techniques are usually implemented in load-bearing elements.

2.2 Historical Review

Glass is one of the most ancient materials used in the building industry. The occurrence of natural glass is associated with phenomena like volcanism, meteoritic impact, and electrical atmospheric discharge (Konta, 1988). These phenomena are responsible for originating different types of natural glass: obsidians (Figure 2.2 a)), tektites and fulgurites, respectively.

While natural glass has always existed, the first known signals of the existence of manufactured glass are dated from about 3500 B.C. (O'Regan, 2014), in Egypt. At this time, the produced glass was colored and was typically used in jewelry or for vessels. The first production shops appeared in Mesopotamia approximately 2000 years later. One of the earliest techniques utilized to obtain glass was the “*core-forming*” and consisted in involving molten glass in a removable core made from sand or clay. After cooling at environmental temperature, the core was removed and the glass was cut and polished (Figure 2.2 b).

The first remarkable breakthrough in the glass production occurred in Syria with the development of the “*glass blowing*” technique (Figure 2.2 c)). This technology was spread across all Mediterranean civilizations by the Romans around I A.D. The Roman Empire was also responsible for creating and enhancing new procedures like the “*cast glass*” technique and the “*cylinder*” method that enable the production of flat glass in large dimensions. The developed techniques allowed the development of clear glass objects and the first mirrors.



a) *Natural Glass (Obsidian)*
[Image 9]



b) *Egyptian core-formed glass vessel* [Image 10]

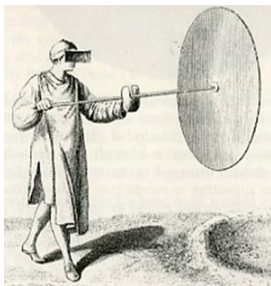


c) *Roman bottle (free-blowing glass)* [Image 11]

Figure 2.2 - Ancient glass objects.

With the downfall of the Roman Empire, the evolution of the glass industry slowed down. It was only in the middle age that the production of glass regained expression and disseminated through all Europe. At this point, the main contributors to the improvement of the Roman procedures were the French, with the adoption of larger molds and the creation of annealing lehrs. It was also in France that the development of the “*crown*” process occurred in the beginning of the 14th century (Figure 2.3 a)). This technique consisted in blowing glass into a crown or a small hollow tube which was then flattened by reheating and spinning the melted glass into a flat disk and was the first to produce flat glass panes. It became one of the main ways to obtain window glass, firstly applied in the windows of medieval churches.

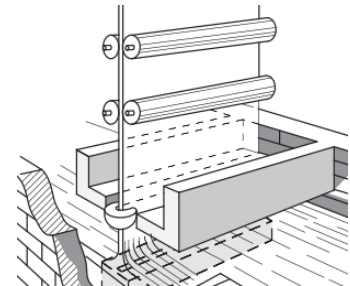
Nevertheless, it was only with the incomparable technological advances that took place during the Industrial Revolution that the automated production of flat glass was possible, firstly in the early 19th century, through the invention of a machine which automated the “*cylinder*” method by William Pilkington (Figure 2.3 b)), and later with the appearance of various drawn flat sheet processes from which it stands out the Belgian Fourcault (Figure 2.3 c)) and the American Colburn Processes (O’Regan, 2014).



a) *The crown process*
[Image 12]



b) *The cylinder method*
[Image 13]



c) *The drawn process - Fourcault*
[Image 14]

Figure 2.3 - Glass production techniques.

The mass production of flat glass was only possible with the discovery of the “*float*” process in 1959 by Alistair Pilkington from the Pilkington Brothers (Haldimann, *et al.*, 2008). Before the invention of this technique, glass had to be polished in order to go from being translucent to being fully transparent, which took a considerable amount of work and resulted in elevated costs associated with the production of this material. By producing fully transparent glass with flat brilliant surfaces, the float process did not require the final material to be polished, which caused the price of flat glass to significantly decrease. For being able to produce glass of elevated quality and reduced costs, since the invention of the float process, the glass industry was able to respond positively to the growing demands regarding the energetic efficiency of glass. This procedure is extensively explained in section 2.3 of the present dissertation.

2.3 The Industrial Production

The float process is one of the main techniques to obtain flat glass. As previously explained, this technique offers an alternative that is not only cheaper but also has superior quality than other mass production processes. Currently, by and allowing the efficient production of high-quality flat glass, the float method is responsible for the production of about 90% of the worldwide flat glass (Haldimann, *et al.*, 2008).

This process is initiated by melting the raw materials in a furnace at a temperature close to 1500°C to form molten glass (O'Regan, 2014). Soon after that, the molten glass is poured into a bath of molten tin at around 1100°C (Figure 2.4). Since the density of the glass is much lower than the density of the tin, the glass is able to float above it, forming glass sheets with uniform thickness and smooth surfaces. While the surface facing the tin is designated “tin side”, the other surface is referred to as “air side” (Louter, 2011). As the glass flows in the tin bath, its temperature is lowered until about 600°C. Thereafter the glass is removed from the bath and placed in an oven called the annealing lehr at 200°C, where it is cooled down at a very slow rate, preventing the glass from building up residual internal stresses. Subsequently, the glass sheets are inspected for visible defects and cut.

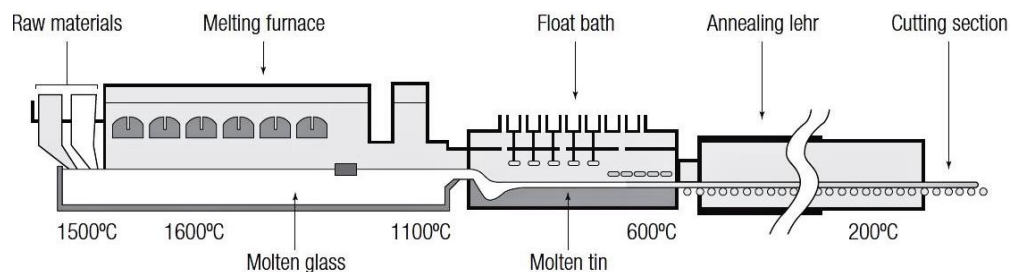


Figure 2.4 - Schematic representation of the float process, (O'Regan, 2014).

According to Guidance for European Structural Design of Glass Components (JRC, 2014), the maximum standard size for annealed float glass panels is 3.21 m x 6.0 m. Nonetheless, it is possible to obtain larger panels on special request. The float process can originate panel with various thicknesses that variate from 2 mm until 25 mm, although the latter is rarely applied because of the associated high costs and manufacturing difficulties.

Notice that, even though this procedure results in annealed glass, other materials can be obtained from it. By processing annealed float glass, it is possible to achieve fully-tempered glass, laminated glass, heat-strengthened glass, curved glass, or even chemically-strengthened glass, which will be addressed in subsequent sections.

2.4 Composition and Mechanical Properties

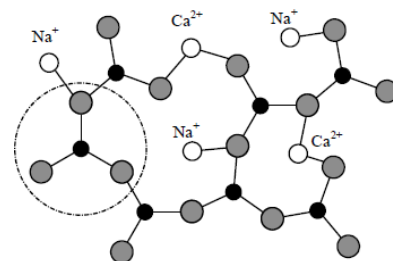
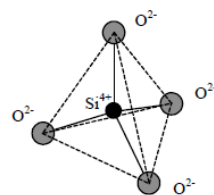
In its large majority, glass can be described as any inorganic, homogeneous and amorphous solid product. It can be composed of a considerable variety of materials. Glass is usually divided into two types: silicate glass (SLSG) and borosilicate glass (BSG), depending if the main element of its composition is calcium oxide or boron oxide, respectively. During the current investigation, soda-lime silicate glass was applied. The chemical composition of this glass type is presented in Table 2.1.

Table 2.1 - Chemical composition of soda-lime silica glass, (Louter, 2011).

Element	Symbol	Mass [%]
Silica sand	SiO ₂	69 – 74
Lime (calcium oxide)	CaO	5 – 14
Soda	Na ₂ O	10 – 16
Magnesia	MgO	0 – 6
Alumina	Al ₂ O ₃	0 – 3
Others	-	0 – 5

Glass is usually obtained by melting several materials and which has been cooled to a solid state without crystallization. During the cooling process, the molten mixture does not crystallize, turning instead into a frozen solid over a specific glass transformation temperature range. Nevertheless, it is possible to obtain glass by means of other processes such as vapor deposition, sol-gel processing, and neutron irradiation of crystalline materials (Louter, 2011).

The internal structure of this material is composed of an irregular network of tetrahedral modules each one of them composed by one silicium atom and four oxide atoms (Figure 2.5 a)), and intermediate alkaline parts. This characteristic internal structure (Figure 2.5 b)) translates into a lack of regular surfaces for internal dislocations, which is why glass is unable to deform in a plastic manner, which results in the brittleness that characterizes this material.



a) 3D representation of the tetrahedral module

b) 2D representation of the internal structure

Figure 2.5 - Structure of soda-lime silica glass, (Louter, 2011).

The most relevant properties of soda-lime silicate glass can be observed in Table 2.2. Its density is similar to the density of concrete and the value of its Young's modulus is identical to the value of Young's modulus of aluminum (Louter, 2011).

Table 2.2 - Properties of annealed soda-lime silicate glass, (adapted from Haldimann, *et al.*, 2008).

Property	Symbol	unit	Value
Density	ρ	kg/m ³	2500
Knoop hardness	$HK_{0,1/20}$	GPa	6
Young's modulus	E	GPa	70
Poisson's ratio	ν	-	0.23
Tensile bending strength	f_t	MPa	45
Specific thermal capacity	c_p	J*kg ⁻¹ *K ⁻¹	720
Coefficient of thermal expansion (between 20 and 300°C)	α	K ⁻¹	9*10 ⁻⁶
Thermal conductivity	λ	W*m ⁻¹ *K ⁻¹	1
Average refractive index within the visible spectrum	N	-	1.52

The tensile bending strength cannot be assumed as a material constant. This parameter depends on various aspects such as the condition of the surface, the size of the element, the intensity and duration of the loading, the residual stress, and the environmental conditions.

From a mechanical perspective, glass presents an almost perfect linear-elastic and isotropic behavior. As shown in Figure 2.6, its stress-strain relation is perfectly linear until the sudden fracture of the glass steel. The breakage of glass develops in this manner because this material is incapable of yielding in order to redistribute high stresses like other structural materials such as steel.

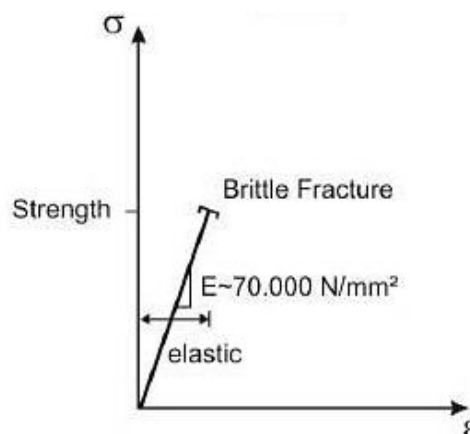


Figure 2.6 - Stress-strain diagram of float glass, (JRC, 2014).

2.5 The Fracture

2.5.1 Introduction

Being a brittle material, glass is characterized by failing in an unsafe way. As mentioned before, this mechanical behavior is originated by the fact that glass is not able to redistribute stresses through plastic yielding, which makes it extremely sensitive to stress concentrations. For this reason, and due to the susceptibility of the structural response of glass to several environmental and mechanical parameters, it is not safe to assume the value of the glass strength to be a material constant, as will be explained in the following sections

2.5.2 Fracture Mechanics

The theoretical strength of glass is considerably high and can be determined through the known forces of the interatomic bonds of its molecular structure. Equation (1) was established by Orowan and allows the determination of the theoretical failure stress of any material (σ_m), which corresponds to the necessary stress to break a bond (Louter, 2011).

$$\sigma_m = \sqrt{\frac{E \cdot \gamma}{r_0}} \quad (1)$$

Considering the properties of soda-lime glass (Young's modulus, $E=70\text{GPa}$; fracture surface energy, $\gamma=3\text{J/m}^2$; and equilibrium spacing of the atoms, $r_0=0.2\text{nm}$), the theoretical strength obtained through the application of this equation to common silica has the value of 32GPa . In spite of the considerable obtained result, the admitted value for practical applications of the glass tensile bending strength is only 45MPa . Griffin attributed the significant difference between the theoretical and practical values of the glass strength to the microscopic flaws that exist along the glass surface (Louter, 2011). These imperfections are present in the glass surfaces since its production and that additional damages can easily be inflicted in the glass while processing and handling it or even during its service life due accidental circumstances.

Griffins' flaws are essentially invisible to the human eye and are responsible for originating an accumulation of tensile stresses in the glass, which increases its risk of cracking in those areas. The occurrence of stress concentrations is critical to glass because it is unable to redistribute these stresses, which can result in the propagation of the existing flaws. Even in constant stresses, it is possible for the size of the cracks to increase, leading to the rupture of the glass,

which is why the practical strength of glass is much lower than the theoretical. Consequently, it becomes logical to conclude that the strength of a glass element depends on the depth of its largest flaw (critical flaw). The larger the critical flaw depth, the lower the tensile strength of the glass can be expected to be (Figure 2.7).

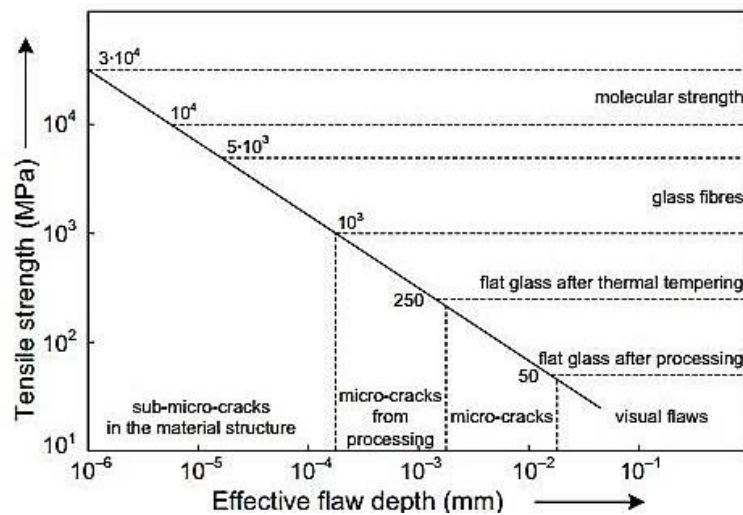


Figure 2.7 - Typical tensile strength as function of the flaw depth, (Haldimann, *et al.*, 2008).

Once the flaws’ distribution along the glass surface is random, the larger the glass element, the bigger the chance of the existence of a significantly large critical flaw, which will ultimately result in a lower tensile strength. Figure 2.8 shows the statistical distribution of the glass tensile strength according to the conditions of its surface.

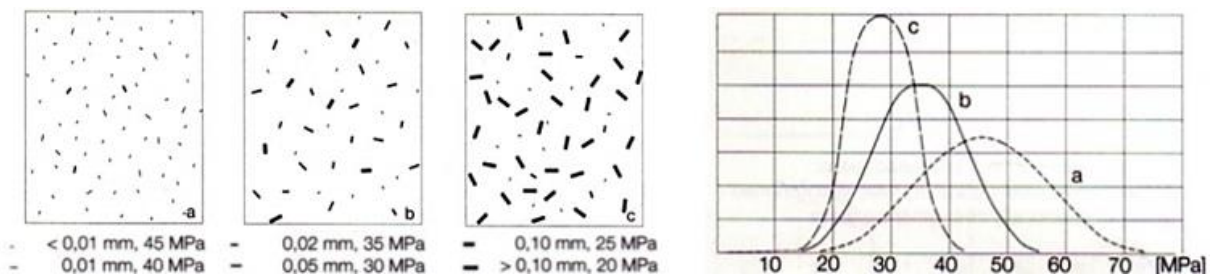


Figure 2.8 – Statistical distribution of the tensile strength of glass with the increase of superficial damage, with a) surface of a new glass, b) surface of glass after climatic actions, and c) surface of glass with time-related damages (adapted from Valarinho, 2010).

It is also important to mention that the tensile strength of the edges of glass sheets is generally lower than the strength in the interior regions. The reason for this discrepancy is the fact that the surface of flat glass specimens is much more damaged.

2.5.3 Stress Corrosion

The surface flaws of glass are characterized by a time-dependent behavior when tensioned, which causes them to grow even at constant stress levels (Louter, 2011). The main cause for this occurrence is the slow crack growth that develops in glass, which is associated with an environmental phenomenon commonly referred to as “*Stress Corrosion*”. According to Louter (Louter, 2011), Stress Corrosion was discovered in 1899 by Grenet and is responsible for inducing damage in glass when this material is in the presence of water or high levels of humidity, along with long-term loading of the glass element. This phenomenon causes the surface flaws to gradually increase when the glass presents crack opening tensile stresses. This means that, even if the glass is not stressed up to its characteristic tensile stress, it can still collapse after being loaded during a certain period of time, because its critical flaw will eventually grow until a size significant enough to cause the glass failure.

Stress Corrosion is associated with a chemical process described by the “*Classical Stress Corrosion Theory*”. The chemical reaction that develops between water and the silica molecules of the glass element results in the sharpening and lengthening of the crack tip, causing the development of even higher stress levels (Equation (2) and Figure 2.9) (Louter, 2011).

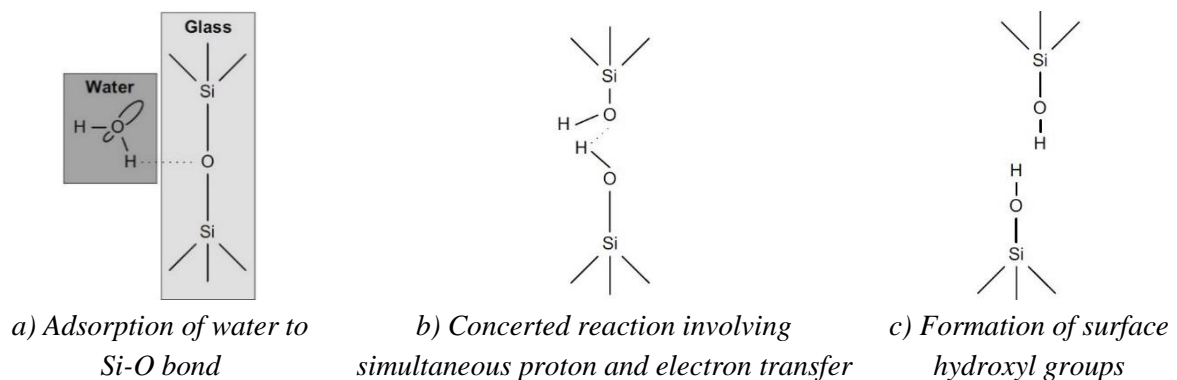
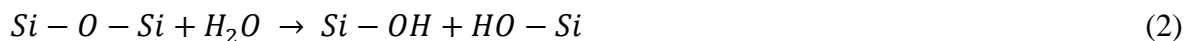


Figure 2.9 – Schematic representation of the chemical reaction of stress corrosion at the crack tip, (Haldimann, *et al.*, 2008).

The kinetics of the chemical process described by the “*Classical Stress Corrosion Theory*” are responsible for influence the rate at which the surface flaws increase, that is, the crack velocity (v). The relation between crack velocity and the stress intensity factor (K_I) is usually considered to predict the lifetime of glass elements (Haldimann, *et al.*, 2008). The stress intensity factor represents the value of the elastic stress intensity that develops near the crack tip.

In the Linear Elastic Fracture Mechanics (LEFM), there have been distinguished three fracture modes: Mode I (opening mode): corresponds to normal separation of the crack walls develops under the influence of tensile stresses (Figure 2.10 a)); Mode II (sliding mode): corresponds to longitudinal shearing of the crack walls in a direction normal to the crack front (Figure 2.10 b)); Mode III (tearing mode): corresponds to lateral shearing parallel to the crack front (Figure 2.10 c)) (Louter, 2011, apud Lawn,1993).

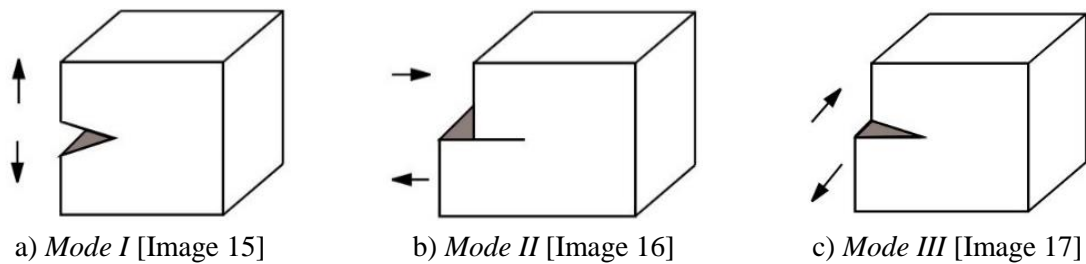


Figure 2.10 – Fracture modes according to the LEFM.

It was established that for Mode I loadings the value of K_I can be calculated through Equation (3) (Louter, 2011).

$$K_I = Y \cdot \sigma_n \cdot \sqrt{\pi \cdot a} \quad (3)$$

The stress intensity factor is related to: Y , a geometry factor that depends on the geometry and depth of the crack, the specimen geometry, the stress field, and the proximity of the crack to the specimen boundaries; σ_n , the nominal tensile stress normal to the plane of the crack; and a , the crack size, which can be equal to the depth of the crack or to half of its length. Further details on stress corrosion and sub-critical crack growth are presented in section 3.2.1.

2.6 Reinforcing Techniques

2.6.1 Introduction

Nowadays, the application of load-bearing glass elements in the building industry is becoming increasingly common. However, the handling of a material known to have a relatively unsafe fracture behavior must be performed considering appropriate reinforcing techniques. To guarantee an adequate enhancement of the failure mechanism of glass, it is usual to implement two measures acquired from the car industry: lamination and thermal treatment. Both techniques aim to minimize the probability of complete failure of the glass element, as well as

improving its post-rupture behavior. It is important to note that, in spite of the application of these reinforcing techniques, it is still possible for the rupture of the glass element to develop due to the overlap of high local stress points in all glass layers as consequence of assembly errors or even unexpected situations like severe or repetitive impact.

2.6.2 Lamination

This concept was first introduced in 1910 (O'Regan, 2014). This safety procedure consists in increasing the strength and resistance of structural glass elements by constructing them through the superposition of several glass layers bonded to each other through an adhesive interlayer.

Initially, the glass layers were bonded with sheets of celluloid plastic materials. This type of interlayer exhibited a weak mechanical response in the presence of water or humidity, causing the laminated glass to have a low durability. One of the first materials applied as an adhesive layer that allowed the assembly of significantly resistant and durable laminated glass components was the polyvinyl butyral (PVB). The utilization of this foil interlayer remained exclusive to the automotive industry until the 1970s, when the building industry adopted it for claddings. Although PVB interlayers are widely used, this material is characterized by limited stiffness and reduced strength translates into a relatively poor post-breakage strength. Several foil interlayers like thermoplastic polyurethane (TPU), ethyl vinyl acetate (EVA) and SentryGlas (SG) were later developed. Nowadays, the utilized interlayers are constituted by foil or resin and present significantly enhanced resistant properties. In the building industry, the foil interlayers are the most frequently applied type of interlayer. The bond between the glass and the foil interlayer is created through an autoclave lamination process. The adhesive resins are usually applied with a cast-in-place process in which the space between the glass layers is filled with the resin. Subsequently, this material is cured with UV-radiation.

The main purpose of this reinforcement technique is to keep the glass fragments from falling apart in case of glass fracture, preventing the occurrence of harmful situations. Additionally, it offers significant improvements in the post-breakage behavior of the glass elements. By keeping the glass fragments in place, the interlayer allows an arching effect to develop in the broken layer, which allows it to still be able to carry the load. The overlapping of glass sheets also enables the load to be carried by the remaining layers even after one glass sheet fails.

By presenting higher stiffness and strength than the most commonly used adhesive material (PVB), it is expected that SentryGlas will considerably strengthen glass laminates, improving

their behavior before and after the rupture (Figure 2.11), which is why the adhesive bond considered in the current investigation was the SG interlayer.

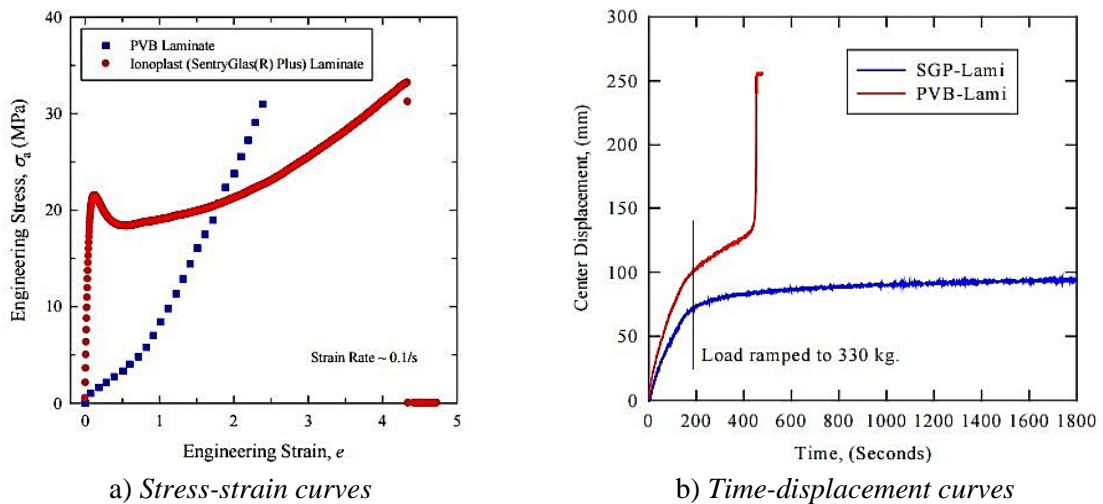


Figure 2.11 – Comparison between SGP and PVB laminates.

The SG adhesive is a foil interlayer and was originally introduced by DuPont in 1998. It is a semi-crystalline thermoplastic polymer sheet material and was initially developed for hurricane and burglary resistant laminated glass. The main reason for the selection of this material is the promising results in bonding metal and glass elements. It is guaranteed by the manufacturer that this adhesive layer is capable of improving significantly both the strength and stiffness of glass elements before and after fracture. Some of the most relevant physical and mechanical properties of the SentryGlas interlayer are displayed in Table 2.3.

Table 2.3 - Properties of the SG interlayer, according to DuPont, (Louter, 2011).

Property	Symbol	unit	Value
Tensile strength	f_t	N/mm ²	34.5
Elastic modulus	E	N/mm ²	300
Glass Transition temperature	T_G	°C	55-60
Elongation at tear	ϵ_T	%	400
Density	ρ	kg/m ³	950

As mentioned before, this material is susceptible to external mechanical and environmental parameters such as temperature, humidity, UV-radiation and loading conditions. This causes the value of E to fluctuate, which is why it should not be considered a material constant.

In what concerns the influence of the SG in the behavior of laminated elements, it is important to acknowledge that different support conditions will lead both the glass sheets as well as the

adhesive layers to be solicited in distinct manners, which will ultimately result in distinct global responses. To accurately determine this response, it is crucial to, not only characterize the applied materials, but also to specify its support setup. For linear elements, two loading situations can be distinguished: plate and beam (Figure 2.12) (Belis, *et al.*, 2008).

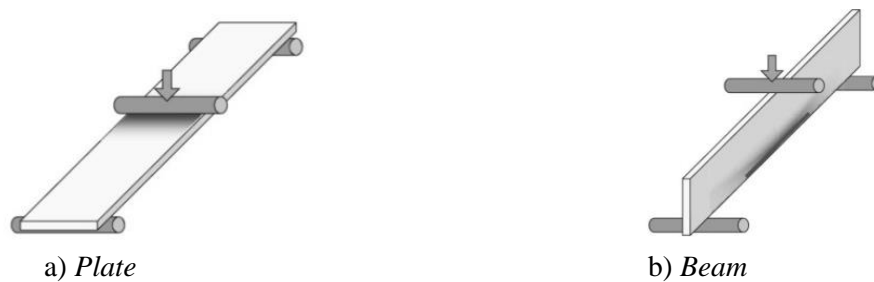


Figure 2.12 - Basic loading situations for laminated glass, (adapted from Belis, *et al.*, 2008).

Regarding plate applications of load-bearing laminate glass, it has been demonstrated by several authors like Hooper (Belis, *et al.*, 2008 apud Hooper, 1973) and Behr (Belis, *et al.*, 2008 apud Behr, *et al.*, 1993) that the interlayer has fundamental role in the mechanical response in unbroken conditions, as it is responsible for supporting significant shear stresses, enhancing the global behavior of the laminate. Posteriorly, this effect was also detected in the post-breakage regimen. These investigations confirm the importance of interlayer in plate applications, increasing the global resistance and rigidity of the laminates in both plastic and elastic regimens.

Contrarily, in beam applications, it has been verified that the majority of the applied loads is supported by the glass sheets and that the effect of the interlayer is irrelevant until the fracture of all glass layers. Despite that, it has been proven that the interlayer is able to increase the shear stress transference capacity between the broken glass layers, which makes it a relevant component in the post-breakage resistance of these type of elements.

In what concerns the level of damages if laminated elements composed of two glass sheets and one interlayer, as is the case of the models adopted in the present dissertation, Kott defined three stages (Belis, *et al.*, 2008 apud Kott, 2006). Stage I represent the situation in which all the glass sheets are still intact which means that the bending stress distribution in the glass depends mostly on the shear modulus of the adhesive layer (Figure 2.13 a)). In Stage II, the rupture of one of the glass sheets has already occurred and the existing bending stresses are mainly supported by the remaining unbroken glass layer (Figure 2.13 b)). The final stage (Stage III) corresponds to the situation in which both glass layers are broken and all the tensile stresses are supported by the lamination film which causes it to suffer considerable deformations and ultimately can result in the complete collapse of the structure (Figure 2.13 c)).

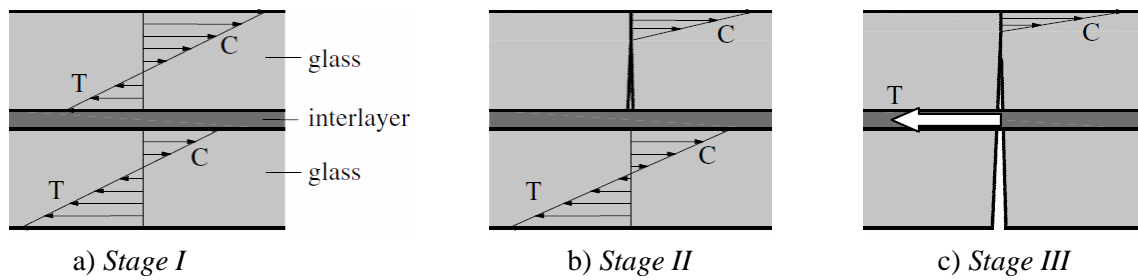


Figure 2.13 – Stages of laminated glass during failure, (Belis, et al., 2008).

2.6.3 Thermal Treatment

The first signals of the existence of tempered glass date from about 3000 BC (O’Regan, 2014). Nowadays, it has been established that, for structural applications of glass, tempering is one of the most important processing methods (Haldimann, *et al.*, 2008). The application of heat treatments can greatly enhance the practical strength of annealed float glass. Ultimately this causes a considerable improvement in the resistance of glass elements.

In the heat treatment processes, the glass layers are heated until roughly 620 to 675 °C (the glass transformation temperature (T_G)) and subsequently cooled by air jets (Figure 2.14).

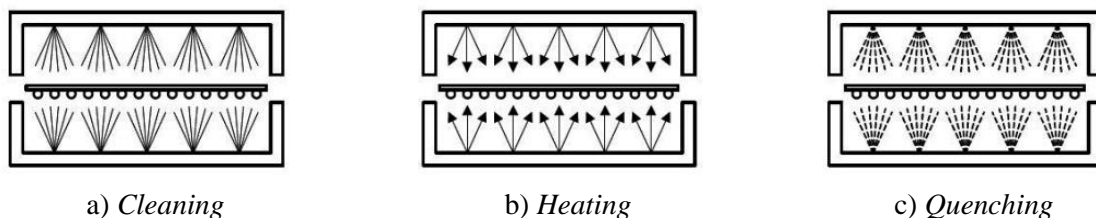


Figure 2.14 - Representation of the tempering process, (Haldimann, *et al.*, 2008).

The thermal treatment causes the external surface to cool much faster than the internal area of the glass layers. As a result, compressive residual stresses are originated in the glass surfaces and tensile residual stresses are originated in the interior of the glass (Figure 2.15).

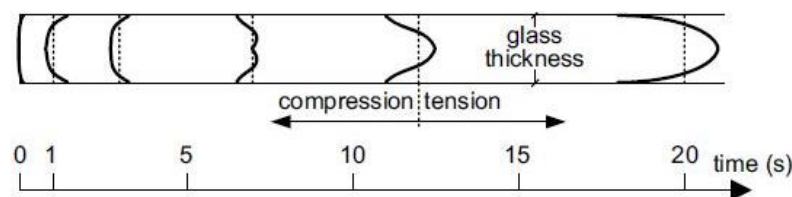


Figure 2.15 - Stress field during the tempering process, (Haldimann, *et al.*, 2008).

It is important to note that this reinforcement technique is only effective because of the low coefficient of thermal expansion that characterizes glass, which enables a slow progression of the heat and allows the internal stresses to develop. As long as the external tensile stresses are lower than the acting compressive residual stresses, this procedure protects the surface flaws from growing, as represented in Figure 2.16.

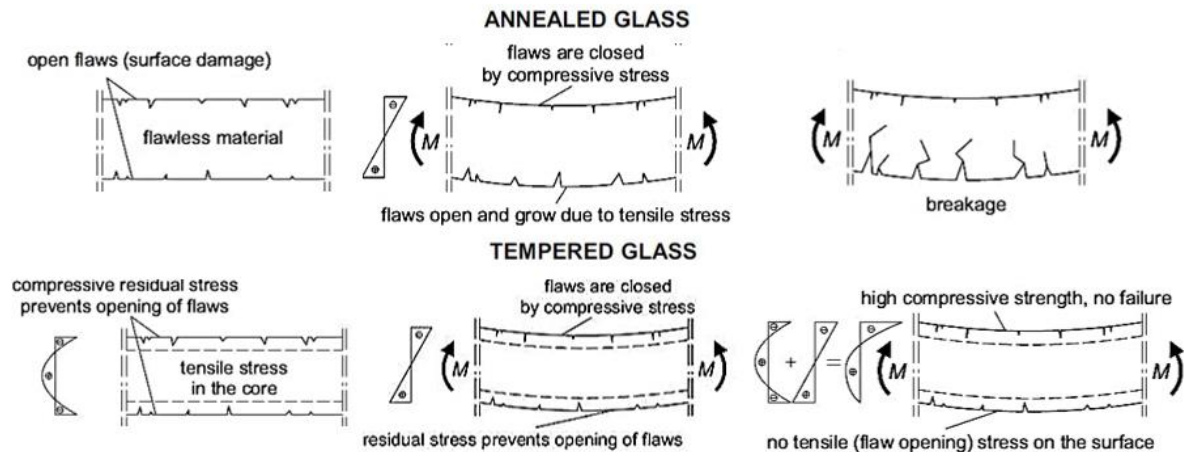


Figure 2.16 - The principle of glass tempering, (adapted from Haldimann, *et al.*, 2008).

To prevent the disruption of the energy balance between the internal and surface residual stresses, procedures like cutting, drilling, or grinding should be performed before the application of thermal treatment. Through this procedure, it is possible to obtain two types of tempered glass: the fully-tempered glass and the heat-strengthened glass.

Fully-tempered glass has the highest level of residual stresses which causes it to fail in very small fragments (Figure 2.17 a)). Even though its load-bearing capacity is the highest (Table 2.4), the post-breakage behavior presented by fully-tempered glass is relatively poor due to the reduced fragmentation pattern (Figure 2.18).

The heat-strengthened glass results from a slower cooling of the external surfaces, which causes it to display lower residual stresses and to break in larger fragments than fully-tempered glass (Figure 2.17 b)). This type of glass displays an advantageous combination between relatively high load-bearing capacity and a fragmentation pattern big enough to enable a fair post-breakage behavior (Figure 2.18).

In the case of annealed float glass, the value of internal stresses is insignificant. For this reason, it breaks in considerably larger fragments than heat-treated glass, which causes it to have the lowest fragmentation of the three analyzed glass types (Figure 2.17 c)).



a) Fully-tempered glass b) Heat-strengthened glass c) Annealed glass

Figure 2.17 - Fracture pattern of different glass types, (adapted from Louter, 2011).

The expected tensile bending strength of annealed and tempered glass can be observed in Table 2.4.

Table 2.4 - Characteristic tensile bending strength of different glass types, (Louter, 2011).

Glass type	Characteristic tensile bending strength
Annealed	45 MPa
Heat-strengthened	70 MPa
Fully-tempered	120 MPa

As represented in Figure 2.18, the values of the compressive surface stresses introduced by the tempering process can vary between 80MPa and 170MPa for fully-tempered soda-lime silica glass. In the case of heat-strengthened glass, this value fluctuates between 24MPa and 52MPa.

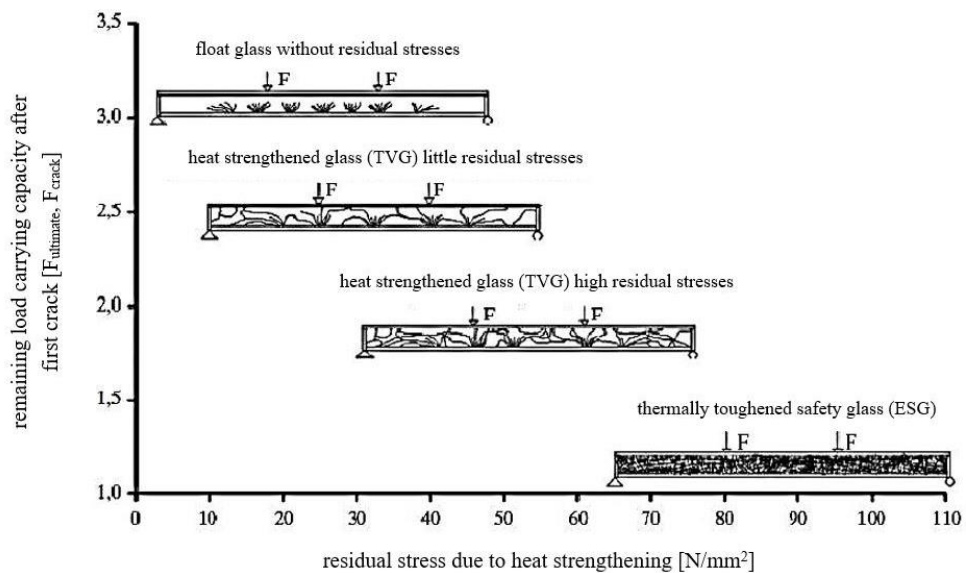


Figure 2.18 - Relation of residual pre-stress and remaining load-carrying capacity for different glass types, (Louter, 2011).

As demonstrated in Figure 2.17, the smaller the fragments that result from the rupture of the glass sheet, the worse the post-breakage behavior of the laminated glass will be, as the “arch” effect enabled by the lamination film becomes less efficient with the diminishment of the fragments (Haldimann, *et al.*, 2008).

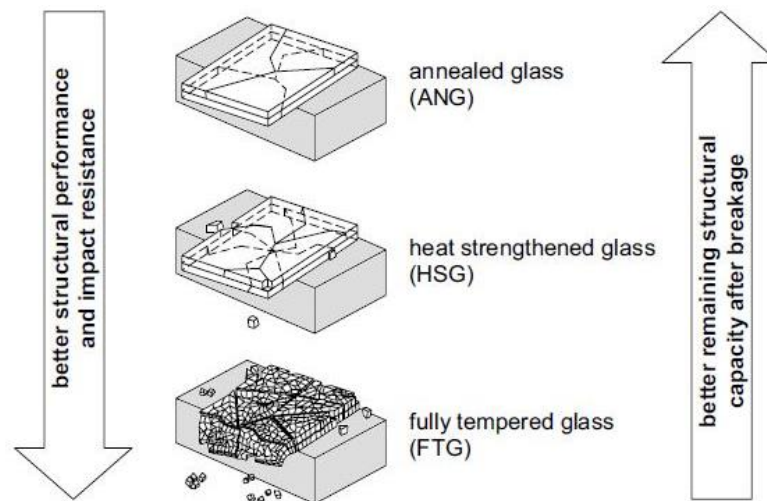


Figure 2.19 - Post-breakage behavior of laminated glass for different glass types, (Haldimann, *et al.*, 2008).

As a result, it is expected that, even though annealed glass is characterized by the lowest tensile bending strength, its restricted fracture type will result in a significantly better post-breakage structural response as well as allow a substantial load-carrying capacity. For that reason, this was the chosen material to incorporate in the analyzed beams.

3 LONG-TERM EFFECTS ON STRUCTURAL GLASS

3.1 Introduction

In spite of being a relatively durable material, the strength of structural glass is influenced by several factors from which it stands out the duration of the actions to which these elements are subjected. As previously mentioned, the effects of long-term mechanical and environmental loads have a considerable impact in the behavior of structural glass, affecting the characteristics of not only the glass sheets but also of the adhesive layers. Among long-term effects, the deterioration of the surface of glass elements and consequent loss of strength caused by Stress Corrosion, and the susceptibility of the properties of the interlayer to long-term actions are significantly important.

In the following sections, the main mechanisms responsible for the deterioration of the glass and the resistance of the adhesive layer over time are described. There will also be presented several existing studies in which the influence of long-term effects on both glass and laminate compounds is well noticed. It is hoped that the information presented in this chapter will contribute to a better understanding of the relevance of the investigation developed in the current dissertation.

3.2 Mechanisms Responsible for the Long-term Behavior of Laminated Glass

3.2.1 In the Glass

As it has been established in the previous chapter, glass has a time-dependent behavior when tensioned, which is mainly induced by an environmental phenomenon called Stress Corrosion, as it is responsible for the deterioration the surface of glass in the presence of water molecules. The main consequence of this environmental corrosion is a phenomenon referred to as “sub-critical crack growth”, which consists in the growth of the flaws that exist on the surface of glass, even if the glass element has a stress value below the theoretical tensile bending strength of glass (Haldimann, *et al.*, 2008). Consequently, this occurrence will cause the glass element

will break at lower tensile stress values, and it is for that reason that the practical value of the tensile bending strength of glass is much lower than the theoretical one.

Naturally, glass with different compositions display distinct resistances to Stress Corrosion. Although the performed experimental research was based on soda-lime glass, which is a widely-applied material in the structural glass applications, the chemical bonds that characterize silica glass grant it a significantly higher corrosion resistance (Ronchetti, et al., 2013).

The growth of the surface flaws is related to several factors such as the properties of the glass element and the flaw itself, the stress history and the relation between the crack velocity and the value of the stress intensity factor. According to what was established in section 2.5.2, the stress intensity factor (K_I) represents the elastic stress intensity close to the tip of the fracture (Equation (4)), and is dependent on the characteristics and location of the crack on the glass, and on the geometric properties and stress distribution of the glass (Haldimann, et al., 2008).

$$K_I = Y \cdot \sigma_n \cdot \sqrt{\pi \cdot a} \tag{4}$$

The relation between K_I and the crack velocity (v) is represented in Figure 3.1 This relation depends on various aspects such as humidity, temperature, corrosive media and pH values, chemical composition of the glass and the loading rate (Haldimann, et al., 2008).

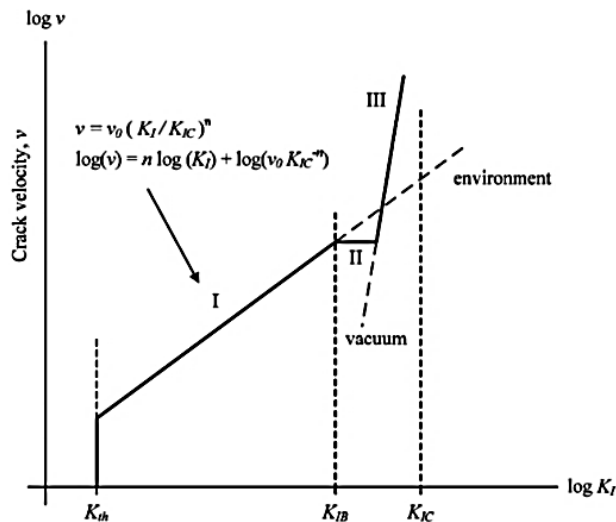


Figure 3.1 - Schematic representation of the relation between the (v) and (K_I), (Louter, 2011).

As presented in Figure 3.1 when the value of K_I reaches or surpasses the value of the critical stress intensity (K_{IC}), the crack velocity behaves independently of the environment, increasing rapidly until a characteristic crack propagation speed (1500 m/s for soda-lime glasses).

Ultimately, the evolution of the crack at this stage results in the unavoidable fracture of the glass (Haldimann, *et al.*, 2008). This phenomenon is translated by Irwin's fracture criterion and is given by Equation (5) (Louter, 2011).

$$K_I \geq K_{Ic} \quad (5)$$

It is acceptable to assume, for all practical purposes, that the value of K_{Ic} for modern soda-lime glass is between 0.6 and 1.0 MPa.m^{0.5} (Gy, 2003).

During phase I, the growth of the cracks develops under the influence of tensile stresses, being highly susceptible to the influence of environmental humidity or the presence of water. This is due to the fact that water molecules are responsible for increasing the superficial flaws of the glass element, as explained before. Below the value of K_{th} , which for soda-lime silica glass is usually about 0.2 to 0.3 MPa.m^{0.5}, it is unlikely for any crack to increase (Haldimann, *et al.*, 2008).

In phase II, the value of the crack velocity is independent of K_I . At this point, the kinetics of the chemical reaction responsible for Stress Corrosion stop depending on the activation of the chemical process and start being controlled by the water supply rate. With the growth of the fracture and the progression of the velocity of the crack, the time that it takes for the water molecules to be transported to the crack tip increases, which ultimately results in a shortage of water.

As the stress intensity factor approaches rapidly to the value of K_{Ic} , the crack velocity becomes completely independent of the environment. In phase III, the value of v will continue to increase until it reaches the characteristic crack propagation speed of glass. It is in this phase that cracks evolve until its critical stage, diminishing the strength of the glass element. Ultimately this will cause the glass to fail completely.

3.2.2 In the Adhesive

As referred in section 2.6.2, the utilized adhesive layer is composed by a polymer material. In this section, the particularities of the behavior of this material will be presented.

Polymers consist of large chain-like molecules composed of repeating simple monomer units, linked to each other through physical and/or chemical bonds (Louter, 2011). It becomes important to recognize that the chemical bonding forces can be up to 10³ stronger than the

physical bonding forces. While physical bonds can be reversed when subjected to heat, solvents or mechanical forces, chemical bonds are practically irreversible. Furthermore, different types of bonds result in the existence of different structures: linear (Figure 3.2 a)), branched (Figure 3.2 b)), cross-lined (Figure 3.2 c)) and entangled (Figure 3.2 d)).

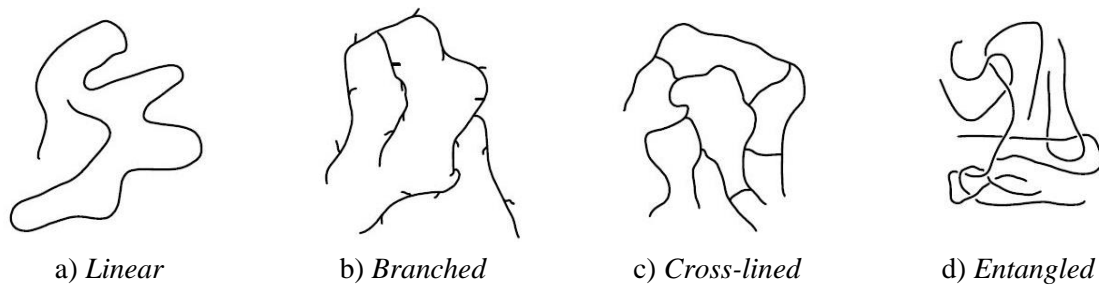


Figure 3.2 – Schematic representation of the structure of polymer materials, (Louter, 2011).

According to their molecular structure, polymers can be classified in thermosets, elastomers, and thermoplastics (Louter, 2011). For the current investigation, the thermoplastic polymers are of particular importance, once the applied adhesive (SentryGlas) is itself included in that category.

Thermosets are originated through the chemical reaction between different components such as resin or hardener. They are usually described as network polymers due to their characteristic heavily cross-linked and entangled structure. Once these polymers have solidified, they do not soften or melt when subjected to elevated temperatures. Although its secondary (physical) bonds tend to suffer when heated, causing a reduction on the E-modulus of the polymer, the cross links prevent the thermosets total melting. When subjected to extremely elevated temperatures, this material decomposes.

Elastomers are composed by chemically cross-linked macromolecules. Its loosely bond network structure is characterized by a low cross-link density, which allows this material to display large elastic deformations. The cross-links of this polymers grant it the ability to return to its original form upon the removal of the applied loads, even after significant deformations. Similarly to what occurs in thermosets, when heated, elastomers do not display viscous behavior or melt, thanks to the effect of its chemical bonds.

Thermoplastic polymers are made by chain polymerization and are known to be composed by linear or branched macromolecules bonded to each other via physical links. The more complex the resulting structure is, the less ductile the behavior of these polymers at room temperature will be. Due to the absence of cross-links in thermoplastic polymers, these materials have no

defined melting point, displaying instead a decrease of viscosity with the increase of temperature, which translates in the softening of the material (Louter, 2011).

Upon loading, polymers are known to present three different deformation types: instantaneous elastic deformation, which is caused by the instantaneous modification of the atomic distance and by the distortion of the valence angles between fixed chemical bonds (Figure 3.3 a)); time-dependent viscoelastic deformation due to the stretching of the molecular chains (Figure 3.3 b)); time-dependent viscous deformation resultant from the movement of the molecular chains (Figure 3.3 c)). It is important to mention that, from among these types of deformation, only the viscous deformation is completely irreversible.

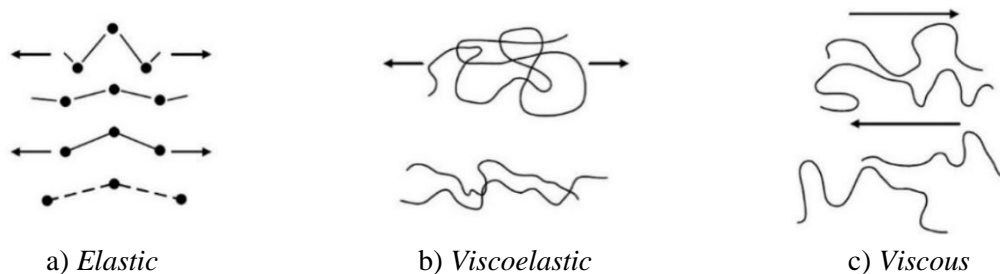


Figure 3.3 – Schematic representation of the deformation in polymers, (Louter, 2011).

The mechanical behavior of polymers is extremely dependent on external factors such as temperature, time, loading rate, UV- radiation, and environmental parameters like humidity or oxygen (among others) (Figure 3.4).

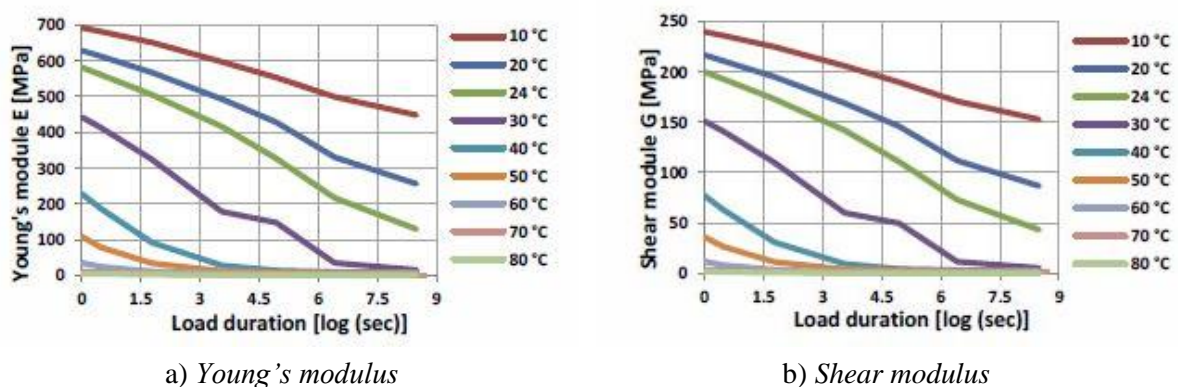


Figure 3.4 – Degradation of the SG properties with the increase of temperature and load-duration, (Stelzer, 2010).

Besides the dependence on all these external factors, the behavior of the polymer layer is highly influenced by the glass transition temperature (T_G) and by the magnitude and rate of the applied

load. The glass transition temperature corresponds to the temperature value where the largest change of stiffness prior to melting takes place. At temperatures below T_G or for high loading rates, polymers usually display rigid and brittle behavior because their molecules are unable to relocate fast enough. On the other hand, for slower loading rates or at temperatures above T_G , polymers exhibit tough and ductile behavior (Louter, 2011).

The presence of water molecules is also capable of influence the mechanical behavior of these materials. By absorbing water, a diminishment of the glass transition temperature may occur, which will affect the overall response of the polymer by altering its stiffness, yield stress, strain at failure and toughness (Louter, 2011).

3.3 State of Knowledge

3.3.1 Introduction

The main objective of this sections is to present several previous works were the effect of long-term actions on the behavior of glass elements and of laminated glass structures is well noted.

3.3.2 Glass

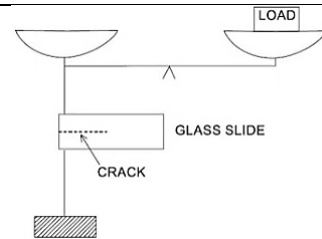
As explained before, glass suffers a deterioration of its properties over time. This deterioration is mainly caused by Stress Corrosion but other aspects like loading history also influence the long-term behavior of glass. The severity of the impact that this phenomenon has on the strength of the glass is highly dependent not only on the environmental conditions but also on the tension installed in glass specimen, on the size of the surface flaws, on the temperature changes and on the surface and edge finishes.

Regarding the physical consequences of fatigue in glass elements, an experimental investigation was developed by Guin and Wiederhorn (Guin and Wiederhorn, 2003). Through this research, they evaluated the residual features of cracks after holding them at certain stress values, during varying time periods. The conducted experimented consisted in propagating a crack on a glass sheet at $K_I = 0.37 \text{ MPa}\cdot\text{m}^{0.5}$ and then reducing it to values below the fatigue threshold of soda-lime silicate glass, in order to arrest the crack growth. Posteriorly, the samples

were subjected to the initial K_I value, in order to measure the amount of time that took for the propagation of the crack to restart (Table 3.1).

Table 3.1 - Experimental research by Guin and Wiederhorn (2003).

Author(s):	Guin and Wiederhorn.
Objective(s):	Determination of the effect of hold-time of the cracks in the restart of the growth of the crack.
Experimental Tests:	Crack propagation, interruption, and reinstatement to measure the necessary time for the crack growth to restart.
Parametric variation:	<p>Samples:</p> <ul style="list-style-type: none"> - Soda-lime silicate glass microscopic slides (75 x 25 x 1.5 mm) <p>Hold stress-intensity factor (K_{Ih})</p> <ol style="list-style-type: none"> 1) $K_{Ih} = 0.24 \text{ MPa} \cdot \text{m}^{0.5}$ 2) $K_{Ih} = 0.1 \text{ MPa} \cdot \text{m}^{0.5}$ <p>Hold-time: 1 hour up to 200 hours</p>



From the obtained results, it was possible to verify that the deterioration of the surface of the glass is highly influenced not only by the stress values but also by the duration that the glass specimen is subjected to that stress (Figure 3.5). In the samples held at $K_I = 0.24 \text{ MPa} \cdot \text{m}^{0.5}$, it was observed that the longer the hold-time, the longer it took for the cracks to restart growing when the initial stress intensity factor was re-established (Figure 3.5 a)). The values obtained in the samples held at $K_I = 0.1 \text{ MPa} \cdot \text{m}^{0.5}$ indicated that the growth of the crack started almost immediately, independently of the hold-time (Figure 3.5 b)).

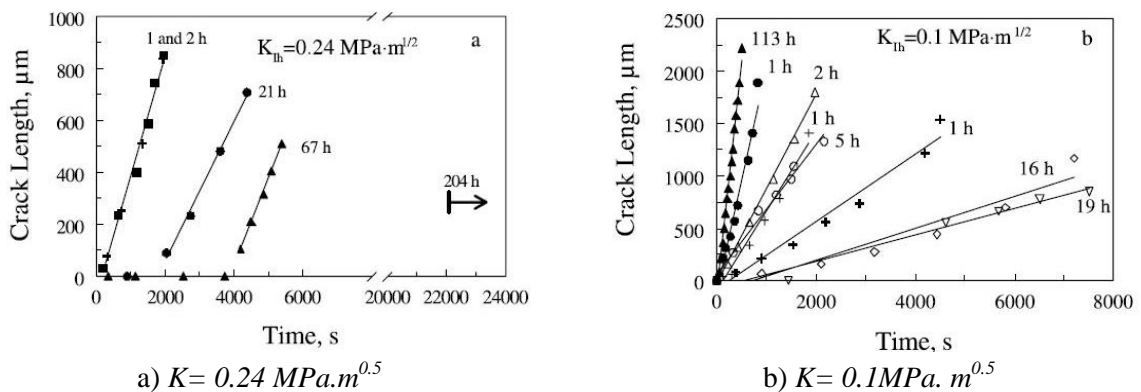


Figure 3.5 – Time-delay to restart a crack held at different hold stress-intensity factors, (Guin and Wiederhorn, 2003).

This investigation allowed to confirm that load history is a crucial factor to take into consideration when analyzing the behavior of glass elements, affecting its physical integrity and, consequentially, in the load-bearing capacity that the glass is able to display.

3.3.3 Laminated Compounds

Due to the elevated risk of fracture and to the fact that the strength of the glass tends to decrease over time, it is usual to apply laminated glass in situations where it is important that these elements have high load-bearing capacity. Yet, it is essential to bear in mind that the behavior of the laminated compounds depends on the response that each of its components provides both in normal unbroken conditions and during its failure stages. Previous studies support the theory that the interface between glass and the bond layer does not suffer any damage, so perfect adhesion between is usually assumed until the occurrence of the first crack. Consequently, only the properties of the interlayer influence the coupling between the components of the laminate.

To evaluate the differences between the time-dependent behavior of several materials applied as adhesive layers, Bati and coauthors developed an extensive research to laminated glass beams from which the 4PB tests are of greater interest to the framework of the current dissertation (Table 3.2) (Bati, et al., 2010).

Table 3.2 - Experimental research by Bati and coauthors (2010).

Author(s):	Bati, Ranocchiai, Reale and Rovero.
Objective(s):	1) Mechanical characterization of laminated glass beams subjected to bending;
Experimental Tests:	Four-point bending tests to obtain time-displacement diagrams.
Parametric variation:	<div style="display: flex; align-items: flex-start;"> <div style="flex: 1;"> <p>Laminated glass (PVB) dimensions:</p> <p>(1) 55 x 5 x 2.152 (cm)</p> <p>(2) 55 x 7 x 2.152 (cm)</p> <p>Laminated glass (EVA) dimensions:</p> <p>(1) 55 x 7 x 2.22 (cm)</p> <p>Simple glass ply dimensions:</p> <p>(1) 55 x 5 x 1 (cm)</p> <p>(2) 55 x 7 x 1 (cm)</p> <p>Laminated glass (SG) dimensions:</p> <p>(1) 55 x 7 x 2.22 (cm)</p> </div> <div style="flex: 1; text-align: center;"> </div> </div>

The measured deflections are presented in Figure 3.6 and confirm the strong influence that the viscosity of the adhesive layers has on the mechanical response of composite beams. The results showed that each of the analyzed polymers affected the mechanical response of the beams in a different manner and that their performance degraded at different rates, as consequence of their time-dependent behavior. The evolution of the deflections in all the tested samples is almost linearly dependent on time. It is also noted that the SG-laminates displayed stronger bonds and favorable long-term behavior, by presenting considerably smaller deflections.

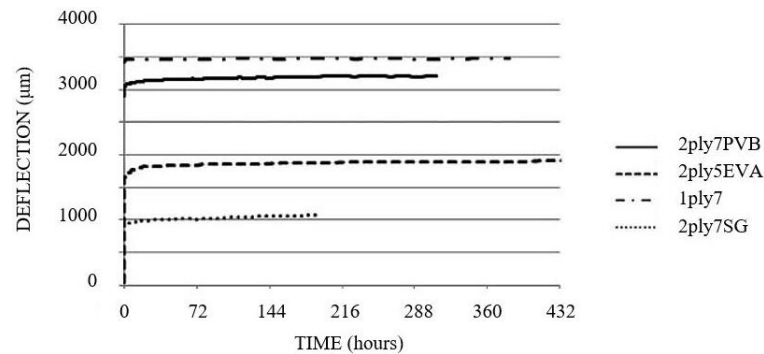
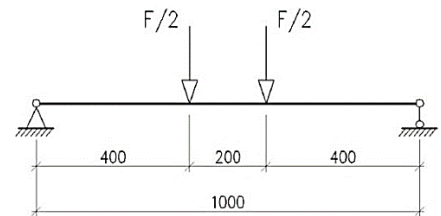


Figure 3.6 - Results of the 4PB tests, (adapted from Bati, *et al.*, 2010).

To understand the durability aspects of laminated glass plates with different interlayers, a series of 4PB tests according to EN 1288-3:2000 (Table 3.3) were performed by Serafinavicius and coauthors (Serafinavicius, *et al.*, 2013). In the performed long-term 4PB tests, the samples were subjected to three temperature values, for 24-hour intervals each.

Table 3.3 - Experimental research by Serafinavicius and coauthors (2013).

Author(s):	Serafinavicius, Lebet, Louter, Lenkimas and Kuranovas.
Objective(s):	Investigation of durability aspects of laminated glass in the framework of long-term tests.
Experimental Tests:	Four-point bending tests with constant load in order to measure middle span deflections, volatile displacements between the glass layers and longitudinal strains over time.
Parametric variation:	<p>Sample composition:</p> <ul style="list-style-type: none"> - 2 annealed glass sheets (t=6 mm) - Lamination film of PVB, EVA or SG (t=1.52mm) <p>Dimensions: - Length =1100 mm - Height =360 mm</p> <p>Evaluated Temperatures: +20°C, +30°C and 40°C</p>



The results revealed that the behavior of the polymer adhesive layers is influenced by the variation of temperature and time, since the measured parameters increase not only when the range of temperature is changed but also at constant values of temperature.

While EVA and SG laminates displayed similar results, PVB laminates presented the worst behavior, which is particularly visible in the results presented in Figure 3.7. The obtained results demonstrated that, under long-term loading, that the SG-laminates had the best performance, displaying considerably smaller values of the measured parameters, even at the highest considered temperature. When comparing the results of PVB and SG laminates it is important to refer that the percentage of differences between the recorded deflections, volatile displacement and tensile stresses are of 71%, 99% and 46%, respectively.

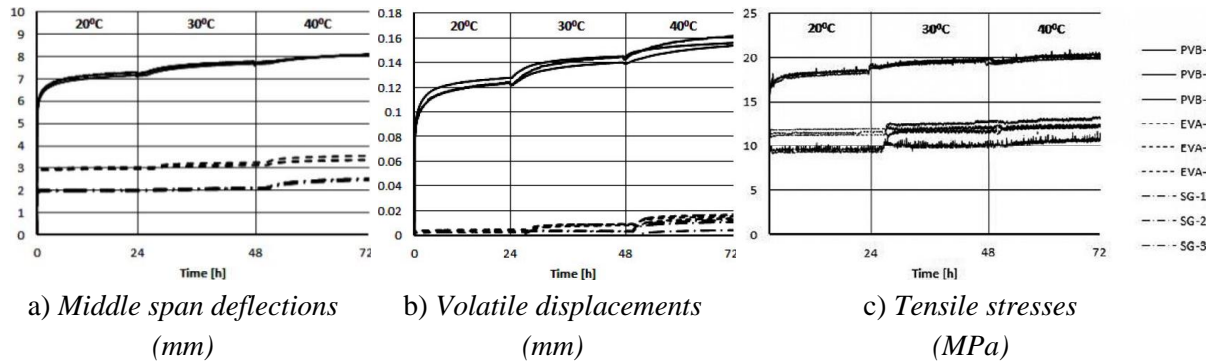
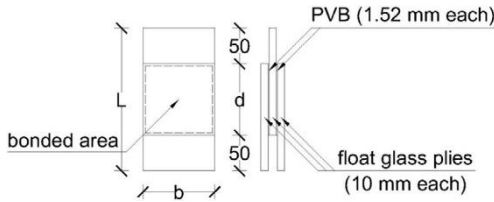



Figure 3.7 - Experimental results of four-points bending tests at +20°C, +30°C and +40°C, (adapted from Serafinavicius, *et al.*, 2013).

Also, regarding the long-term viscoelastic behavior of laminated glass elements, an experimental research was developed by Biolzi and coauthors (Biolzi, *et al.*, 2014). This behavior was investigated by means of a series of mechanical tests performed on glass-PVB double-lap joints (Table 3.4).

Table 3.4 - Experimental research by Biolzi and coauthors (2014).

Author(s):	Biolzi, Cagnacci, Orlando, Piscitelli and Rosati.	
Objective(s):	Investigation of the viscoelastic behavior of laminated glass.	
Experimental Tests:	Application of compressive loadings to double lap joints in order to obtain load and displacement variations as a function of time.	
Parametric variation:	<p>Sample composition:</p>  <p>Dimensions of the glass plies: b=100, 125 or 200 mm d = 100, 125, 150, 200 or 250 mm l = 200,225, 250, 300 or 350 mm</p>	
	Evaluated Parameters: Temperature (T); Relative Humidity (H); Load Duration (L); Unload Time (U).	
	Tested Situations: a) T: 50°C, H: 70%, L: 13 days, U: 0 days; d) T: 20°C, H: 90%, L: 40 days, U: 26 days; b) T: 30°C, H: 70%, L: 30 days, U: 7 days; e) T: -5°C, H: 50%, L: 23 days, U: 0 days; c) T: 20°C, H: 50%, L: 37 days, U: 32 days; f) T: -20°C, H: 50%, L: 6 days, U: 0 days;	

In Figure 3.8 it is possible to observe the results of one of the samples tested in each of the considered situations. It is important to refer that the applied loads intended to originate constant values of the shear stress in the lamination films. However, the PVB displayed considerable relaxation for temperatures above 20° C, which implicated the multiple load adjustments. Note that the main displacements take place upon these adjustments and that, the removal of the applied load results in the partial recuperation of the vertical deformations. Furthermore, it is also visible that, even in periods where the applied load is constant, the vertical displacements of the samples continue to grow, which confirms the time-dependency of the behavior of laminated glass compounds.

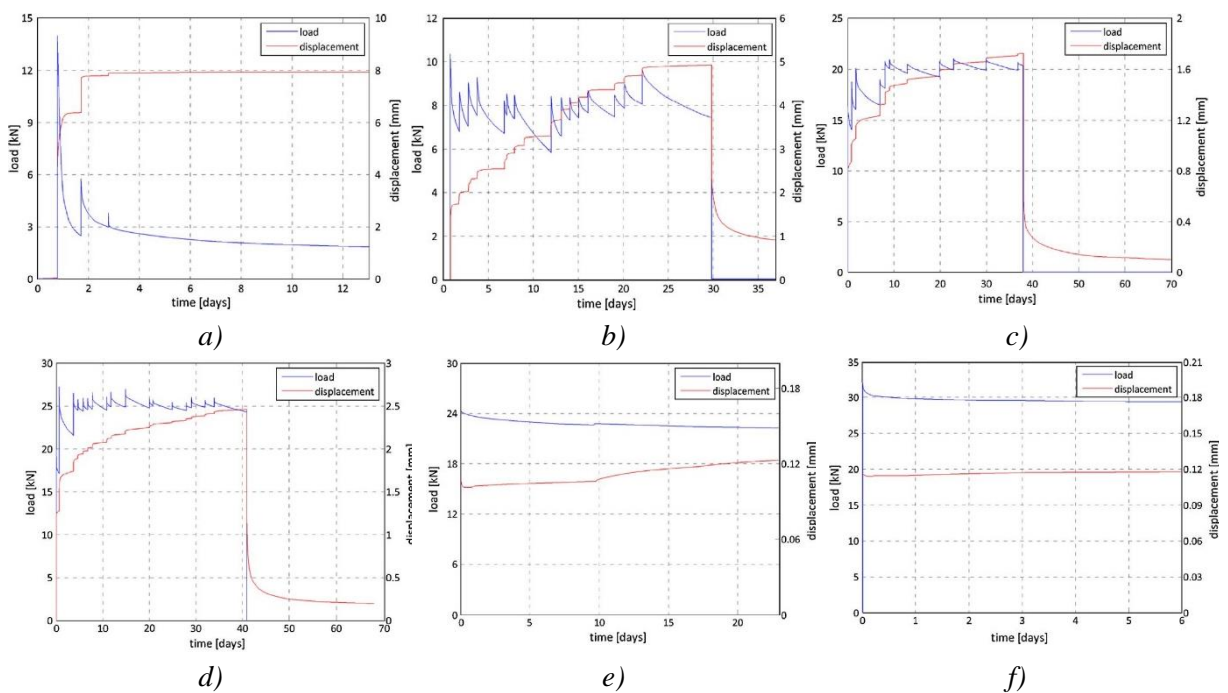
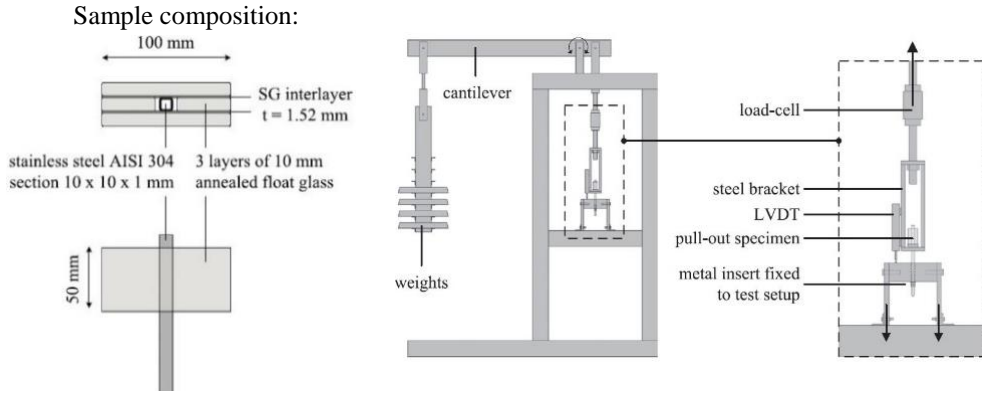
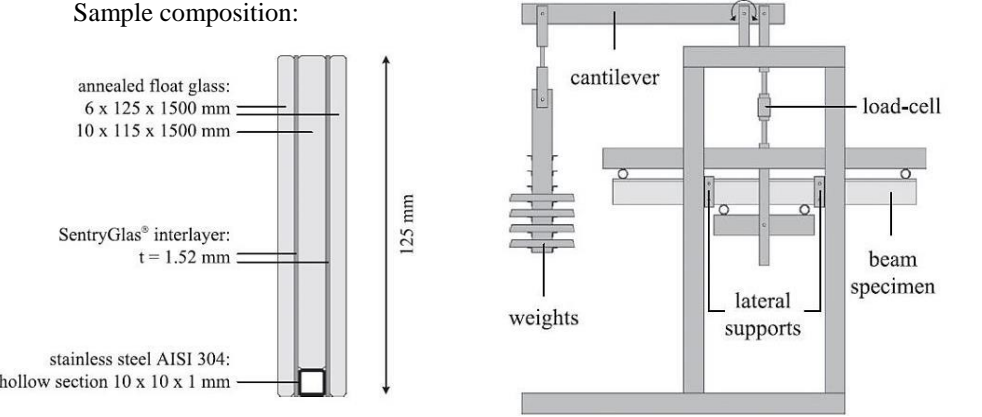


Figure 3.8 – Load and displacement as a function of time, (adapted from Biolzi, et al., 2014).

As expected, the specimens subjected to negative temperatures (Figure 3.8 e) and f)) displayed a more linear evolution of the displacements, whose values are significantly lower than those verified in the remaining situations. The reason for this is that these tests were performed at temperature values are well below the transition temperature of PVB (20°C).

Within the framework of the long-term behavior of structural glass, the experimental investigation regarding SG-laminated reinforced glass beams performed by Louter and coauthors (Louter, et al, 2011) is of great importance (Table 3.5).

Table 3.5 – Experimental research by Louter and coauthors (2011).

Author(s):	Louter, Belis, Veer and Lebet.
Objective(s):	Investigate the durability of structural glass beams composed by annealed glass, stainless steel reinforcement and SG interlayer sheets, when conditioned by several parameters.
Experimental Tests:	Small scale pull-out tests to obtain load-displacement curves in order to investigate the shear transfer capacity of the SG.
Parametric variation:	 <p>The diagram shows the sample composition and the test setup. The sample consists of a stainless steel AISI 304 section (10 x 10 x 1 mm) embedded in three layers of 10 mm annealed float glass, with an SG interlayer (t = 1.52 mm) between the glass layers. The total width is 100 mm and the height is 50 mm. The test setup includes a cantilever beam with weights, a load-cell, a steel bracket, an LVDT, and a metal insert fixed to the test setup.</p> <p>Evaluated Parameters: Temperature (-20°C, 23°C, 60°C and 80°C); Thermal Cycling; Humidity Exposure; Load-duration.</p>
Experimental Tests:	Medium scale four-point bending tests to obtain load-displacement curves in order to investigate the structural response of the SG-laminated reinforced beams.
Parametric variation:	 <p>The diagram shows the sample composition and the test setup. The sample consists of two layers of annealed float glass (6 x 125 x 1500 mm and 10 x 115 x 1500 mm) with a SentryGlas® interlayer (t = 1.52 mm) between them, and a stainless steel AISI 304 hollow section (10 x 10 x 1 mm) embedded in the bottom layer. The total height is 125 mm. The test setup includes a cantilever beam with weights, a load-cell, lateral supports, and a beam specimen.</p> <p>Evaluated Parameters: Load-duration, Temperature (-20°C, 23°C and 60°C); Thermal Cycling; Humidity Exposure.</p>

In the performed long-term pull-out tests, the SG-interlayer presented stress-intensity related creep, as the inserted metal began to slip gradually, even at constant loads. It was noticeable that, at higher loading levels, the rate slip of the reinforcement increased considerably. This occurrence is related to the viscoelastic properties of the SG, which, as previously established, are influenced by both temperature and load duration. Through the long-duration bending tests, it was observed that the fractured samples displayed vertical creep deformation under constant loading (Figure 3.9).

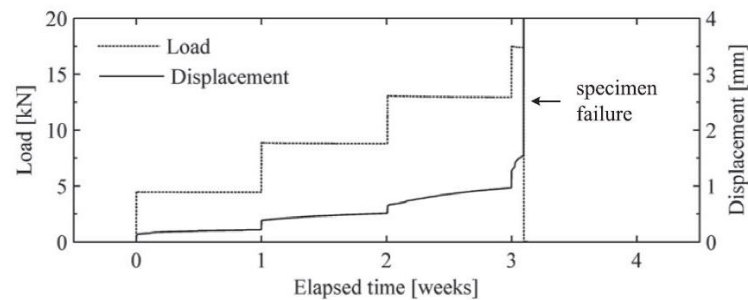


Figure 3.9 – Long-term pull-out tests - loads and displacements, (Louter, et al, 2011).

In the long-term bending tests, the beams displayed vertical displacements under constant loading. This deformation was mainly induced by the creep of the interlayer between the glass sheets and the applied reinforcement, causing the gradual slip of this last component and stimulation the propagation of the cracks. This crack propagation resulted in a reduction of the stiffness of the samples, which led to the increase of the vertical displacements. Still, the samples showed excellent post-breakage behavior, as even though its creep deformation continued to increase during the full duration of the experimental test, they did not collapse and were still able to carry the applied load. These results indicate that SG-laminated reinforced glass beams provide are characterized by a considerably safe post-breakage behavior, even when subjected to long-duration loads, which makes its application highly redundant.

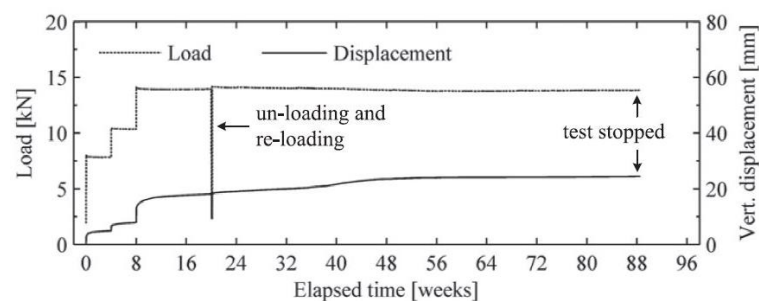


Figure 3.10 – Long-term bending tests - loads and vert. displacements, (Louter, et al, 2011).

3.4 Design Code Framework

The design of glass structures should be performed through a procedure identical to those applied to other structural materials, resulting of an iterative process including design codes, analytical calculations, and experimental tests. It must be guaranteed that the glass elements are able to respond adequately to the requirements of both Ultimate and Serviceability limit states, ensuring its structural safety and limiting its deflections (Valarinho, 2010).

When designing glass elements, one must take into consideration the brittle nature of the material, as well as the level of safety that each element must be able to provide not only in unbroken conditions but also during and after rupture. Being able to break unexpectedly, it also becomes important to evaluate the probability of failure of each glass element and the correspondent consequences (Delincé, et al., 2008), which must lead to higher attention while designing glass elements and in lower tolerances associated with their production and assembly procedures. According to the structural function, the applied loads, and the failure consequences of each element, it is possible to classify it as primary or secondary. Primary elements like columns and beams are generally meant to support loads from superior elements, which translates in the requirement of high levels of robustness and damage tolerance. On the other hand, secondary elements such as horizontal glazing are not intended to do so, which is why they do not require the same level of safety and reliability.

In spite of the considerable evolution that took place in the industry of glass and of the generalization of the glass applications in structural elements, there is still little documentation available and the existing practical design codes are not consensual. While nationally, there is no documentation which focuses particularly on structural glass elements, internationally the situation is different. Currently, the most applied approach is the prEN 16612, but the glass Eurocode is expected to include components from standards of several member states from which stand out the following countries: Germany, Austria, Czech Republic, Netherlands, France, Italy, and United Kingdom. For more detailed information, consult the Guidance for European Structural design of Glass Components (JRC, 2014).

In linear elements constituted by isotropic materials, the value of both stresses and deformations can be analytically determined through elementary theories from the domain of the strength of materials, provided that the connection between all the components that constitute it can be considered completely rigid (Firmo, 2015). Many of the existing design codes include procedures based on this assumption, disregarding the behavior of the lamination film and its impact on the global long-term response of laminated glass elements, which results in solutions that, in spite of being relatively safe, are considerably uneconomic and whose behavior is not sufficiently defined. In order to incorporate the long-term effects of the interlayer in the structural behavior of laminated elements, as the bond between the glass sheets and the adhesive layer is relatively flexible and is known to deteriorate with time, it becomes necessary to establish more complex formulations.

Nonetheless, some of the existing approaches take into consideration that the bending strength of glass depends on a variety of influencing factors such as the size of the critical flaw, the size

of the element, the stress distribution, the environmental conditions, and the load-duration (JRC, 2014). So that the effects of long-duration loads in the performance of glass elements could be included in the determination of the practical strength of glass, the factor of load duration (k_{mod}) was defined (Table 3.6). It depends on the load duration (t) and on the constant of corrosion (c), which is related to the susceptibility of the glass zone to external actions. It is also important to note that different types of loading are associated with specific load durations and possess different values of the k_{mod} (Table 3.7).

Table 3.6 - Determination of k_{mod} according to different design codes (from JRC, 2014).

Design Code:	Factor of load duration:	Variables:
NEN 2608	$0,25 \leq k_{mod} = \left(\frac{5}{t}\right)^{1/c} \leq 1$	t: load duration in seconds c: constant of corrosion
prEN 16612	$k_{mod} = (0,663 \cdot t)^{-1/c}$	t: load duration in hours c: constant of corrosion
CNR-DT-21	$k_{mod} = (0,585 \cdot t)^{-1/c}$	t: load duration in hours c: constant of corrosion

Table 3.7 - Load durations and respective values of k_{mod} , according to different design codes (from JRC, 2014).

Load Duration	Type of loading and k_{mod}		
	DIN 18008	ÖNORM B 3716	prEN 16612
Permanent	Permanent load and permanent climatic loading, $k_{mod}=0,25$	Permanent load and climatic load, $k_{mod}=0,6$	Dead-loads, self-weight, $k_{mod}=0,29$
Medium	Climatic loading and snow, $k_{mod}=0,4$	Snow, personnel loading on glass floors and drivable floors, $k_{mod}=0,6$	Yearly temperature variation, $k_{mod}=0,39$ Snow, $k_{mod}=0,44$ Barometric pressure, $k_{mod}=0,5$ Daily temperature variation, $k_{mod}=0,57$
Short	Horizontal traffic load and wind, $k_{mod}=0,7$	Horizontal traffic load, maintenance load and wind, $k_{mod}=0,7$	Wind (short, multiple), $k_{mod}=0,7$ Personnel loads (short single gust), $k_{mod}=0,89$ Wind (single gust), $k_{mod}=1,0$

The load-duration coefficient is, subsequently, included in the determination of the resistant force of glass elements (R_d). The design value of R_d for glass elements is differently determined in the various European member states. Its value is influenced by various parameters such as: type of glass (annealed or heat-treated), type of production method in the case of heat-treated glass, loading situation (as plate or as beam) and duration, material safety factor, redundancy of laminated glass, reduction of the design value caused by edge effects or depending on the surface profile, consideration of special applications, among others (JRC, 2014).

Being particularly important for the current research, currently applied equations for dimensioning of annealed float glass are presented in Table 3.9.

Table 3.8 - Determination of R_d according to different design codes (from JRC, 2014).

Design Code:	Design value (R_d):	Variables:
NEN 2608	$R_d = \frac{k_{mod} \cdot k_a \cdot k_e \cdot k_{sp} \cdot f_k}{\gamma_{M,A}}$	<p>$\gamma_{M,A}$: material partial factor (1.8 if the wind is the dominant load, 2.0 for remaining loads)</p> <p>k_a: coefficient of non-linearity ($k_a=1,644 \cdot A^{1/25}$ (A: loaded area in mm²))</p> <p>k_e: coefficient depending on the type of loading (0.8 for perpendicular to plane loads, 0.62 for in-plane loads)</p> <p>k_{sp}: factor for the glass surface profile (1.0 for float glass and 0.8 for patterned glass)</p> <p>k_{mod}: factor of load duration</p> <p>f_k: characteristic bending strength of annealed glass</p>
CNR-DT 210	$R_d = \frac{k_{mod} \cdot k_{ed} \cdot k_{sf} \cdot \lambda_{gA} \cdot \lambda_{gl} \cdot f_k}{R_M \cdot \gamma_M}$ $+ \frac{k'_{ed} \cdot k_v \cdot (f_{b,k} - f_{g,k})}{R_{M,v} \cdot \gamma_{M,v}}$	<p>γ_M: material partial factor (2.55)</p> <p>$\gamma_{M,v}$: material partial factor (1.35)</p> <p>R_M: multiplicative factor for annealed and prestressed glass, dependent on the class of consequence (I class – 0.7, II class – 1.0)</p> <p>$R_{M,v}$: multiplicative factor for annealed and prestressed glass, dependent on the class of consequence (I class – 0.9, II class – 1.0)</p> <p>$f_{b,k}$: bending strength according to the product standard</p> <p>k_{mod}: factor of load duration</p> <p>k_{ed} and k'_{ed}: coefficients on the edge and(or) holes finishing</p> <p>k_{sf}: coefficient dependent on the surface treatments</p> <p>k_v: coefficient dependent on the prestress or chemical treatment</p> <p>λ_{gA}: size effect coefficient ($0.75 \leq \lambda_{gA} = \frac{0.24m^2}{k \times A} \leq 1.0$; A= loaded surface; k= boundary condition coefficient)</p> <p>λ_{gl}: edge quality coefficient (for polished edges $\lambda_{gl} = \left(\frac{0.1667 \times 0.45m}{k_b \times l_b}\right)^{1/5} \leq 1$; for ground edges $\lambda_{gl} = \left(\frac{0.0741 \times 0.45m}{k_b \times l_b}\right)^{1/12.5} \leq 1$)</p> <p>$k_{mod}$: factor of load duration</p> <p>$f_{g,k}$: characteristic bending strength of annealed glass</p>
DIN 18008	$R_d = \frac{k_{mod} \cdot k_c \cdot f_k}{\gamma_M}$	<p>γ_M: material partial factor (1.8)</p> <p>k_c: coefficient respecting the type of construction (1.8 for linearly supported panels, otherwise 1.0)</p> <p>k_{mod}: factor of load duration</p> <p>f_k: characteristic bending strength of annealed glass</p>

<p>prEN 16612</p> <p>prNBN S23-002</p>	$R_d = \frac{k_{mod} \cdot k_{sp} \cdot f_{g,k}}{\gamma_{M,A}}$	<p>$\gamma_{M,A}$: material partial factor (1.8)</p> <p>k_{sp}: factor for the glass surface profile (1.0 for float glass and 0.75 for patterned glass)</p> <p>k_{mod}: factor of load duration</p> <p>$f_{g,k}$: characteristic bending strength of annealed glass</p>
<p>Ö B 3716</p>	$R_d = \frac{k_{mod} \cdot k_b \cdot f_k}{\gamma_M}$	<p>γ_M: material partial factor (2.0 for wired and patterned glass, 1.5 for float, laminated float glass and heat-treated glass)</p> <p>k_b: coefficient depending on the type of loading (1 for perpendicular to plane loads, 0.8 for in-plane loads)</p> <p>k_{mod}: factor of load duration</p> <p>f_k: characteristic bending strength of annealed glass</p>

It also becomes important to refer the existing approaches for the determination of both the stresses and deflections that defined loading conditions provoke in glass elements. Within the developed European standards, the Equivalent Thickness Methods are of considerable importance. These methods allow to determine the thickness that a monolithic beam should have in order to behave itself in terms of deflections and stresses as the laminated glass beam under evaluation. The effective thickness can be established through the consideration of a shear transfer coefficient, Γ , which will translate the portion of the shear actions that is transferred between the glass plies through the interlayer (Equation (6)). The Wölfef-Bennison model is frequently applied in order to determine the deflection-effective and the stress-effective thicknesses, $h_{ef;w}$ and $h_{i;ef;\sigma}$, of laminated elements composed by two glass plies (Equation (7) and (8)) (CNR, 2013).

$$\Gamma = \frac{1}{1+9,6 \cdot \frac{h_{int} \cdot E \cdot I_s}{G_{int} \cdot l^2 \cdot d^2}} = \frac{1}{1+9,6 \cdot \frac{h_{int} \cdot E \cdot A^*}{G_{int} \cdot l^2 \cdot b}} \quad (6)$$

$$h_{ef;w} = \sqrt[3]{h_1^3 + h_2^3 + 12 \cdot \Gamma \cdot I_s} \quad (7)$$

$$h_{i;ef;\sigma} = \sqrt{\frac{h_{ef;w}^3}{h_1 + 2 \cdot \Gamma \cdot d_i}} \quad (8)$$

The previous equations involve: the thickness of the interlayer (h_{int}); the width of the beam (b); the length of the beam (l); the Young's modulus of the glass (E); the moment of inertia per unit of length (I_s); the shear modulus of the interlayer (G_{int}); the thickness of the i^{th} glass ply (h_i); the distance of the gravity centre of the i^{th} glass ply to the gravity centre of the laminated element (d); and the total generic area of the glass plies cross sections (A^*).

For more information regarding the presented approaches for both the determination of the resistant force of glass and of its deflections and stresses under the influence of long-term loadings, the consultation of the referred standards is recommended.

4 EXPERIMENTAL TESTS

4.1 Introduction

As previously established, the behavior of glass load-bearing structures is still not fully characterized, particularly in situations where they are subjected to long-term loading. For this reason, and in spite of the considerable expansion that took place in the glass industry, there are still many undefined aspects. Because of these uncertainties, the approaches considered by the existing design codes and by nowadays structural glass designers turn out to be uneconomical, implicating several expensive and complicated procedures, which include the development of full-scale experimental tests and complex computer models. The fact that these procedures are out of range of most of the ordinary designers also contributes for the suppression of the expansion of glass as a structural element.

The experimental research developed in the framework of the present dissertation aimed to produce results that would contribute to overcome the shortage of knowledge regarding the long-term behavior of structural glass.

Since as it was considered important that the obtained results could represent real parameters, the performed experimental investigation aimed to simulate an authentic situation, as if a real structure was being monitored. So that the experimental test could originate results passible of being obtained in real structures, which contributes to enhance the applicability and redundancy of the experimental tests, several aspects were taken into consideration:

1. The experimented models consisted in full-scale beams, with geometrical properties similar to those applied to real structures, and whose composition includes materials widely used in the development of glass laminates:
2. The applied thermal load consisted on the natural daily and seasonal fluctuations. The option of including non-manipulated thermal load was considered so that the models were subjected to real temperature values, as the application of short severe thermal loads hinders the full applicability of the experimental results and their representativeness of real structural behavior.

3. The consideration of laminated glass beams in both cracked and intact conditions was essential to the performed investigation. It allowed not only the characterization and comparison of the long-term behavior of laminated glass elements of models with different physical conditions, but also the evaluation of the contribution of the interlayer.

It was expected that the experimental research provided redundant results, contributing not only for a better understanding of the long-term behavior of laminated glass but also for the precise calibration of future numeric models.

The following sections aim to expose the aspects associated with the performed experimental research, including information regarding the geometry of the models, the test layout and protocol, the chosen instrumentation, the obtained results and respective comments.

4.2 Geometry and Experimental Layout

The tested models consisted of double-layer 10 mm annealed glass plies with a 1.52 mm thick layer of SentryGlas®. The glass sheets, whose dimensions are 3000 x 300 mm, were perfectly leveled and present polished beveled edges. The geometry of the models and the adopted experimental layout are depicted in Figure 4.1.

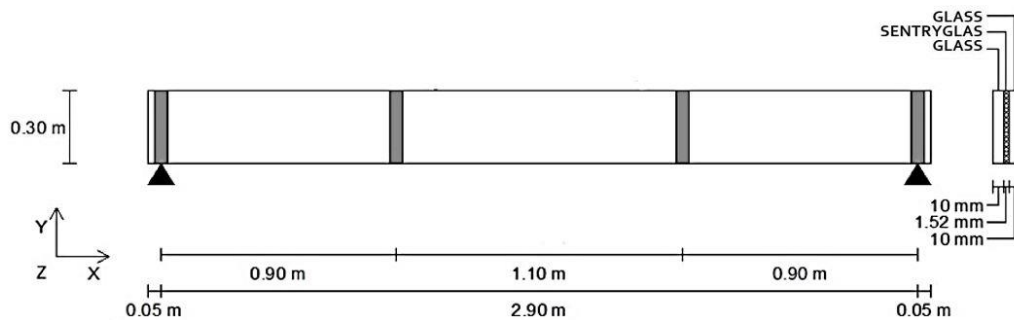
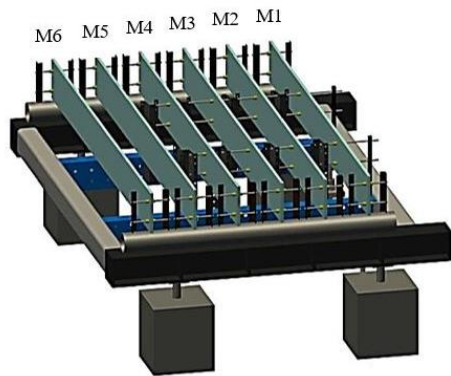


Figure 4.1 – Experimental layout and model geometry.

The performed experimental research included six full-scale models. Note that models 1, 2, 3, and 4 are fractured and models 5 and 6 are intact. To properly identify the models, a representation of the test apparatus is presented (Figure 4.2 a)). The laminated glass beams were supported by an external system constituted by several elements characterized by high rigidity (Figure 4.2 b)). This is of the utmost importance in the sense that the deformations expected in the models are considerably small and the measuring instruments are very sensitive to external disturbances.



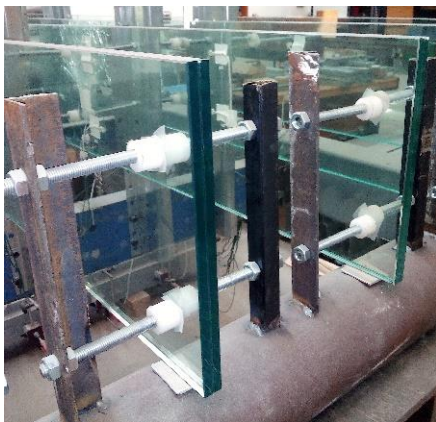
a) Model identification



b) Layout's perspective

Figure 4.2 - Model identification and layout's perspective.

The models were simply supported vertically at each end. Since the tested models were particularly slender, their movements were also restricted laterally in the proximity of the vertical supports by means of endless screws capped with nylon heads, to prevent the occurrence of buckling phenomena (Figure 4.3 a)). The cracked beams also had lateral supports at $1/3$ and $2/3$ of the length of the beams (Figure 4.3 b)).



a) Simple vertical support and lateral support



b) Lateral support

Figure 4.3 - Details of the adopted vertical and lateral supports.

4.3 Instrumentation

The utilized instruments included: a thermocouple device, whose objective was to monitor the values of the environmental temperature, since this parameter has a critical effect on the behavior of the structure; a set of vertical deflectometers (Figure 4.4 a) and b)), fitted at the bottom of each model at $1/4$ and $1/2$ of the total span of the beams (Figure 4.5 a)), to determine

the evolution of the deformations of the beams; and a set of unidirectional strain gauges (Figure 4.4 c)), placed at key locations (Figure 4.5 b) and c)), which were used to measure the strain evolution, complementing the results of the deflectometers and allowing a proper characterization of the behavior of the beams. It is important to refer that the strain gauges were placed on both sides of the models in order to detect and measure any out-of-plane deformation that might occur during the experimental tests, which is of the utmost importance, since the magnitude of the results is very small, the impact of this phenomenon on the measurements should not be considered.

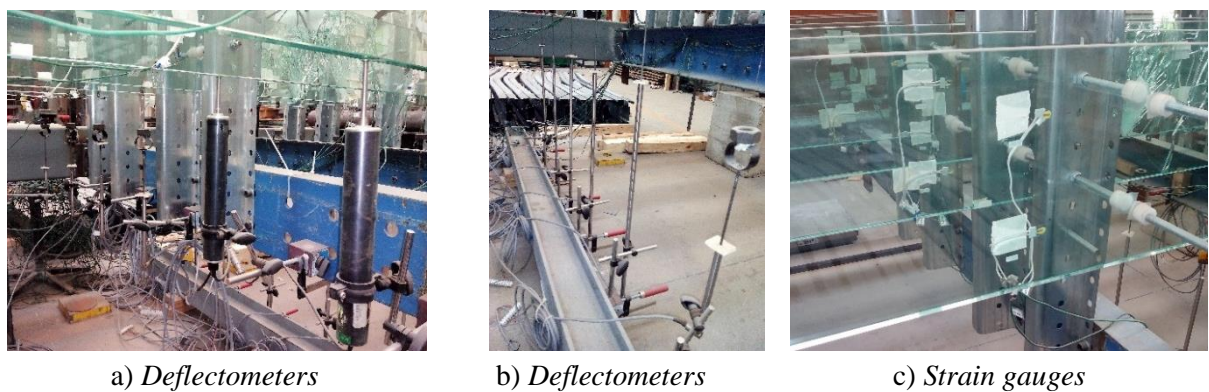


Figure 4.4 – Instrumentation.

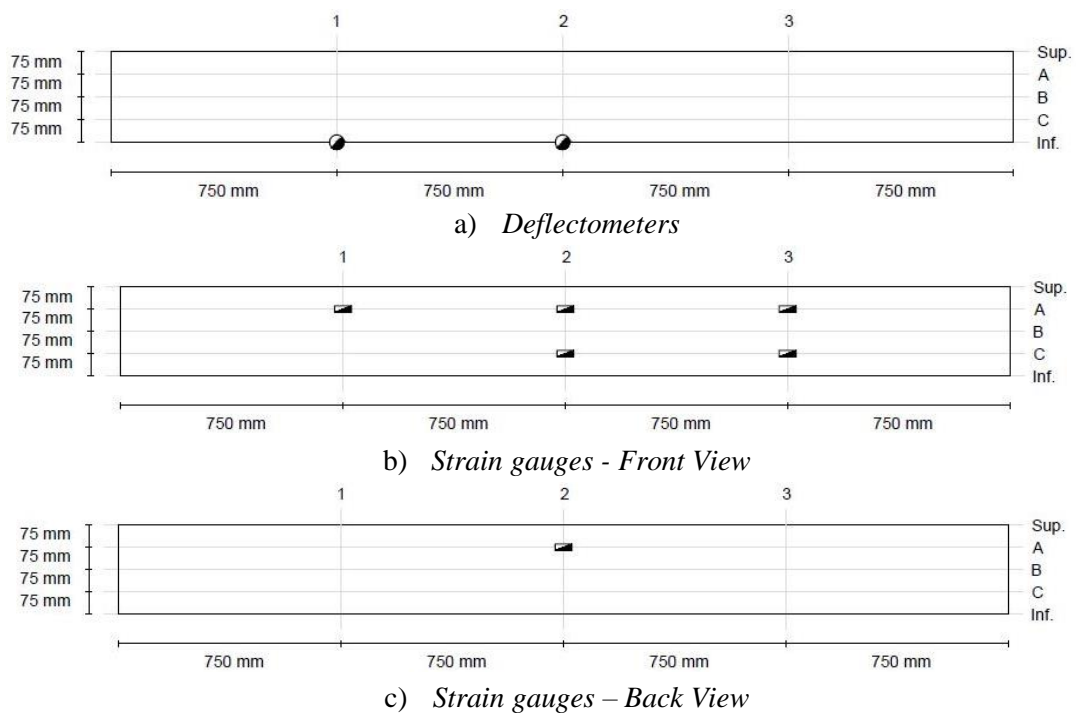


Figure 4.5 - Location of the adopted instrumentation.

4.4 Test Protocol

Firstly, the test apparatus was assembled as described in section 4.2 and the considered recording instruments were attached. After that, an initial loading phase was initiated, in which samples 1 to 4 were subjected to a mechanical vertical load until they fracture (Figure 4.6).

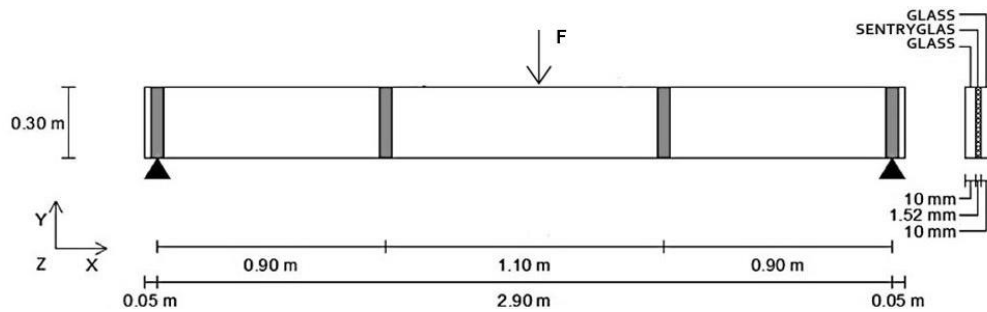
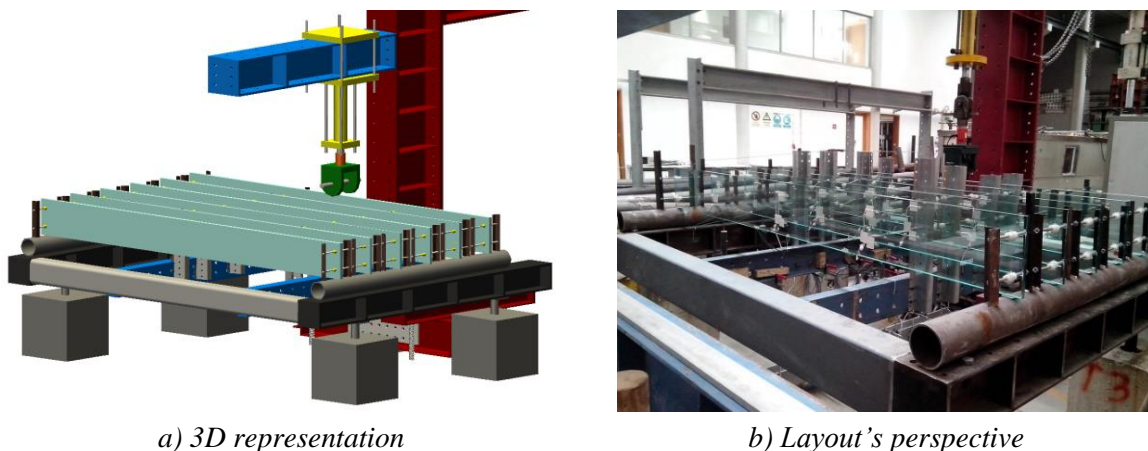


Figure 4.6 – Loading scheme.

The mechanical load was applied by means of a hydraulic jack on each of the first four models, sequentially (Figure 4.7).



a) 3D representation

b) Layout's perspective

Figure 4.7 – Loading-phase layout.

The procedure took approximately 0,1 days, during which both the evolution of the applied force and of the consequent deflections were measured. It is important to refer that all the instruments were zeroed at this stage, which results in the disregard of the impact of the self-weight of the beams in posterior measurements of both strains and deflections.

To understand the impact that resetting the instruments had on the measurements, the theoretical strains caused by the self-weight of the models were determined. This procedure was developed

by means of an auxiliary calculation software (Ftool). In these calculations, it was assumed that the transversal section of the models was only composed by the glass layers, disregarding the presence of the interlayer (Figure 4.8), and that the only acting load was the self-weight of the glass sheets. Glass is characterized by a unit weight of 25 kN/m^3 , which corresponds to a uniformly distributed load of $0,15 \text{ kN/m}^3$ (Figure 4.9).

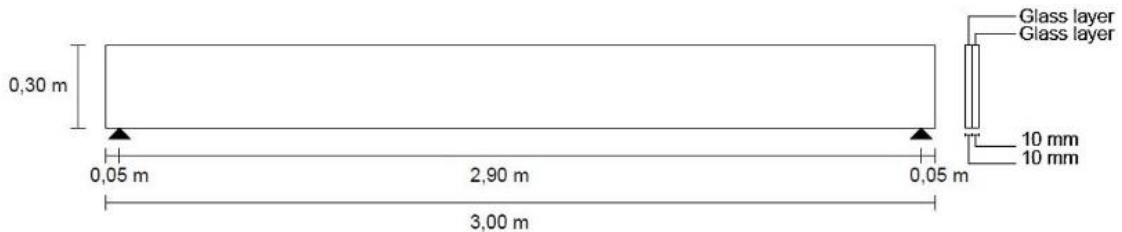


Figure 4.8 – Adopted model geometry for the determination of the theoretical strains.

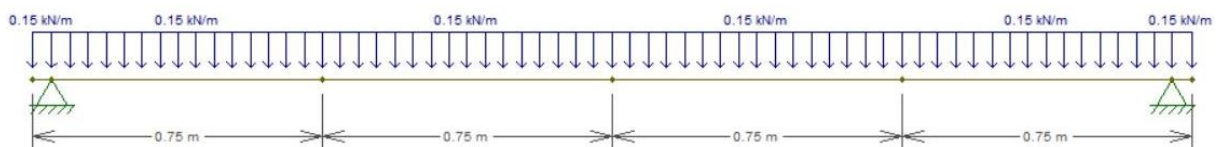


Figure 4.9 - Schematic representation of the considered layout.

The resulting deformed configuration is presented in Figure 4.10.

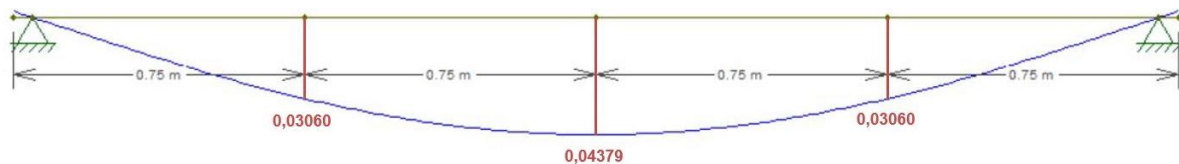


Figure 4.10 – Deformed configuration of the models (vertical displacements in mm).

Due to the assumed simplifications, the obtained theoretical values were not exactly coincident to those that will likely have occurred in the models. The disregard of the presence of the lamination film implicates that a significant part of the deformation of the models and consequent vertical displacements was omitted.

To determine the theoretical strains provoked by the self-weight of the beams, it became necessary to calculate the stresses that this load induced. As self-weight is a vertical load, only the consequent bending moment around y (M_y) contributed for the theoretical stresses of the models. Figure 4.11 displays the bending moment diagram that resulted from the self-weight of the beams. Note that these calculations only revealed the theoretical strains on the intact beams.

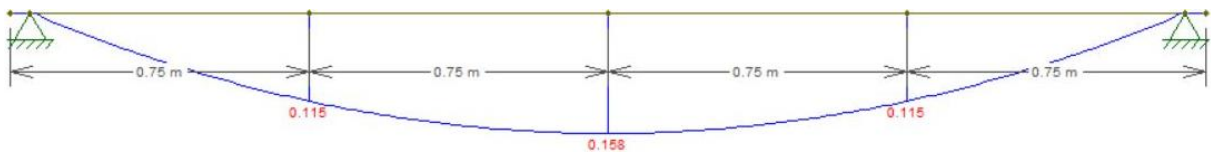


Figure 4.11 - Diagram of the bending moments around y axis (bending moments in kN.m).

Since the experimented beams were not subjected to any axial forces and that the acting loads only cause bending moments around the y axis, the models could be considered simply bended and the stress values of the several section points that correspond to the location of the applied strain gauges could be obtained through Equation (9) (Dias da Silva, V., 1995).

$$\sigma = \frac{M_y}{I_y} \cdot z \tag{9}$$

In this equation, M_y corresponds to the bending moment of the considered transversal section, z is equal to the distance between each point of the section and the neutral axis (which in this case passes through the geometrical center of the transversal section parallel to the y axis), and I_y is the moment of inertia of the transversal section ($I_y = 0.000045\text{m}^4$). The diagram of the theoretical stress of the transversal section of the beams at midspan and at $\frac{1}{4}$ of the span of the beams as shown in Figure 4.12 and Figure 4.13, respectively.

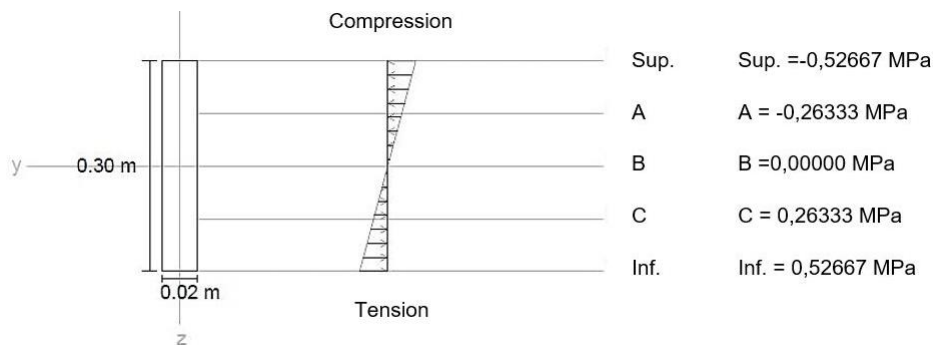


Figure 4.12 – Diagram of the stresses for the bending moment at midspan.

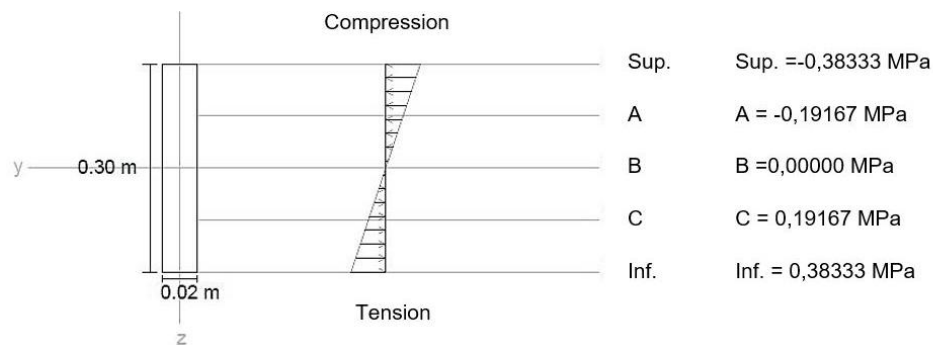


Figure 4.13 - Diagram of the stresses for the bending moment at $\frac{1}{4}$ of the span of the beams.

The theoretical value of the strains of the beams is directly related to the theoretical stress value that occurs in the models and to its Young’s modulus (E). As glass is a homogeneous material with linear elastic behavior until its abrupt rupture, its strains can be obtained through Hooke’s unidimensional law (Equation (10)) (Dias da Silva, V., 1995).

$$\varepsilon = \frac{\sigma}{E} \tag{10}$$

Through the application of Equation (10), it was possible to determine the theoretical values of the strains of the models, in each of the considered key locations (Table 4.1).

Table 4.1 – Theoretical strains in the locations of the considered strain gauges.

Strain gauge location	Stress [MPa]	Strain [m/m]
1A	-0.19167	$2,7381 \times 10^{-6}$
2A	-0.26333	$3,7619 \times 10^{-6}$
3A	-0.19167	$2,7381 \times 10^{-6}$
2C	0.26333	$3,7619 \times 10^{-6}$
3C	0.19167	$2,7381 \times 10^{-6}$
2A(B)	0.26333	$3,7619 \times 10^{-6}$

The determination theoretical strains became essential to properly evaluate the measured strains in each of the experimented models.

Regarding the first loading-phase, the deflection-time and load-deflection diagrams are presented in Figure 4.14 and Figure 4.15. To better understand the evolution of the deflections, the theoretical value of the deflection that the applied force should originate at both ¼ and ½ span is also presented (Figure 4.15 a) and b)). This theoretical value was determined analogously to the deflections resulting from the self-weight of the beams.

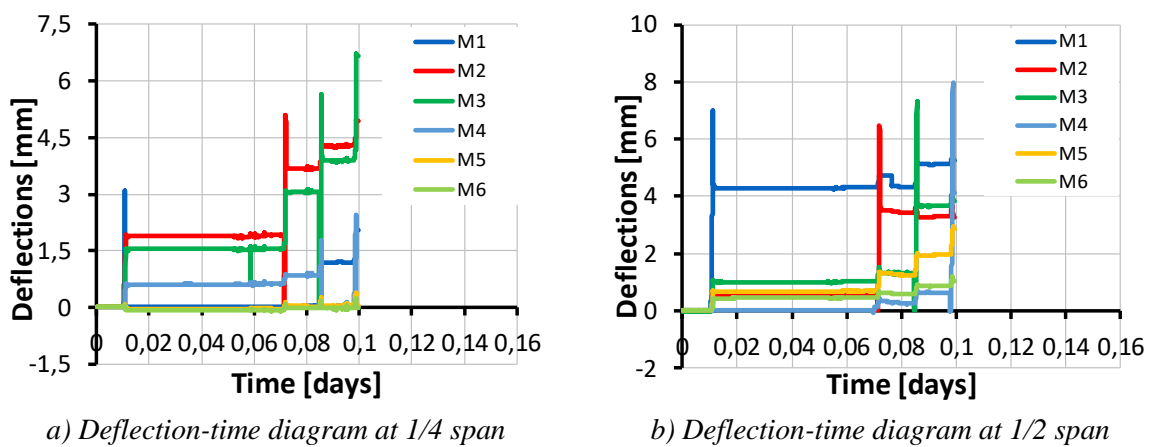


Figure 4.14 - Loading-phase results – Deflection-time diagrams.

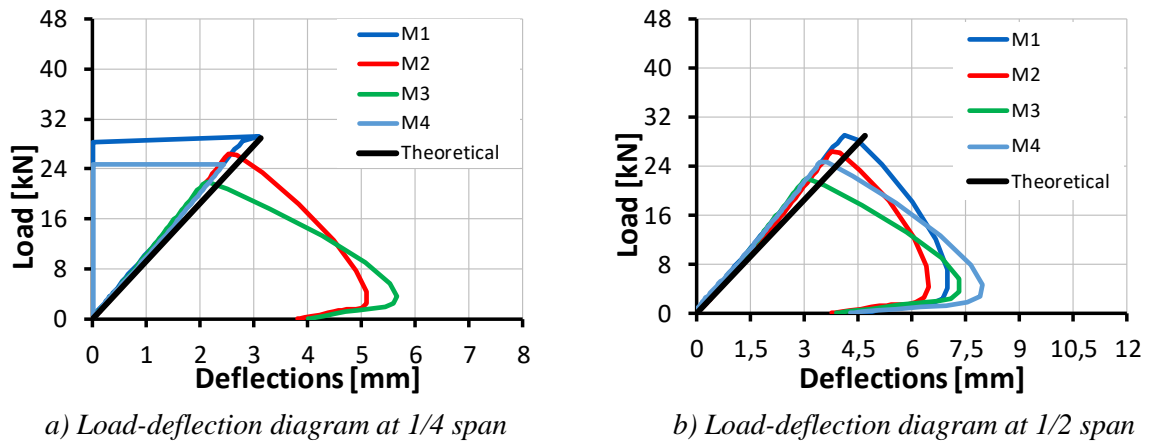


Figure 4.15 – Loading-phase results – Load-deflection diagrams.

In Figure 4.14 a) and b), it is possible to observe the range of the deflection values that characterized each model upon the breakage of models 1 to 4. It is noticeable that, although models M5 and M6 were not mechanically loaded, their deflections were also influenced by the procedure. This occurrence was a result of the fact that all the tested beams shared the same support structure.

The anomalous evolution of M1 and M4 curves presented in Figure 4.15 a) were caused by the rupture of the deflectometers wires consequent to the fracture of the models.

Upon the beginning of the developed long-term experimental tests, the measurement of the extensions and the deflections of the models was restarted, and the equipment was zeroed again in order to remove of the effect of the applied mechanical load. Consequently, the obtained results only revealed the influence of the environmental temperature on both the strains and deflections of the models.

4.5 Experimental Results

In this section, an evaluation of the conditions of the models at the end of the experiments is presented, as well as a brief description of the obtained data.

The patterns of the fractures that characterized the broken models (Models 1, 2, 3 and 4) at the end of the duration of the performed long-term tests can be observed in Figure 4.16. Models 5 and 6 remained intact and without any visible fractures.



a) Model 1 – Front view



b) Model 1 – Back view



c) Model 2 – Front view



d) Model 2 – Back view



e) Model 3 – Front view



f) Model 3 – Back view



g) Model 4 – Front view



h) Model 4 – Back view

Figure 4.16 – Fracture patterns at the end of the experimental research.

The fractures were fan shaped and initiated close to the maximum stress value. Posterior to the occurrence of the first fissure, additional cracks developed in high stressed regions, from the bottom to the top of the beams. As they reached the top of the beams, the evolution of the cracks became a consequence of the smashing forces that develop in this region.

Even with identical loading and support conditions, the fracture patterns were distinct in every model and amongst the glass sheets of each beam. This occurrence was expected because fracture depends mostly on the distribution of its surface flaw, which is random in nature. In Figure 4.17, the front view of the obtained fractures and respective position in each of the fractured models is presented.

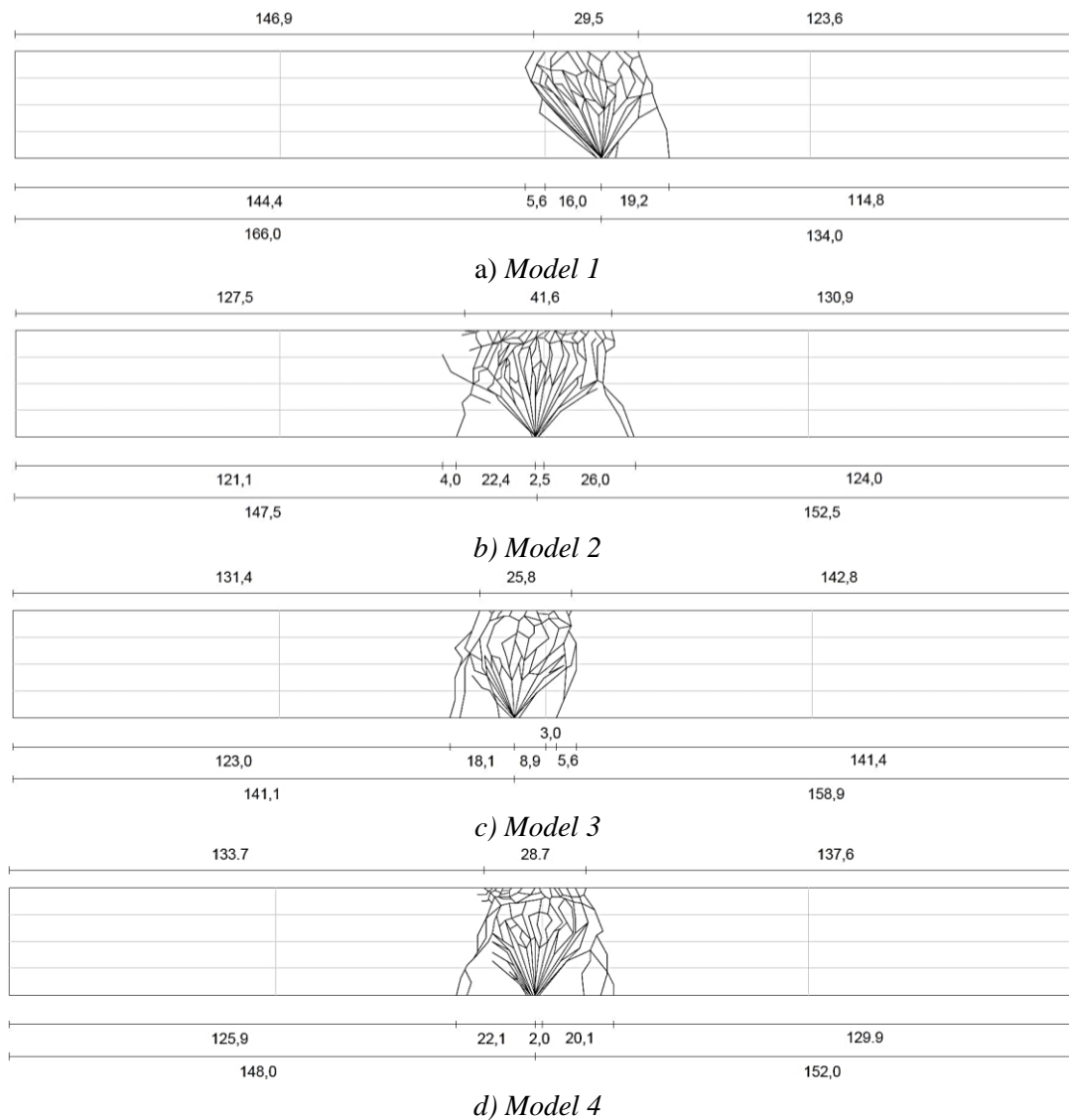


Figure 4.17 - Schematic representation of the final fractures (dimensions in millimeters).

The geometrical properties considered to be relevant in the assessment of the experimental results can be observed in Table 4.2.

Table 4.2 – Geometrical properties of the final fractures.

Model	Distance between the middle of the fracture and the midspan of the model [cm]	Area of the fractured zone [cm²]	Total width of the fractured zone [cm]
1	16	767,99	40,8
2	2,5	804,66	54,9
3	3,0	704,86	35,6
4	2,0	734,78	44,2

Although none of the crack initiation location developed at mid span, it is important to note that the instruments applied at midspan are located inside the fractured areas, as their measurements may be affected by the fracture itself.

Regarding the measured values, it is important to refer that the recording of the evolution of the values was not continuous during the full duration of the experimental research. The data was measured during thirteen periods (Table 4.3).

Table 4.3 – Recording intervals.

Interval	Start Time	End Time
1	22/04/2015, 17:16:19	03/05/2015, 20:26:19
2	06/05/2015, 11:05:20	05/06/2015, 16:05:19
3	08/06/2015, 15:00:37	09/06/2015, 08:50:38
4	09/06/2015, 09:01:54	25/06/2015, 10:11:53
5	26/06/2015, 16:19:53	02/07/2015, 14:29:52
6	02/07/2015, 15:25:59	13/07/2015, 23:35:58
7	15/07/2015, 16:56:25	05/08/2015, 01:36:24
8	05/08/2015, 15:16:15	13/11/2015, 10:56:14
9	02/02/2016, 16:33:02	03/02/2016, 12:13:01
10	03/02/2016, 12:35:20	08/02/2016, 10:55:21
11	08/02/2016, 20:49:54	23/02/2016, 16:59:54
12	23/02/2016, 17:52:54	01/05/2016, 18:02:53
13	02/05/2016, 11:12:43	30/05/2016, 10:42:42

The initial loading phase applied to models 1 to 4 was not included in the final diagrams.

The thermocouple and midspan deflectometer of models 5 and 6 were disconnected after the 11th interval. Several instruments were also disrupted in other occasions, as described in Chapter 5.

5 COMPARATIVE ANALYSIS

5.1 Introduction

As previously established, the loadings of the experimental models included the self-weight of the laminated glass beams and environmental temperature. However, the impact of self-weight was removed from the measurements upon the restart of the instruments. Consequently, it was expected that the values of both deflections and strains would be particularly small, which may have influenced the magnitude of the impact that external effects had in the readings.

In most cases, the measuring devices of long-term tests on structural glass only include a single deflectometer. To minimize the error percentage in the recorded values, the set of instruments of the performed experimental tests included two deflectometers and a set of strain gauges placed at six key locations throughout the models. By analyzing and comparing the strain values in each location, it became possible to establish several conclusions regarding the distribution of the internal forces of the beams and to monitor the occurrence of out-of-plane deformations.

Although the instruments setup was quite detailed, the measured parameters are extremely small and its variation is difficult to be accurately measured. Furthermore, the experimental layout was in a non-isolated facility with heavy machinery, where daily work operations may have affected the results. For these reasons, it was essential to take special care when analyzing the results, as they include many aspects. Therefore, it was necessary to develop a tailored analysis to remove measuring errors from the results.

The causes for irregular readings in the measuring devices are listed below:

1. Application of measuring instruments in positions where glass is broken or shattered;
2. Deterioration of the connection between the deflectometers and the models;
3. Operation of heavy machinery that caused either mechanic or electromagnetic disturbances in the proximity of the experimental layout;
4. Human action (careless/accidental).

The main objective of Chapter 5 was to explain how the experimental data was treated to exclude non-valid measurements and parasite influences, and to interpret the real results.

5.2 Evaluation of the Recorded Deflections

The following evaluation focused on the determination of the interferences of the measured deflections and correspondent causes. The measured deflections are presented in Figure 5.1. Since the deflections on the intact models were much smaller than those on the fractured models, a different scale was necessary to make the fluctuation of these values more perceptible.

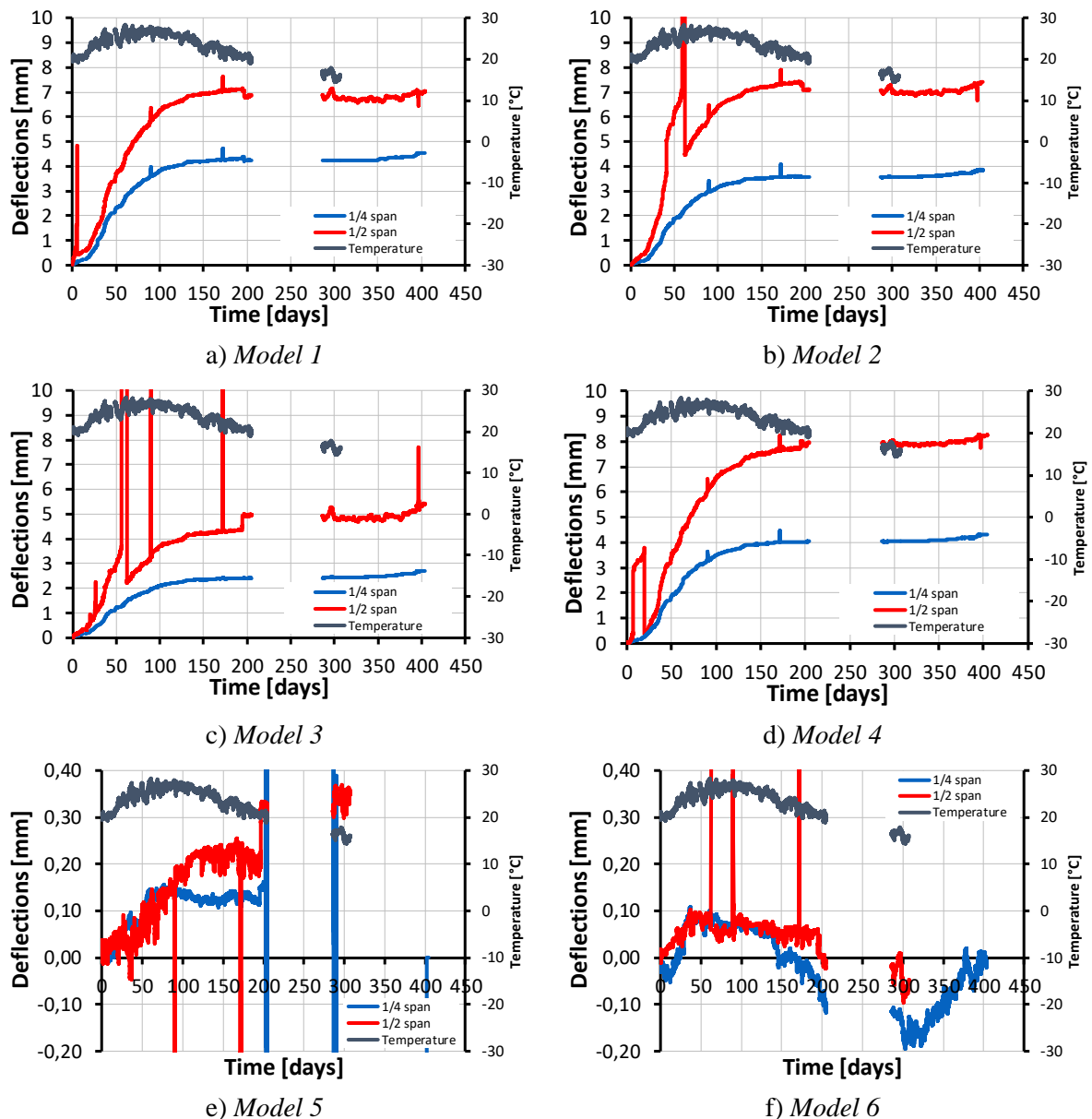


Figure 5.1 – Recorded deflections.

From Figure 5.1 it was possible to realize that all the instruments were able to register the vertical displacements adequately and without no more than a few discrete disturbances. In order to assess if there were any common causes for the disturbances, the flaws registered by each deflectometer were summarized in Table 5.1.

Table 5.1 – Noted disturbances of each deflectometer.

Day	Deflectometer												
	Model 1		Model 2		Model 3		Model 4		Model 5		Model 6		
	1/4	1/2	1/4	1/2	1/4	1/2	1/4	1/2	1/4	1/2	1/4	1/2	
5 th	x	✓	x	x	x	x	x	x	x	x	x	x	x
7 th	x	x	x	x	x	x	x	✓	x	x	x	x	x
26 th	✓	x	x	x	x	✓	x	x	x	✓	x	x	x
40 th	x	x	x	✓	x	✓	x	✓	x	x	x	x	x
51 th	x	✓	x	✓	x	✓	x	x	x	x	x	x	x
56 th	x	✓	x	✓	x	✓	x	x	✓	✓	x	x	x
58 th	x	x	x	✓	x	✓	x	x	x	x	x	x	x
62 th	x	✓	x	x	x	x	x	x	x	✓	x	✓	✓
90 th	✓	✓	✓	✓	x	✓	✓	✓	x	✓	x	✓	✓
171 th	✓	✓	✓	✓	✓	✓	✓	✓	x	✓	x	✓	✓
194 th	✓	✓	x	✓	x	✓	x	✓	✓	✓	x	✓	✓
307 th	x	✓	x	✓	x	✓	x	✓	x	x	x	x	x
396 th	✓	✓	x	✓	x	✓	x	✓	✓	x	x	x	x

Note that the indicated dates were a mere reference in time of the disturbances, as most of them had an effect that propagated over time, affecting more than one measurement. Another aspect to have into consideration is that, according to Figure 5.1, not all of the disturbances listed above had the same impact, since most of them are not even visible in the presented scale.

The deflections of Model 1 (Figure 5.1 a)) evolved as expected. Although the deflectometer of midspan revealed five irregularities that were not visible on the device applied to $\frac{1}{4}$ of the span of the beam (Table 5.1), the flaws that took place on the 90th, 171th, 194th and 396th day of the experiment were common to both instruments. This occurrence may indicate that either this model or the entire support structure was disturbed at those occasions.

The diagrams of Model 2 evolved as expected (Figure 5.1 b)). In spite of appearing to function adequately, the midspan deflectometer presented more irregularities than the one applied on $\frac{1}{4}$ of span. From those flaws, only two were also noted on the $\frac{1}{4}$ deflectometer (Table 5.1).

In Model 3 an unexpected situation occurred, as the midspan deflectometer presented several considerable irregularities that were not noticed by the second device (Figure 5.1 c)). In fact, the $\frac{1}{4}$ deflectometer was only able to notice a single irregularity, not even measuring the flaws that were registered by roughly all the instruments (Table 5.1).

In Model 4, both deflectometers presented an appropriate evolution (Figure 5.1 d)). Although it registered two of the disturbances that are visible in almost every deflectometer, the instrument placed at $\frac{1}{4}$ of span of Model 4 was not able to measure all of the flaws noticed by the midspan deflectometer, as happened in the previous models (Table 5.1).

It is quite perceptible that the midspan deflectometer of the fractured models registered a considerably larger number of irregularities during the experimental test. This situation may be explained by the fact that these instruments are located in the fractured zones of those models. The midspan sections of the fractured models are characterized by significantly low rigidity, which makes them much more susceptible to external mechanical factors, making it difficult for the applied deflectometers to accurately measure the vertical displacements of the experimented models in this location. Furthermore, it is possible that the fractured models have suffered additional deterioration during the long-term experiment like the aggravation of the existing fractures or even the detachment of glass shatters, which affects the values of the deflections.

In Model 5, the $\frac{1}{4}$ deflectometer displayed an initial anomalous evolution, as instead of growing over time, it diminished. This occurrence is not verified in any other model, which is why it becomes difficult to explain. The most probable cause was the faulty setup of the instrument. In addition to that, the measurements correspondent to the 9th and 10th period displayed considerable errors, which is why they were disregarded in posterior evaluations (Figure 5.1 e)). After the 292th day, the values went back to vary accordingly adequately. The values recorded by the midspan deflectometer seem to be adequate, suffering only a few perturbations until its disconnection on the 307th day (Table 5.1).

The instruments applied to the sixth model evolved as expected with the one placed at midspan presenting irregularities on the 62th, 90th, 171th and 307th days, right before it stopped recording (Table 5.1). The deflectometer applied to $\frac{1}{4}$ of span recorded its values without noticing any kind of disturbances.

In the case of the irregularities that were detected by the majority of the deflectometers, it seemed reasonable to assume that they were originated by some kind of external interference which affected the entire support system of the experiment. The irregularities that were only registered by one or two deflectometers may also have been caused by external impacts, although it is more likely to consider that they resulted from perturbations of one of the models, as they end up not affecting the remaining experimental layout

5.3 Evaluation of the Recorded Strains

The following analysis intended to identify the irregularities of the recorded strains and to establish its probable causes. The recorded strains can be observed in Figure 5.2.

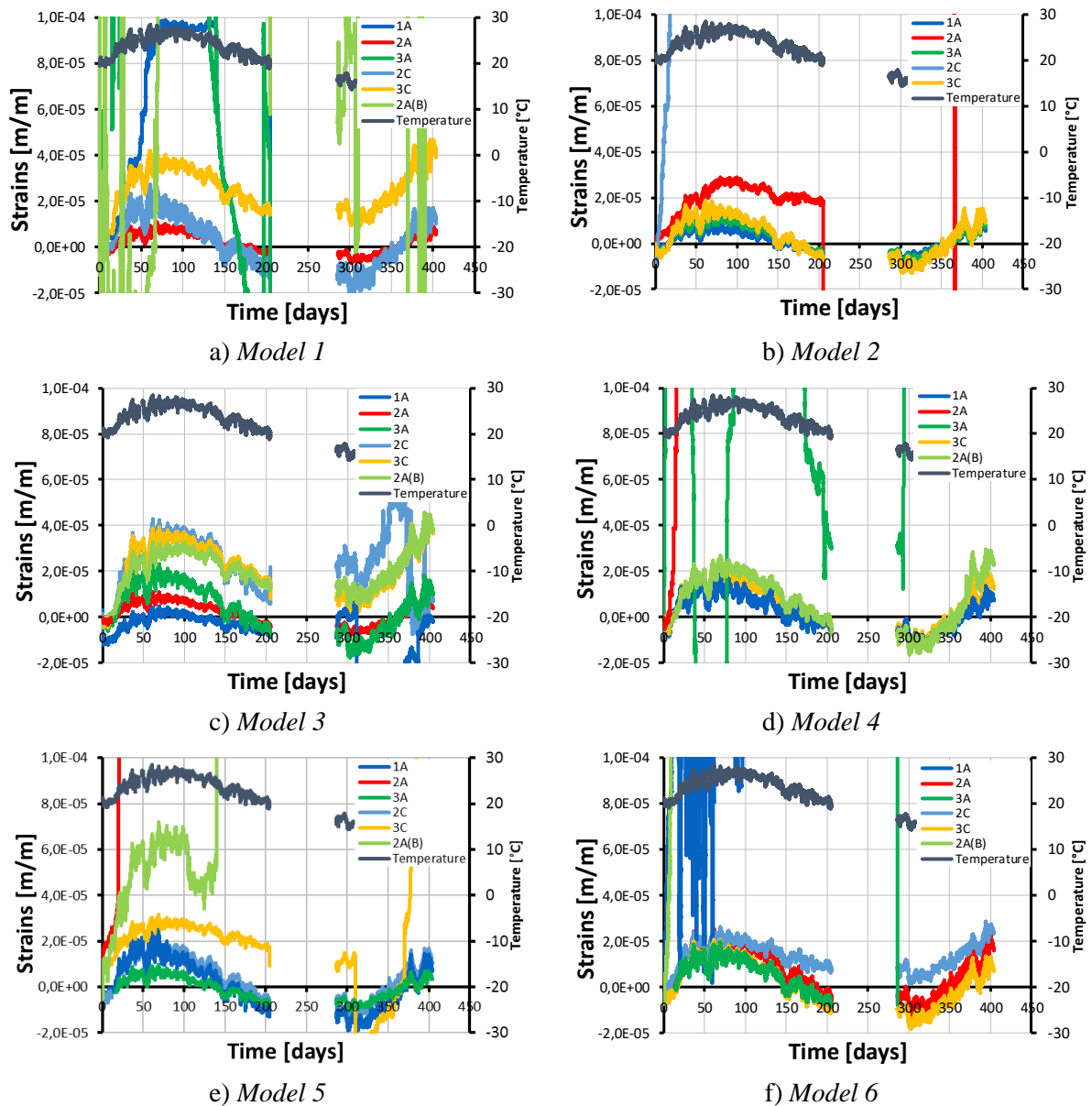


Figure 5.2 – Recorded strains.

It is important to refer that, in Models 1 to 4, the strain-gauges placed at midspan are located in the fractured areas, which makes them more prone to display less accurate results (Figure 5.3).

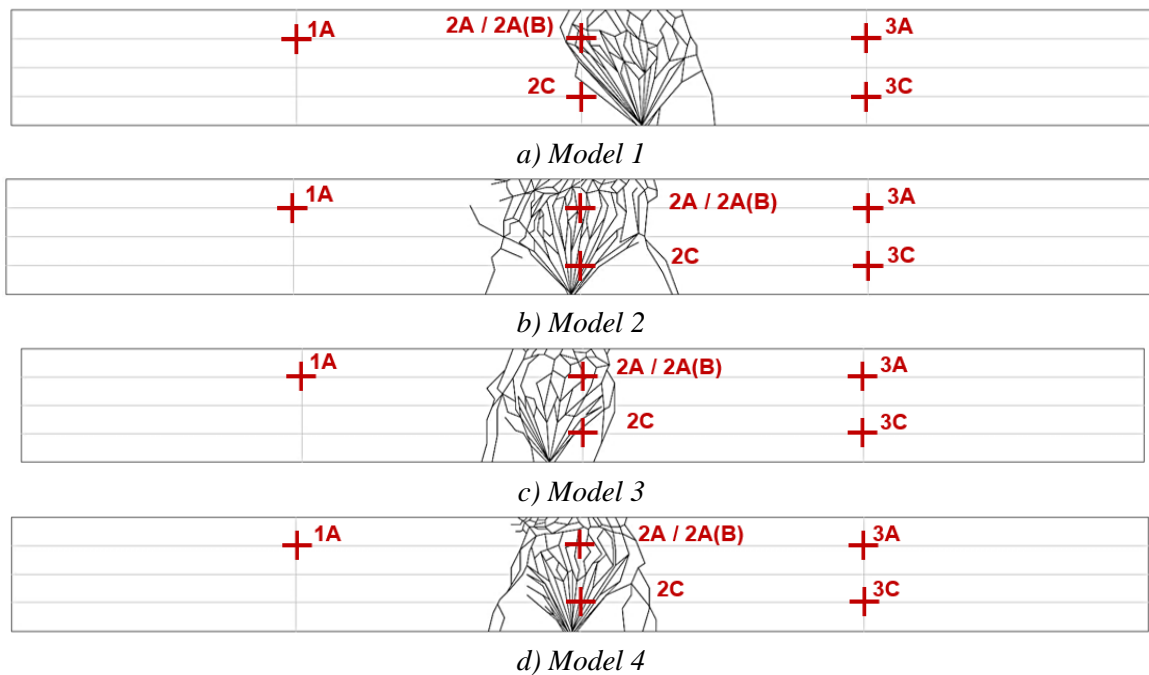


Figure 5.3 –Location of the strain gauges relative to the fractures.

5.3.1 Model 1

The 2A, 2C and 3C strain gauges placed of Model 1 seemed to have recorded fairly good results, as they were consistent with the measured temperatures and did not display the same inconsistencies as the deflectometers (Figure 5.2 a)). This allows to conclude that any irregularities that may take place in these instruments' data were most likely related with rigid body movements of the support structure, caused by external interferences. The values of the remaining instruments displayed several irregularities, which appeared to be independent of the variation of temperature and unrelated to each other, as they developed at different times in each of the strain gauges and displayed distinct variation rates. For that reason, it is probable that they were related to the inefficient attachment 1A, 3A and 2A(B) strain gauges.

The data of the 1A strain gauge revealed an extremely accelerated initial growth and higher susceptibility to the influence of the temperature, displaying wider daily amplitudes than the remaining strain gauges. This occurrence may have been potentiated by the rise of temperature that takes place in the first 120 days of the experiments, but it is a clear sign that the instrument was not properly attached. The abrupt growths that developed on the 29th, 50th, 55th, 63th, 71th, 92th, 170th and 197th day are a probable consequence of the gradual detachment of the instrument. These discrete flaws were removed to allow a better perception of the evolution of the strains. After the 204th day, the data was disregarded as the strains became too inconsistent.

Regarding the 3A strain gauge, its data contained severe flaws from the beginning of the experiment, which is why it was assumed as invalid.

As neither the recorded temperatures nor the midspan deflectometer displayed perturbations as significant as those presented by the 2A(B) strain gauge, the anomalous results presented by this instrument indicate that it was partially detached from the model or that it was applied in a location too fractured to allow accurate readings, which is why they were disregarded.

5.3.2 Model 2

According to the diagram of Figure 5.2 b), the strain gauges placed in the 1A, 3A and 3C locations of Model 2 functioned adequately, as their values appeared to evolve coherently with the fluctuation of temperature without any visible anomalies. The instruments applied in the 2A and 2C locations were unable to properly register the evolution of the strains during the full extent of the experimental research. The 2A(B) strain gauge did not record anything.

The strains measured by the 2A strain gauge fluctuated as expected until the 204th day. This irregularity was likely a consequence of the detachment of the instrument, as it cannot be explained neither by a drastic variation of temperature, which decreased much more moderately, nor by external perturbations of the experimental layout, as the respective deflectometer did not reveal any irregularities at the correspondent time. Since after the 204th day the recorded data was too irregular and had to be ignored in further analysis.

The values of the 2C strain gauge exhibited an accentuated growth since the beginning of the experimental test until the 20th day, after which the instrument seemed to have reached its maximum capacity and became unable to register any further data. The data was disregarded from posterior evaluations as it was considered insufficient to allow adequate comparisons.

5.3.3 Model 3

As perceivable in Figure 5.2 c), the data recorded by every strain gauge was fairly coherent with the variation of temperature during the experimental test, as there were only discrete irregularities detected by the devices placed on the 1A and 2C locations.

The diagram of the strains of the 1A strain gauge displayed two abrupt decreases, at the beginning of the experimental test and on the 310th day (Figure 5.2 c)). Smaller flaws were also

detected on the 204th, 336th and 386th days. None of these irregularities were verified on the deflectometers of Model 3, which is why they were disregarded from posterior analysis.

The variation of the values the 2C strain gauge appear to be much more accentuated than on the 2A (Figure 5.2 c)). Additionally, it was possible to distinguish several discrete flaws on the 204th, 310th, 316th, 344th, 353th, 371th, 377th and 394th, from which none is likely to be related to external layout disturbances, as they were not noted in the midspan deflectometer. These irregularities have most likely been caused by problems associated with the strain gauge such as a faulty connection between the device and the surface of the models or the progressive detachment of the instrument caused by the propagation of the fracture of the model.

5.3.4 Model 4

In Model 4 (Figure 5.2 d)), it was verified that only the strains measured by the 1A, 3C and 2A(B) evolved accordingly to the variation of temperature and without any significant flaws. The 2A and 3A strain gauges displayed inadequate values. The instrumenting placed in the 2C location was unable to register any kind of information.

The strains recorded by 2A instrument evolved as expected until the 5th day, after which they began to increase until the strain gauge reaches its full capacity in the 30th day. This occurrence is unrelated to the variation of temperature, as its values are stable at the correspondent time. However, the midspan deflectometer of this model registered a significant perturbation, which could implicate that the model or even the support system itself was tampered.

The 3A strain gauge registered significantly irregular data since the beginning of the experimental test, which resulted in having to reject it.

5.3.5 Model 5

In Model 5 (Figure 5.2 e)), the strain gauges placed in the 1A, 3A and 2C locations were able to record fairly good results. The remaining devices displayed considerable errors.

Regarding the 2A strain gauge, its initial values were consistent with the variation of the temperature until the sudden increment registered in the 2A strain gauge in the 20th day, which only stops with the overstrain of the instrument on the 72th day, after which it was unable to record more values, as it happened with the 2A strain gauge of Model 4. These anomalous results were not posteriorly analyzed.

The 3C device shows a fall in the values of the strains on the 204th day and on the 310th day which are not noticeable in any of the deflectometers of Model 5 and seem to be independent of the fluctuation of the temperature. This could indicate a problem with the connection between the strain gauge and the model. After the 310th day, the strains seem to increase more drastically than expected, reaching an even more accentuated growth rate after the 370th day. All the data recorded after this point was considered to be irrelevant.

The values of the 2A(B) strain gauge evolved coherently with the temperature until the 140th day, when they began to increase considerably, stabilizing only in the 286th day. After this the values went back to fluctuate according to what was expected. For this reason, the evolution of the strains during this period was disregarded from the analysis

5.3.6 Model 6

In Model 6 (Figure 5.2 f)), the 2A, 2C and 3C strain gauges presented good results as its evolution was consistent with the variation of the temperature values. The remaining devices presented several inconsistencies.

The values measured by the 1A strain gauge had considerable issues and were discarded.

The 3A strain gauge evolved coherently with temperature, with the exception of a considerable discrete increment that took place on the 286th day, which was not detected by the deflectometers of this model. It is expected that by correcting this error the graph will become similar to those resulting from properly functioning strain gauges.

Until the 20th day, the growth of the 2A(B) strain gauge was much more accentuated than expected. This growth was removed from the graph since, after this period, the fluctuation of the values went back to vary as expected. The probable cause for this situation was, the occurrence of out-of-plane deformations. There was also an irregularity in the values of 2A(B) between the 310th and 370th days, which was unrelated to the temperature, as it did not present any relevant alterations at the same time. The occurrence was also noted in the midspan deflectometer of the model, which could indicate that the experimental layout was disturbed.

5.3.7 Final Notes

It is important to note that models 1 to 4 are cracked and that the fractured zone coincides with the locations where the 2A, 2C and 2A(B) strain gauges were placed. This factor can be

responsible for some of the irregularities that occurred in these locations during the performed long-term experiments, as is particularly visible in models 1, 2 and 4.

Although out-of-plane deformations may develop in both intact and fractured models, in fractured models, its impact is less accentuated than in fractured beams, since their shattered areas are much more deformable and because they present an inferior rigidity, allowing the dissipation of the stresses by vertical deflections instead of having to suffer out-of-plane deformations. This occurrence can result in high discrepancies between the strains on the 2A and 2A(B) locations and was particularly noticeable in Models 3 and 6.

It was also possible to note that several devices presented irregular values on the 204th and 310th days. As none of the applied deflectometers was able to record any anomaly at this date, these flaws could have been caused by the influence of an external factor, such as humidity or solar radiation, in the connection between the devices and its corresponding models.

5.4 Data Treatment

As previously indicated, this section contains the details of all the procedures utilized to improve the quality and accuracy of the obtained data.

Firstly, the discrete flaws mentioned in sections 5.2 and 5.3 were removed from the graphs. To do so, the values of the measurements after the end of each irregularity were considered to be equal to the last adequate measurement previous to the occurrence of the discrepancy.

With the objective of achieving continuous diagrams, a second intervention was performed. It was assumed that the growth of the values during the intervals where the instruments were not recording was approximately equal to the media between the variation of the last three days of the data series that comes before the interruption and the variation of the first three days of the subsequent data series. By estimating the evolution of the parameters during these intervals, it was expected to attain a better perception of the real range of values of the measured parameters.

5.5 Final Deflections

The assessment of the deflections was an important procedure to better comprehend the structural behavior of the models. The final diagrams of the deflections in Figure 5.4.

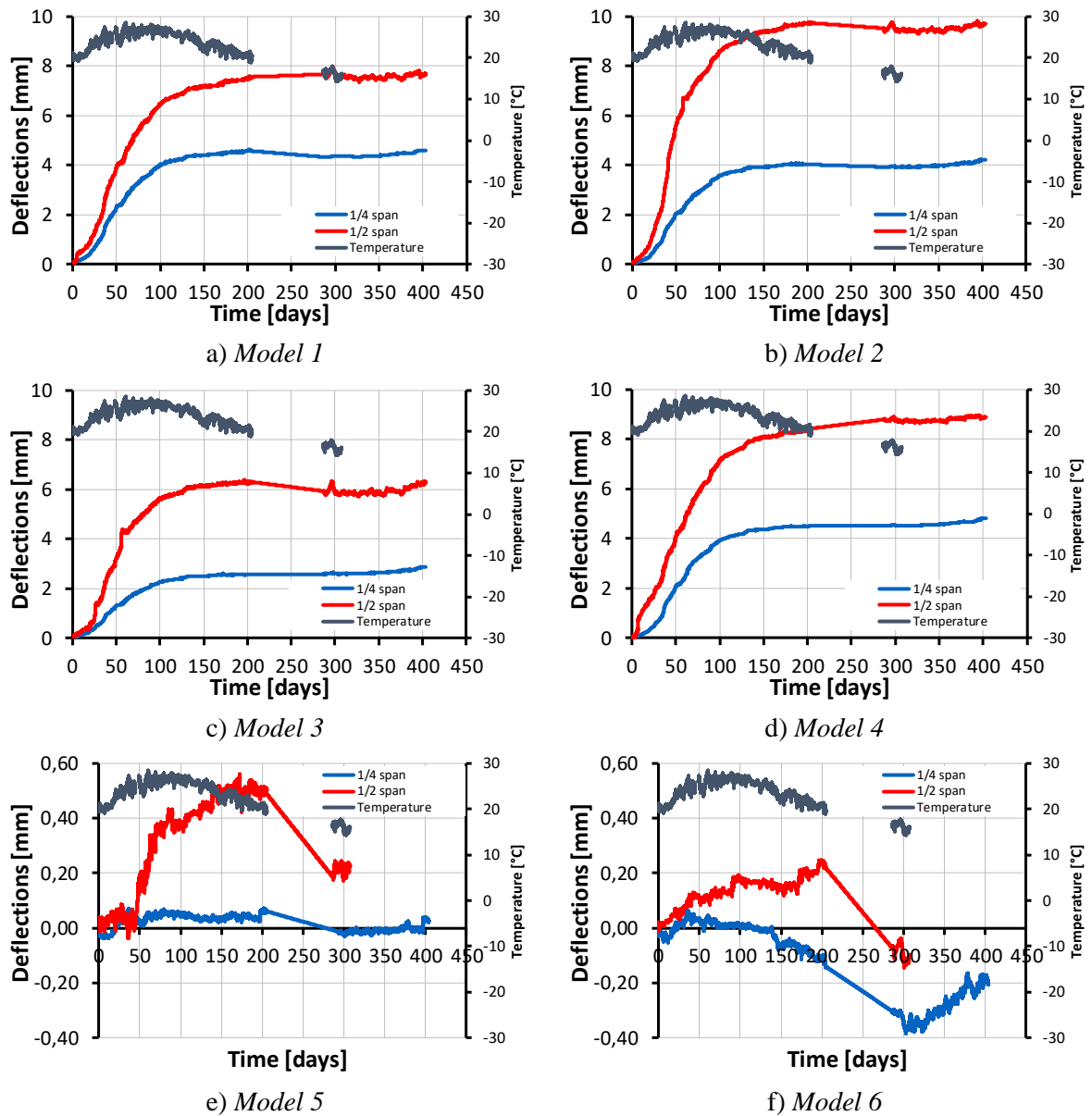


Figure 5.4 – Final deflections at 1/2 and 1/4 of span.

As expected, the deflections measured at 1/4 of span are considerably smaller than those that took place at midspan, which is a natural consequence of the diagram of bending moment. From the obtained results, it was also possible to perceive that the deflections are considerably larger in the fractured models and that its growth is more accentuated in the first 100 days of the experimental tests. This growth is a main consequence of the relaxation of the interlayers.

It was noticeable that the deflections measured in the intact models reached negative values during part of the experiment. Those values were probably induced by the thermal expansion

of the support structure. This occurrence may have resulted in the elevation of the models, causing negative vertical displacement when the lifted distance was larger than the vertical displacement that took place in the model. This situation implicates that the support structure was not completely indeformable as intended, which prevented the deflectometers from recording the evolution of this parameter accurately.

The expansion of the support structure has probably affected all the models. However, it is only perceptible in the intact models because their deflections are much smaller and are not able to completely cancel out the elevation caused by the deformation of the external support system.

5.5.1 Analysis of the Final Deflections

Through the observation of the diagrams presented in Figure 5.5 it was possible to establish additional conclusions regarding the effects of long-term actions in laminated glass beams.

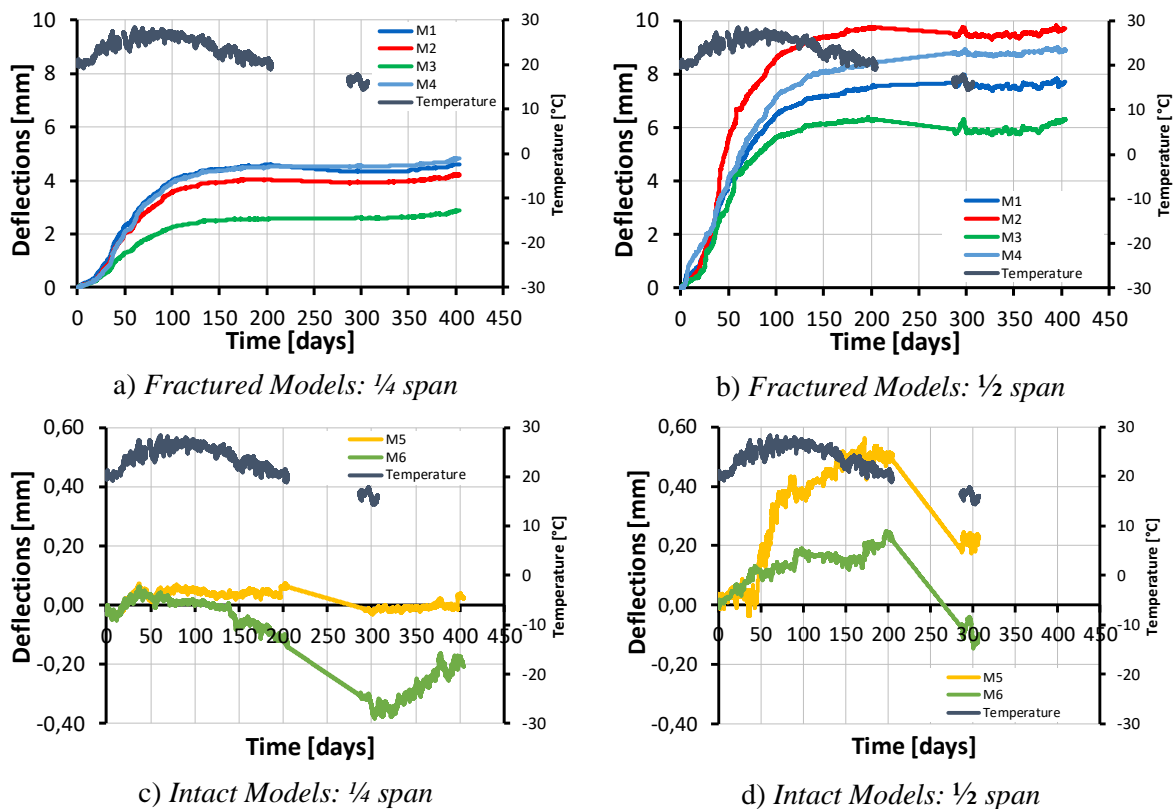


Figure 5.5 – Comparison of the final deflections.

The analysis of Figure 5.5 a) allows to determine that it was Model 4 that displayed the highest deflections and Model 3 that displayed the lowest.

At midspan, the model responsible for presenting the lowest vertical displacements was, once again, Model 3. In what respects the highest deflections, it was clear that the responsible model was Model 2, with a maximum value of 9,8259 millimeters (Figure 5.5 b)).

Regarding the deflections of the intact models, it is clear that Model 5 reached considerably higher values in both $\frac{1}{4}$ and $\frac{1}{2}$ span (Figure 5.5 c) and d)).

To better understand the performed analysis on the final values of the deflections, the maximum values obtained in both fractured and intact models were resumed in Table 5.2 and Table 5.3.

Table 5.2 – Maximum deflections in the fractured models.

Model	Maximum Deflection at $\frac{1}{4}$ span [mm]	Maximum Deflection at $\frac{1}{2}$ span [mm]
1	4,614963	7,966906
2	4,226825	9,825846
3	2,869394	6,395644
4	4,815924	8,978085
Average	4,131777	8,291620

Table 5.3 – Maximum deflections in the intact models.

Model	Maximum Deflection at $\frac{1}{4}$ span [mm]	Maximum Deflection at $\frac{1}{2}$ span [mm]
5	0,072794	0,562960
6	0,061195	0,247830
Average	0,066994	0,405395

It is important to take into consideration the noticeable discrepancy of the values in the broken and the intact models. While the maximum value in the broken models is 4,8159 and 9,8259 millimeters, at $\frac{1}{4}$ and $\frac{1}{2}$ of span, respectively, in the models 5 and 6, the maximum deflections are 0,07279 and 0,5629 millimeters. The maximum values measured in the intact beams correspond to 1,51% and 5,73% of the values of the fractured models both at $\frac{1}{4}$ and $\frac{1}{2}$ span.

5.6 Final Strains

The assessment of the obtained strains allowed to evaluate the long-term effect that the considered actions had on the models and to characterize the stress distribution of the experimented beams. The final diagrams of the registered strains in the six considered locations (1A, 2A, 3A, 2C, 3C, and 2A(B)) are presented in Figure 5.6.

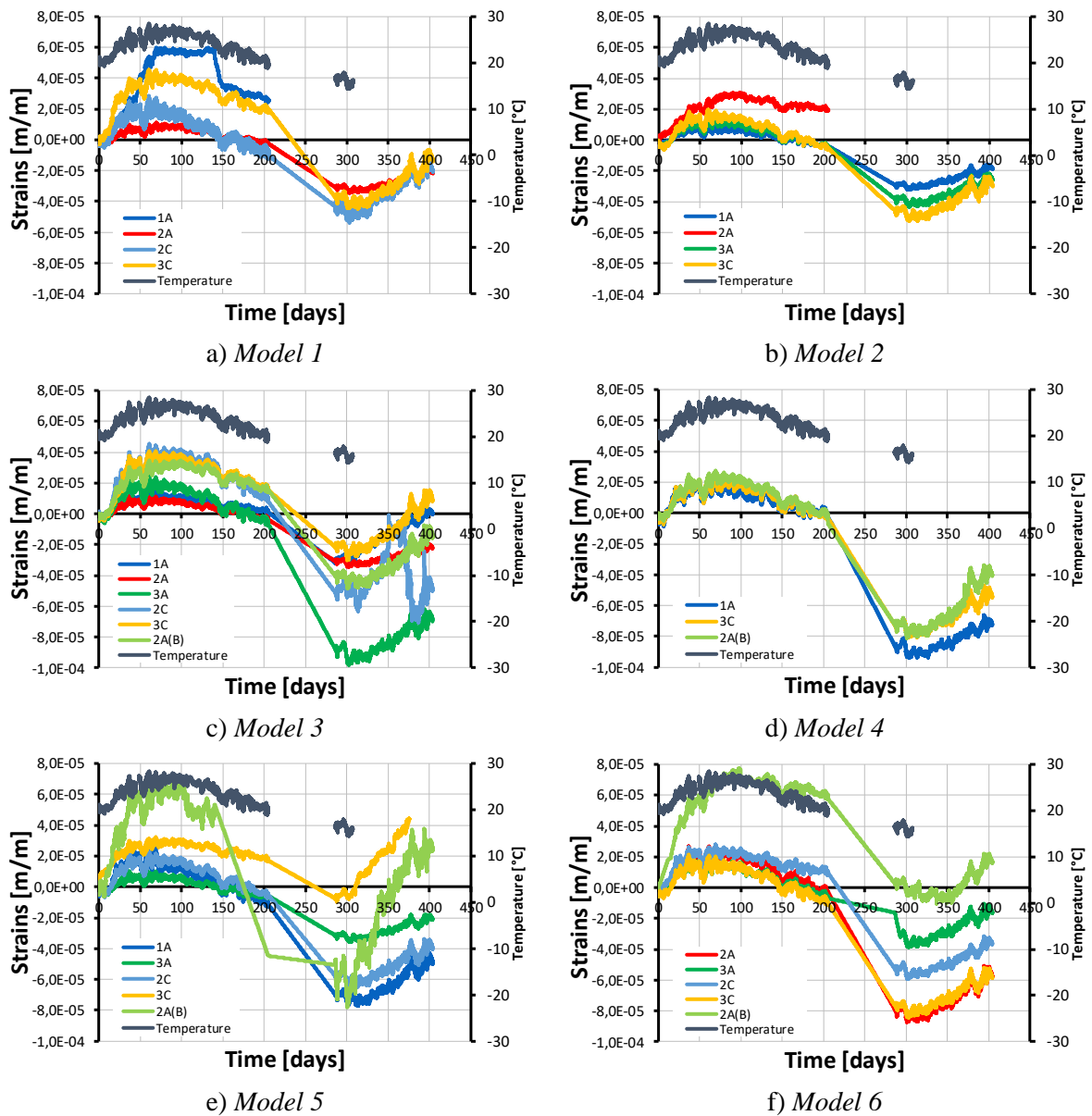


Figure 5.6 – Final strains.

While the differences between the strains measured in the 2A and 2A(B) locations of the same model were likely originated by out-of-plane deformations, the differences of the strains between the remaining instruments were probably induced by the irregular distribution of the internal tensions. This situation is a consequence of several aspects such as the existence of defects in the glass sheets of the models, the faulty assembly of the laminated beams or even the inadequate fixation of the beams to the support system. The evaluation of the final strains allowed to determine that this phenomenon affected every model, as none of the measured strains are exactly equal to those registered in locations that should have identical values.

Contrary to what was detected during the analysis of the deflections, there is no significative difference between the strains of fractured and intact models. This occurrence leads to the conclusion that the physical integrity of the glass sheets does not interfere with this parameter.

5.6.1 Comparison of the Strains in 2A, 2C and 2A(B)

In order to evaluate the strains that take place in the midspan of the models, a comparison between the 2A, 2C and 2A(B) diagrams was performed (Figure 5.7).

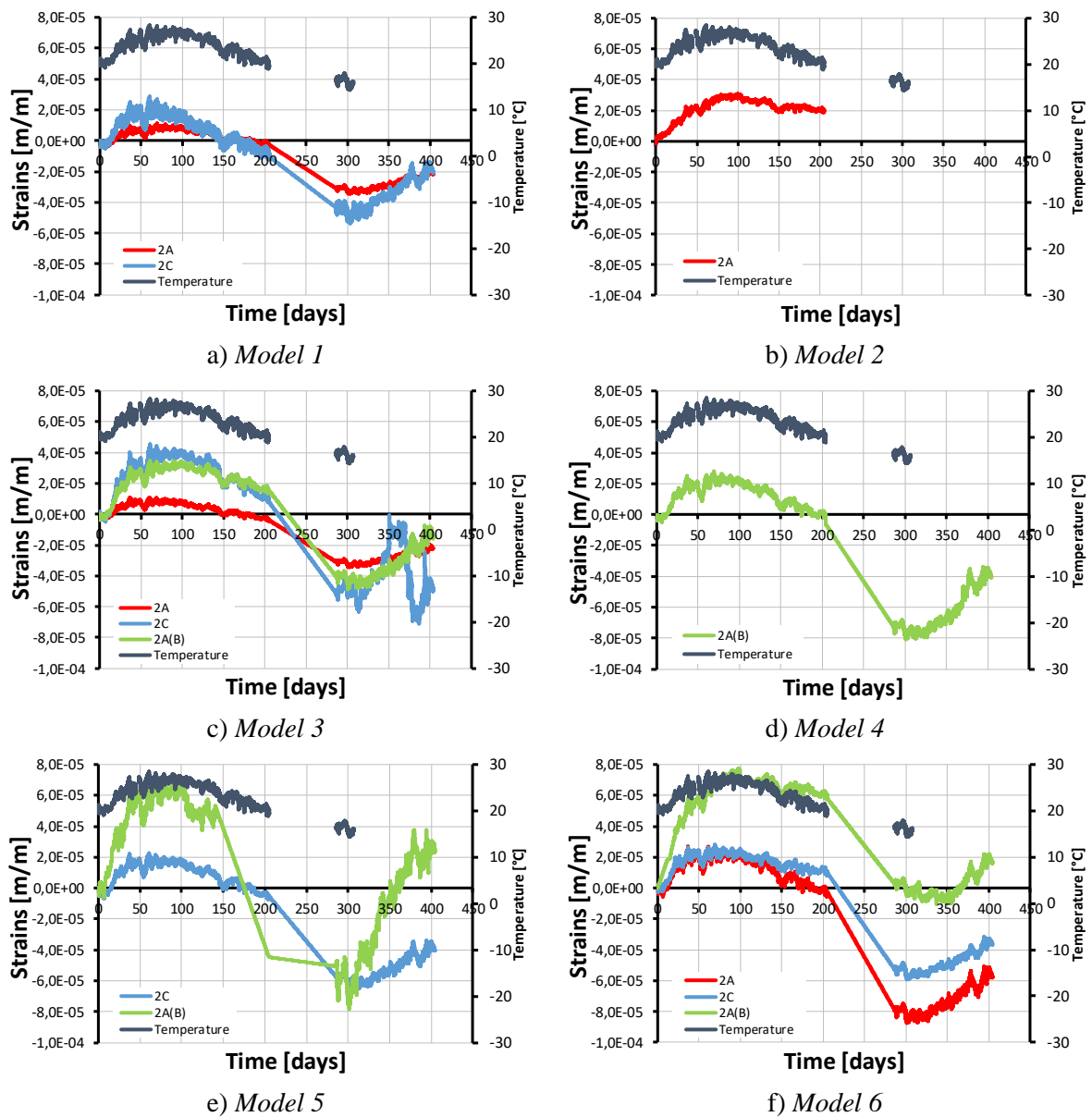


Figure 5.7 – Final strains on the 2A, 2A (B) and 2C locations.

It is important to refer that this analysis also allows to investigate the occurrence and severity of out-of-plane deformations. Although it is likely that this phenomenon affected all the samples, only models 3 and 6 have enough data to allow the confirmation of the occurrence of out-of-plane deformation, as it requires the comparison of the 2A and 2A(B) strains.

In Model 1 (Figure 5.7 a)), the instrument placed in the 2C location displayed a wider range of values, reaching higher strains when subjected to higher temperatures and larger contractions during the colder months of the experimental research. The maximum positive and negative strains by this device correspond approximately $2,85 \times 10^{-5}$ and $-5,5 \times 10^{-5}$ m/m, respectively. Even though there was a visible disparity between their values, the evolution of the 2A strain gauge is quite similar to the 2C, which reaches a maximum of $1,12 \times 10^{-5}$ m/m and a minimum of $-3,5 \times 10^{-5}$ m/m. It is possible that this difference is caused by the stress values that occur in both locations.

In the case of the 2A strain gauge of Model 2 (Figure 5.7 b)), the maximum strain was equal to $3,1 \times 10^{-5}$ m/m, and there were no significant contractions, since the instrument stopped working appropriately on the 204th day.

In Model 3, the 2C strain gauge was characterized by a more accentuated variation than the remaining instruments (Figure 5.7 c)). The maximum and minimum values registered by the 2C device are equal to $3,5 \times 10^{-5}$ m/m and $-4,80 \times 10^{-5}$ m/m. Regarding the 2A and 2A(B) strains, their evolution is similar. Despite that, the strains measured by the 2A(B) instrument are significantly higher when the temperature is elevated and lower at inferior temperatures, which is likely to have been caused by out-of-plane deformations.

The maximum and minimum values measured by the only instrument of Model 4 correspond to $2,75 \times 10^{-5}$ m/m and $-8,10 \times 10^{-5}$ m/m, respectively (Figure 5.7 b)).

Regarding the final values of the midspan strains of Model 5, it becomes important to refer that the 2A(B) strains do not evolve as expected, even after the performed corrections (Figure 5.7 e)). Its anomalous initial growth causes it to reach a maximum strain of $7,05 \times 10^{-5}$ m/m. In addition to that, the growth that was recorded by this instrument is significantly larger than what is observable in the 2C curve.

In Model 6, the effect of out-of-plane deformations is particularly visible since, even after the corrections that were developed, the significant initial growth recorded by the 2A(B) strain gauge is still noticeable, reaching a maximum strain of $7,80 \times 10^{-5}$ m/m and a maximum

contraction of $-1,00 \times 10^{-5}$ m/m (Figure 5.7 f)). Concerning the differences between the 2A and the 2C strains, they were most likely a consequence of higher stress values in the 2C location. Still, it is perceivable that strains of this model evolve similarly to each other.

The following table includes the relevant maximum and minimum strains recorded by the instruments placed at the 2A, 2C, and 2A(B) locations, in each of the analyzed models (Table 5.4).

Table 5.4 – Maximum and minimum strains in the 2A, 2C and 2A(B) locations.

Model	Location	Maximum Strain [m/m]	Minimum Strain [m/m]
1	2A	$2,85 \times 10^{-5}$	$-5,45 \times 10^{-5}$
	2C	$1,12 \times 10^{-5}$	$-3,50 \times 10^{-5}$
	2A(B)	-	-
2	2A	$3,10 \times 10^{-5}$	-
	2C	-	-
	2A(B)	-	-
3	2A	$1,20 \times 10^{-5}$	$-3,50 \times 10^{-5}$
	2C	$4,52 \times 10^{-5}$	$-6,40 \times 10^{-5}$
	2A(B)	$3,50 \times 10^{-5}$	$-4,80 \times 10^{-5}$
4	2A	-	-
	2C	-	-
	2A(B)	$2,75 \times 10^{-5}$	$-8,10 \times 10^{-5}$
5	2A	-	-
	2C	$2,35 \times 10^{-5}$	$-6,55 \times 10^{-5}$
	2A(B)	$7,05 \times 10^{-5}$	$-7,85 \times 10^{-5}$
6	2A	$2,70 \times 10^{-5}$	$-8,80 \times 10^{-5}$
	2C	$2,80 \times 10^{-5}$	$-5,95 \times 10^{-5}$
	2A(B)	$7,80 \times 10^{-5}$	$-1,00 \times 10^{-5}$

5.6.2 Comparison of the Strains in 1A, 3A and 3C

As previously established, the variation of the environmental temperature should induce identical strain values in all the considered locations. Consequently, the differences between the values of the 1A, 3A and 3C strain gauges, in each of the tested models, can only be caused either by measuring errors or by an uneven stress distribution. The latter is responsible for originating different tension levels in locations where it should be identical.

The diagrams of strains measured in the 1A, 3A and 3C locations, in each of the six experimented models, are presented in Figure 5.8. Through their observation, it was possible to establish that every model was affected by uneven stress distributions as, even though most of

its curves are similar to each-other, none of them is identical. Evidently, the severity of this phenomenon differs from model to model.

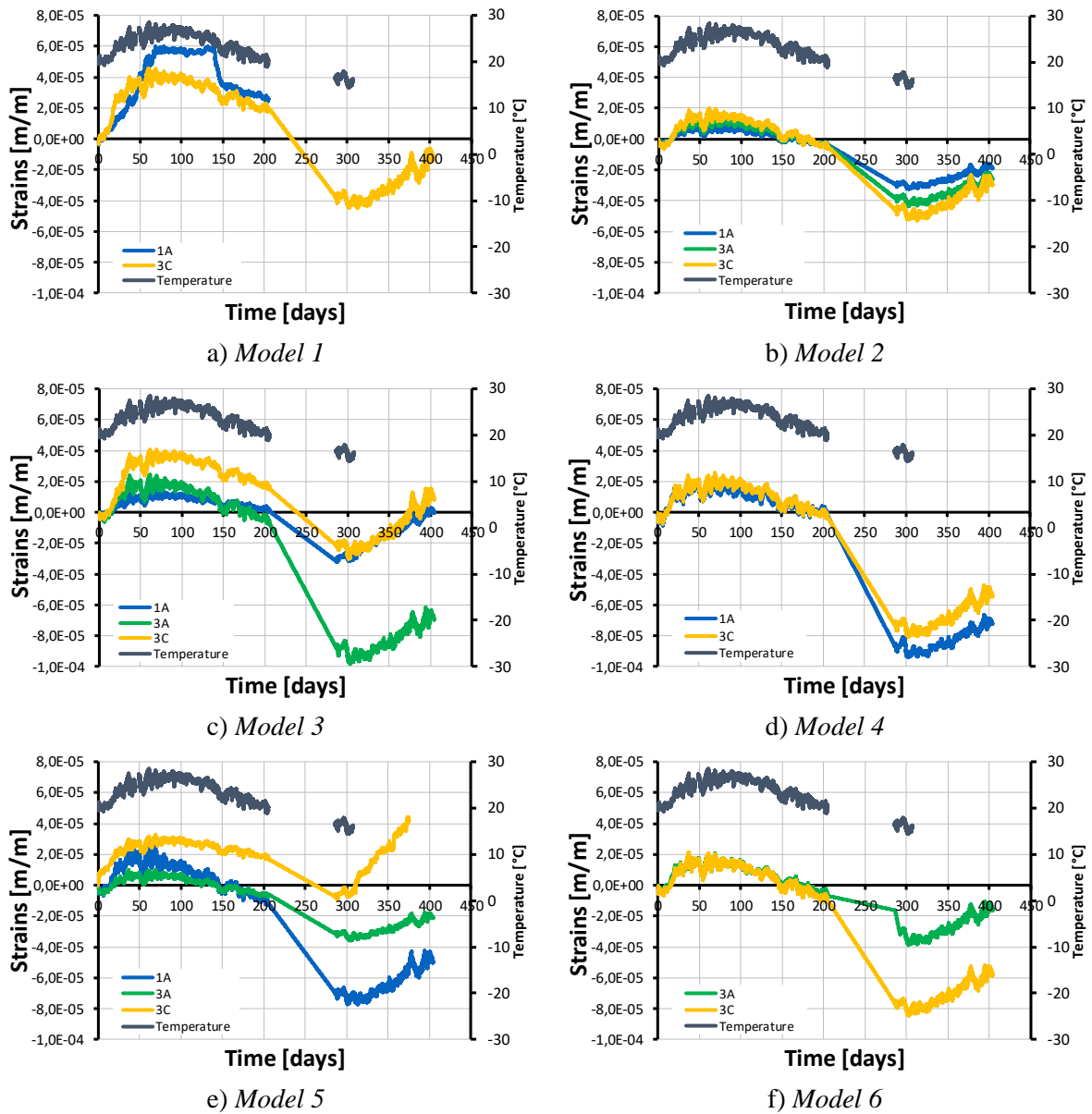


Figure 5.8 – Final strains on the 1A, 3A and 3C locations.

It is appreciable in Figure 5.8 a), that the 1A strain gauge attached to Model 1 displayed an unusual evolution, which makes it difficult to compare with the 3C instrument and to establish if it was caused by the stress levels of that location or by any other reason. Its growth causes it to reach a positive maximum is approximately $6,05 \times 10^{-5}$ m/m. Since this instrument was not able to function adequately after the 204th day, no relevant contractions were recorded.

The strains of the instruments of Model 2 evolved similarly (Figure 5.8 b)), which indicates that this model was subjected to relatively equivalent stress values in the three locations.

In Models 3 and 5 there are visible differences in the strains of the considered locations, with the 3C strain gauge being responsible for the larger strain values (Figure 5.8 c) and e)). Ultimately this is a sign that the stress distribution of these models induced the occurrence of higher tensions on the right side of the laminated glass beams.

Despite the similarity of the curves displayed by the instruments 1A and 3C of Model 4 (Figure 5.8 d)), it is noticeable that the 1A strains are slightly lower. This could indicate that the stress distribution of this model led to higher tensions on the right side.

In the Figure 5.8 f) it is visible that the 3A and 3C values recorded in Model 6 are partly coincident until the 204th day. This occurrence was likely caused by perturbation on the experimental layout, which subsequently affects its internal stress distribution.

The following table includes the relevant maximum and minimum strains recorded by the several instruments in each analyzed model (Table 5.5).

Table 5.5 – Maximum and minimum strains in the 1A, 3A and 3C locations.

Model	Location	Maximum Strain [m/m]	Minimum Strain [m/m]
1	1A	$6,05 \times 10^{-5}$	-
	3A	-	-
	3C	$4,55 \times 10^{-5}$	$-4,15 \times 10^{-5}$
2	1A	$1,05 \times 10^{-5}$	$-3,25 \times 10^{-5}$
	3A	$1,55 \times 10^{-5}$	$-4,30 \times 10^{-5}$
	3C	$2,00 \times 10^{-5}$	$-5,25 \times 10^{-5}$
3	1A	$1,45 \times 10^{-5}$	$-3,25 \times 10^{-5}$
	3A	$2,50 \times 10^{-5}$	$-3,10 \times 10^{-5}$
	3C	$4,12 \times 10^{-5}$	$-9,75 \times 10^{-5}$
4	1A	$2,25 \times 10^{-5}$	$-9,40 \times 10^{-5}$
	3A	-	-
	3C	$2,55 \times 10^{-5}$	$-8,10 \times 10^{-5}$
5	1A	$2,70 \times 10^{-5}$	$-7,75 \times 10^{-5}$
	3A	$1,05 \times 10^{-5}$	$-3,55 \times 10^{-5}$
	3C	$4,45 \times 10^{-5}$	$-1,00 \times 10^{-5}$
6	1A	-	-
	3A	$2,05 \times 10^{-5}$	$-8,50 \times 10^{-5}$
	3C	$2,15 \times 10^{-5}$	$-3,55 \times 10^{-5}$

5.6.3 Analysis of the Final Strains

Posteriorly, it became interesting to evaluate the strains that took place in each of the considered locations (Figure 5.9), as it enhances the development trends of the strains at each location.

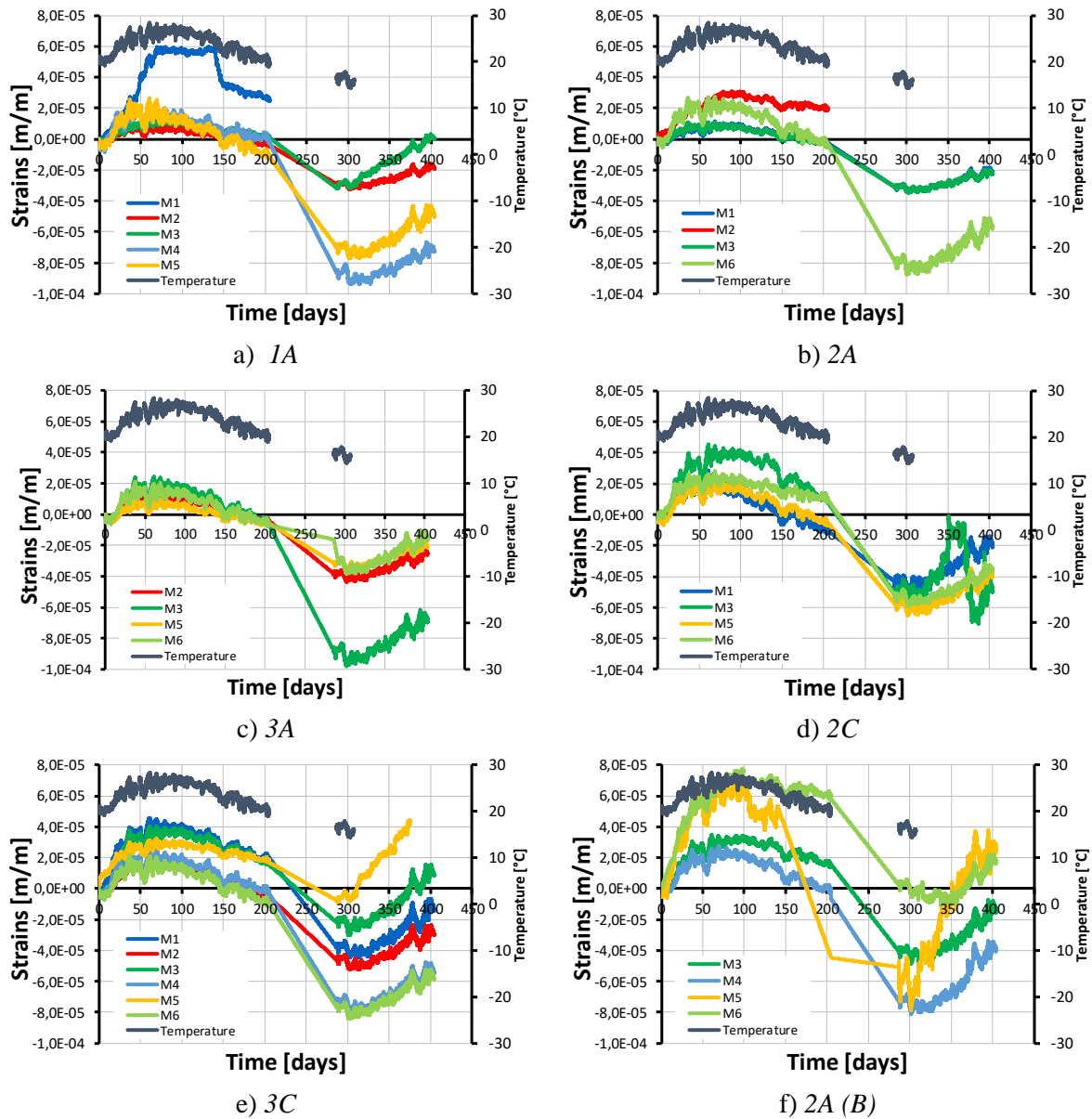


Figure 5.9 – Comparison of the final strains.

To understand the behavior of the experimented beams, the range of values achieved by the instruments at each location was determined, as well as its corresponding mean maximum and

minimum values (Table 5.6). These values translate the magnitude of the strains that could be expected from laminated glass beams with the experimented characteristics.

Table 5.6 - Maximum and minimum strains in each location.

Location	Maximum Strain [m/m]	Minimum Strain [m/m]	Average Maximum Strain [m/m]	Average Minimum Strain [m/m]
1A	$6,05 \times 10^{-5}$	$-9,40 \times 10^{-5}$	$2,70 \times 10^{-5}$	$-5,91 \times 10^{-5}$
2A	$3,10 \times 10^{-5}$	$-8,80 \times 10^{-5}$	$2,46 \times 10^{-5}$	$-5,92 \times 10^{-5}$
3A	$2,50 \times 10^{-5}$	$-8,50 \times 10^{-5}$	$1,79 \times 10^{-5}$	$-4,86 \times 10^{-5}$
2C	$4,52 \times 10^{-5}$	$-6,55 \times 10^{-5}$	$2,70 \times 10^{-5}$	$-5,60 \times 10^{-5}$
3C	$4,55 \times 10^{-5}$	$-9,75 \times 10^{-5}$	$3,30 \times 10^{-5}$	$-5,30 \times 10^{-5}$
2A (B)	$7,80 \times 10^{-5}$	$-8,10 \times 10^{-5}$	$5,28 \times 10^{-5}$	$-5,44 \times 10^{-5}$

Despite the relevance of the present values, it is worth mentioning that, if the anomalous results were completely ignored, the average strains and contractions would be much more consistent.

5.6.4 Isolation of time-related strains

As previously established, the obtained results only depend on the variation of the environmental temperature. Therefore, it was considered relevant to determine the theoretical values of the deformation of the models due to the temperature variation. The length variation of the models, ΔL , is related to the variation of the temperature, ΔT , and to the coefficient of thermal expansion of glass, c , (Equation (11)) (adapted from Dias da Silva, V., 1995).

$$\Delta L = \alpha \cdot \Delta T \quad (11)$$

Assuming that the variation of temperature had the same impact in the entire model, the fluctuation of the strains should be identical in all the considered locations. The application of Equation (11) allowed to determine the theoretical value of the total length variation that the models should experience due to the environmental temperature variation (Figure 5.10).

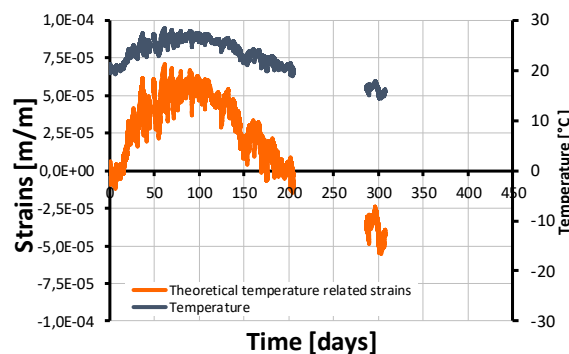


Figure 5.10 – Theoretical temperature related strains.

Since these strains are related to temperature only, they represent the longitudinal deformability that the beams endured, which is constant throughout the models and thus, equal in all the positions of the strain gauges. For this reason, the differences between the theoretical and the experimental values is related to other aspects such as in-plane and out-of-plane bending. The in-plane bending is caused by the self-weight load, which was removed from the readings. This implicates that the differences between the theoretical temperature related and the readings in the strain gauges are caused by out-of-plane bending and time-related deformation of the interlayer alone deformation (Figure 5.10). Since the objective of the experimental research was to establish the effect of the latter, the contribution of out-of-plane bending must also be removed from the results. This may be achieved by using homologous strain gauges in the same location from front and back planes. In fact, if out-of-plane bending had not occurred, the strain gauges would present equal readings. In the cases that it is not verified, the discrepancies between their readings can be used to detect and accurately determine the out-of-plane related strains. After this, they may be removed from the measurements, which allows to isolate the time-dependent deformation.

Regarding the occurrence of out-of-plane deformations (Figure 5.11), it was considered important to estimate its impact on models 3 and 6, as this phenomenon is responsible for inducing additional strains, which are variable along the thickness of the beams (Figure 5.12).

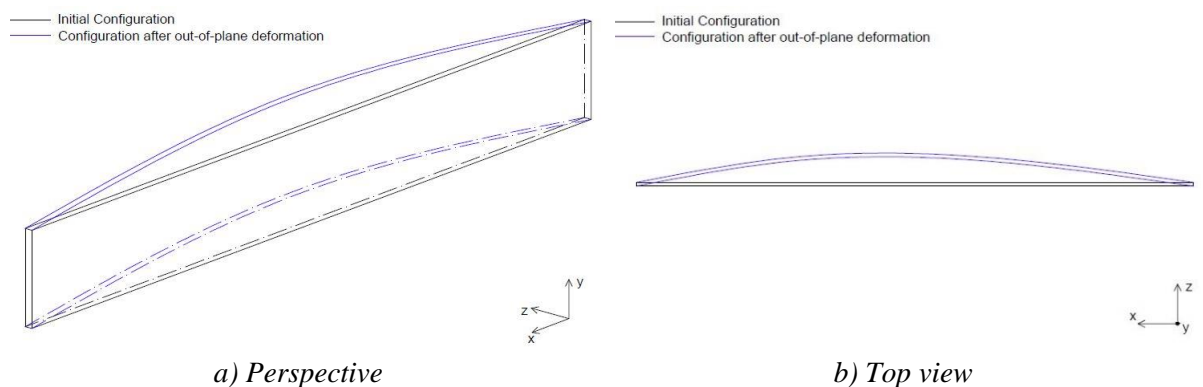


Figure 5.11 – Out-of-plane deformation in the experimental models.

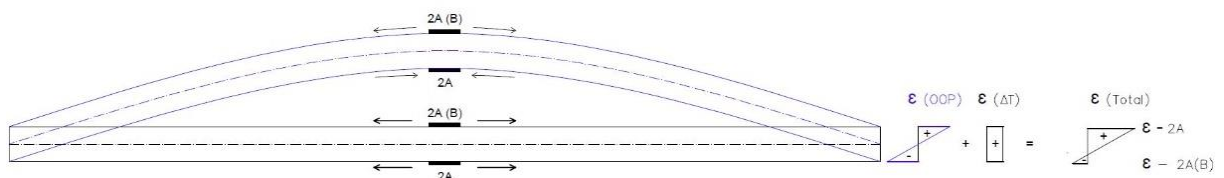


Figure 5.12 - Example of the effect of the out-of-plane deformations on the models' strains.

As observable in Figure 5.12, the strains that characterize the middle section of the models translate the real impact that the fluctuation of the temperature had on the strains of the models, which is why they were determined (Figure 5.13). The obtained curves confirm that the long-term behavior of the models is highly dependent on the variation of the environmental temperature.

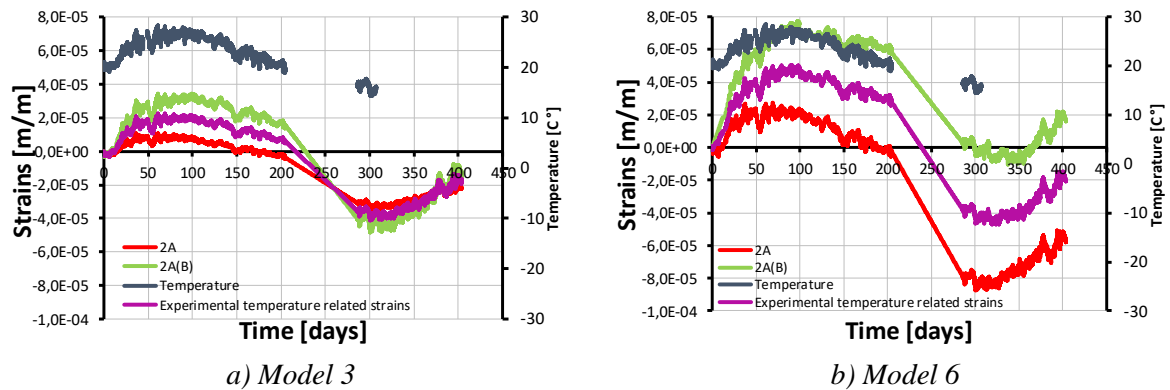


Figure 5.13 – Determination of the experimental temperature related strains.

Furthermore, the isolation of the experimental temperature related strains allows a direct comparison between the experimental and theoretical values of the strains (Figure 5.14).

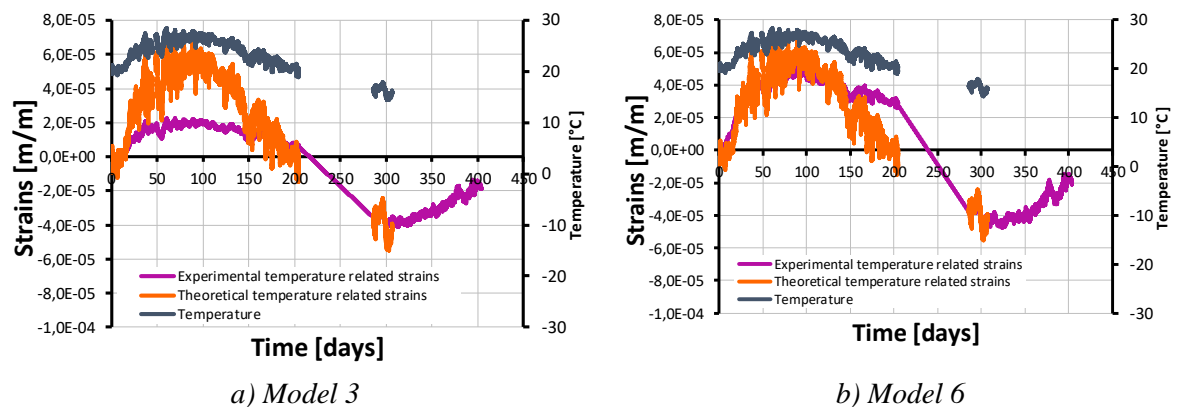


Figure 5.14 – Comparison between the experimental and theoretical temperature related strains.

As observable in Figure 5.14, the results in the non-fractured model show a better agreement with the theoretical values than those of the fractured beam.

6 FINAL COMMENTS

6.1 Conclusions

Throughout the present document, it was made clear that, despite being known for its fragility, the application of glass as load-bearing elements has evolved significantly over the past few decades. The current dissertation intended to contribute for the diminishment of the uncertainties regarding the mechanical response of laminated glass beams by means of an experimental investigation which focused mainly on the effect that environmental temperature and the self-weight of the models had on their long-term global behavior.

It has been verified that glass elements are highly susceptible to the effect of long-term actions, due to the occurrence of stress corrosion and to the fact that the materials that constitute most of the lamination films are polymers, whose properties are known to be influenced by external mechanical and environmental factors. The experimental results confirm those assumptions, as even the daily fluctuation of temperature affected the strains and the deflections of the models.

In the absence of any recognized protocol establishing the loading of long-term tests, a strategy for soliciting the models in the intended manner was defined. It is expected that the considered strategy allowed the models to be adequately solicited for the developed experimental research.

In the performed experimental research two different situations were evaluated through the consideration of both fractured and intact models. By doing so it was possible to observe the mechanical behavior before and after breakage.

Even though not all the instruments displayed proper results, the obtained results were fairly consistent to what was expected as they evolved similarly to each other when neither the instruments nor the test layout was disturbed. This consistency of the registered values ultimately contributes to the increase of the trust in the quality of the results and, consequently, in the applications of glass as load-bearing elements.

Although the final graphs revealed that there was little difference between the values of the strains of intact and fractured models, they clearly showed that there was a significant

discrepancy between the values of the deflections of the intact models from the fractured ones as they displayed much lower vertical displacements.

It was also possible to conclude that, even though the physical integrity of the models had a significant impact on the vertical displacements, the strains were mainly affected by the environmental temperature.

It was concluded that the considered composite structure presented a positive behavior, as its lamination film allowed it to support the considered actions without displaying excessive deformations and strains.

6.2 Proposals for Future Developments

With the finalization of the engaged studies and in order to complement all the performed investigation, a few suggestions for future developments are proposed:

1. Further investigation regarding the long-term behavior of glass is by means of additional full scale experimental tests, which should address not only the impact of self-weight and environmental temperature, but also a more extended load framework, as the effect of actions like humidity, extreme temperatures and cyclic loads, is also still poorly understood and could cause worse consequences in the load-bearing capacity of the laminated glass beams. Both fractured and intact models should be evaluated, being of particular importance the assessment of, not only the strains and the deflections, but also of the evolution of the fracture pattern. Additionally, these experimental studies should also include models with different compositions which will allow to determine more efficient solutions, as distinct glass sheets and interlayers will most certainly perform differently.
2. Development of a finite element model calibrated with the experimental results, which would allow to perform a more detailed parametric analysis.
3. Consideration of all the data obtained regarding the effect of long-term loads in laminated glass beams in the establishment adequate design codes, as it is essential to the further expansion of the application of laminated glass beams.

6.3 Publications

The investigation developed within the present dissertation made possible the realization of a conference article.

7 IMAGE CREDITS

Image 1	<i>The Glass Home</i>	http://omnigp.com/20-beautiful-glass-buildings-world/	27/04/2016
Image 2	<i>The Dome of the Reichstag Building</i>	https://michaelseye.files.wordpress.com/2013/10/t2b5234.jpg	27/04/2016
Image 3	<i>The Louvre Pyramid</i>	http://joinusinfrance.com/episode-21-the-louvre-museum/	27/05/2016
Image 4	<i>The Sage Gateshead,</i>	http://www.chroniclive.co.uk/whats-on/music/soul-singers-60s-stylistics-come-5817722	27/04/2016
Image 5	<i>Structural Glass applied in beams</i>	Louter, C., (2011). "Fragile yet Ductile – Structural Aspects of Reinforced Glass Beams", PhD Dissertation, Delft University of Technology, Delft, Netherland.	28/06/2016
Image 6	<i>Structural Glass applied in columns</i>	https://karmatrendz.wordpress.com/2009/08/11/civic-center-in-st-germain-en-laye-by-atelier-9-portes-philippe-harden/	28/06/2016
Image 7	<i>Structural Glass applied in stairs</i>	https://www.pinterest.com/pin/914862395152991/	28/04/2016
Image 8	<i>Structural Glass applied in a pedestrian bridge</i>	https://empoweryourknowledgeandhappytrivia.wordpress.com/2015/07/15/grand-canyon-skywalk-how-high-is-it/	28/04/2016
Image 9	<i>Obsidian</i>	https://talk.turtlerockstudios.com/t/obsidian-skins/47726?page=3	30/04/2016
Image 10	<i>Egyptian core-formed glass vessel</i>	http://www.toledomuseum.org/kiosk/ancient-asian-european-glass/ancient-glass/pivotal-moments-in-ancient-glass/core-formed-vessels-in-egypt/	30/04/2016
Image 11	<i>Roman bottle (free-blowing glass)</i>	https://www.pinterest.com/judithcameron/ancient-glass/	30/04/2016
Image 12	<i>The crown process</i>	https://bopardconservationproject.wordpress.com/about/a-glossary-of-stained-glass-terms/	02/05/2016
Image 13	<i>The cylinder method</i>	https://bopardconservationproject.wordpress.com/about/a-glossary-of-stained-glass-terms/	02/05/2016
Image 14	<i>The drawn process - Fourcault</i>	http://www.newglasstech.com/?page=product&cat=Specialities&product=restauration&lang=en	02/09/2017
Image 15, 16 and 17	<i>Mode I; Mode II; Mode III.</i>	https://www.sharcnet.ca/Software/Ansys/17.2/en-us/help/ans_frac/Hlp_G_STRFRINTRO.html	09/05/2017

8 BIBLIOGRAPHIC REFERENCES

Bati, S. Briccoli, Ranocchiai, G., Reale, C., Rovero, L., (2010). “Time-Dependent Behavior of Laminated Glass”, *Journal of Materials in Civil Engineering* ©, American Society of Civil Engineers (ASCE), pg. 389-396.

Behr, R., Minor, J., Norville, H., (1993). “Structural behavior of architectural laminated glass”, *Journal of Structural Engineering*, American Society of Civil Engineers (ASCE), pp. 202-222.

Belis, J., Depauw, J., Callewaert, D., Delincé, D., Van Impe, R., (2008). “Failure mechanisms and residual capacity of annealed glass/SGP laminated beams at room temperature”, *Engineering Failure Analysis*, Elsevier, pg. 1866-1875.

Biolzi, L., Cagnacci, E., Orlando, M., Piscitelli, L., Rosati, G., (2014). “Long term response of glass-PVB double-lap joints”, *Composites*, Elsevier, pg. 41-49.

CNR – Advisory Committee on Technical Recommendations for Construction, (2013). “Guide for the Design, Construction and Control of Buildings with Structural Glass Elements”, Italian National Research Council (CNR), Rome.

Delincé, D., Callewaert, D., Belis, J., Van Impe, R., (2008). “Post-breakage behavior of laminated glass in structural applications”, *Proceedings of Challenging Glass*, Delft, Netherlands, pg. 459-467.

Dias da Silva, V., (1995). “Mecânica e Resistência dos Materiais”, 2ª Edição. Zuari, Coimbra, Portugal.

DuPont@. Downloaded at June 25, 2016.
http://www2.dupont.com/Building_Innovations/zh_CN/assets/downloads/SGPintro_E.pdf

Firno, F., (2015). “Análise experimental/FEM de vigas híbridas vidro-aço”, Masters Dissertation, Department of Civil Engineering of Coimbra’s University, Coimbra, Portugal.

Guin, J., Wiederhorn, S. M., (2003). “Crack Growth threshold in soda lime silicate glass role of hold-time”, *Journal of Non-Crystalline Solids*, Elsevier, pp. 12-20.

Gy, R., (2003). “Stress corrosion of silicate glass: a review”, *Journal of Non-Crystalline Solids*, Elsevier, pp. 1-11.

- Haldimann, M., Luible, A., Overend, M., (2008). “Structural Use of Glass”. International Association for Bridge and Structural Engineering (IABSE), Zurich, Switzerland.
- Hooper, J. A., (1973). “On the bending of architectural laminated glass”, International Journal of Mechanical Sciences, Elsevier, pp. 309- 334.
- Joint Research Centre of the European Commission, (2014). “Guidance for European Structural Design of Glass Components - Support to the implementation, harmonization and further development of the Eurocodes”, Luxembourg: Publications Office of the European Union.
- Konta, J. (1988). “Second International Conference on Natural Glasses. Prague, 1987”, Charles University, Prague.
- Kott, A. (2006). “Zum Trag- und Resttragverhalten von Verbundsicherheitsglas”, Federal Institute of Technology, Zurich.
- Louter, C., (2011). “Fragile yet Ductile – Structural Aspects of Reinforced Glass Beams” PhD Dissertation, Delft University of Technology, Delft, Netherland.
- Louter, C. Belis, J., Veer, F., Lebet, J., (2011). “Durability of SG-laminated reinforced glass beams: Effects of temperature, thermal cycling, humidity and load-duration”, Construction and Building Materials, Elsevier, pg. 280-292.
- O’Regan, C., (2014). “Structural use of glass in buildings”, The Institution of Structural Engineers, London.
- Ronchetti, C., Lindqvist, M., Louter, C., Salerno, G., (2013). “Stress-corrosion failure mechanisms in soda-lime silica glass”, Engineering Failure Analysis, Elsevier, pg. 427-438.
- Serafinavicius, T., Lebet, J., Louter, C., Lenkimas, T., Kuranovas, A., (2013). “Long-term laminated glass four-point bending test with PVB, EVA and SG interlayers at different temperatures”, Procedia Engineering, Elsevier, pg. 996-1004.
- Stelzer, I. (2010) “High Performance Laminated Glass”, Challenging Glass 2, Delft, Netherlands.
- Valarinho, L., (2010). “Construção em vidro estrutural: comportamento mecânico de vigas mistas vidro-GFRP”, Masters Dissertation, Department of Civil Engineering and Architecture, Superior Technical Institute, Technical University of Lisbon, Lisbon, Portugal.